Title
UV Second-Harmonic Studies of Concentrated Aqueous Electrolyte Interfaces

Author
Otten, Dale Edward

Publication Date
2010

Peer reviewed|Thesis/dissertation

UV Second-Harmonic Studies of Concentrated Aqueous Electrolyte Interfaces

by

Dale Edward Otten

A dissertation submitted in partial satisfaction of the

requirements for the degree of

Doctor of Philosophy

in

Chemistry

in the

Graduate Division

of the

University of California, Berkeley

Committee in charge:

Professor Richard J. Saykally, Chair
Professor Daniel M. Neumark
Professor Clayton J. Radke

Fall 2010

UV Second-Harmonic Studies of Concentrated Aqueous Electrolyte Interfaces

by Dale Edward Otten

Abstract

UV Second Harmonic Spectroscopy of Concentrated Aqueous Electrolyte Interfaces

by

Dale Edward Otten

Doctor of Philosophy in Chemistry

University of California, Berkeley

Professor Richard Saykally, Chair

The nature of liquid-vapor interfaces is a rapidly developing field of research, aimed at ascertaining the properties and structure of this unique microscopic environment. The mechanism of aqueous electrolyte partitioning and chemistry in the aqueous-vapor interface region is explored herein, using the surface selective technique of second-harmonic generation to probe these systems via strong electronic resonances in the ultraviolet.

In Chapter 1, the current descriptions of the neat water- and electrolyte solution-vapor interfaces are reviewed. Mechanistic explanations for anion adsorption to such interfaces are highlighted as an object of research. Previous applications of the surface second-harmonic technique to aqueous electrolyte systems are also described, and the results of these studies are built upon herein.

In Chapter 2 the principles of applying second harmonic generation as a spectroscopic probe of liquid-vapor interfaces are discussed, followed by a consideration of the adapted Langmuir model used to interpret such studies. This model is then developed to include both cations and anions as a consequence of the requirement of electroneutrality of the solution-vapor interface. The resulting expressions are then identified as diagnostics for mechanisms of ionic adsorption to the solution interface. A discussion of the technical requirements and developments necessary to apply femtosecond ultraviolet second-harmonic spectroscopy to these systems in a reliable and reproducible manner is also presented in Chapter 2.

The models developed in Chapter 2 are used to interpret the interfacial adsorption processes of aqueous sodium nitrite and sodium nitrate solutions in Chapter 3. Nitrite surface activity is found to exhibit second-order bulk concentration dependence which is then interpreted to indicate the adsorption of nitrate and sodium into the interface region as ion-pairs. These ion-pairs are found to adsorb with a standard Gibbs free energy of -37±1 kJ·mol^{-1}. The related sodium nitrate electrolyte is not found to be strongly surface active.

The temperature dependence of the surface activity of aqueous potassium thiocyanate is explored in Chapter 4, and in terms of an adapted Langmuir adsorption model is found to be an exothermic process ($\Delta H^{\circ} = -5.9 \pm 0.2$ kJ·mol^{-1}) with a weakly unfavorable entropic component ($\Delta S^{\circ} = -8 \pm 1$ J·mol^{-1}). The process is also found to exhibit first-order dependence on bulk electrolyte concentration, indicating that the cation and anion translations are not highly correlated. These results are discussed in the framework of current theories of anionic interface adsorption mechanisms and alternative explanations are considered.

The UV photochemical products of aqueous potassium and sodium thiocyanate are also observed to obscure the second-harmonic response of thiocyanate in the interface, and elemental sulfur is proposed to be excluded from the bulk solution into the interface in this system. In Chapter 5 the effect of oxidation on the interface of aqueous sodium iodide solutions is also investigated, determining that much like thiocyanate the second-harmonic signal is obscured by the products that are generated. The potential for exploring rate-law behavior at aqueous electrolyte interfaces by this method is also established. Lastly, the ultraviolet second-harmonic spectrum of sodium iodide at molar and millimolar concentrations is found to be qualitatively different to previously reported spectra. Two postulates are made to explain this variance, one being an experimental configuration difference, the other being due to the oxidation products found in these systems.

To my mother, my father, and my wife

Contents

Chapter 1 - The Liquid-Vapor Interface

The boundaries between phases of matter have long been exploited for their unique properties. The myriad applications in catalysis, chemical analysis, and chemical separation only 'scratch the surface' of the importance that such boundaries have in our modern world. The natural world also runs on interfaces, partitioning water between sea and air, energy between Earth and space. Even the fundamental workings of life itself rely on compartmentalization and controlled flow of energy and molecules that result from the existence of such boundaries. The unique properties and applications that interfaces engender has lead to the huge and growing field of surface science that aims at increasing our knowledge of these macroscopic systems that inherently contain a microscopic dimension. The commonly touted ubiquity of water is only surpassed by the ubiquity interfaces that exist in our natural world.

The liquid-vapor interface is a necessarily asymmetric region; in one direction the properties tend towards those of the vapor phase while in the opposite they tend to that of the bulk phase. Creation of an interface engenders an energetic cost as it requires the truncation of the cohesive interactions that hold the independent phases together. This additional surface energy is observable macroscopically as surface tension. In water this energy is large, exerting a restoring force of 72 m$\mathrm{N \cdot m^{-1}}$ at 25°C as the liquid attempts to minimize the unsatisfied hydrogen bonds at its surface[1, 2]. As a consequence of the coexistence of condensed water and vapor phase, some finite region must exist where the molecular structure transitions from one phase to the other, *e.g.* the interfacial region. This transition engenders unique properties to the liquid-vapor interface region, and the development of the current microscopic description of this region is the subject of this chapter.

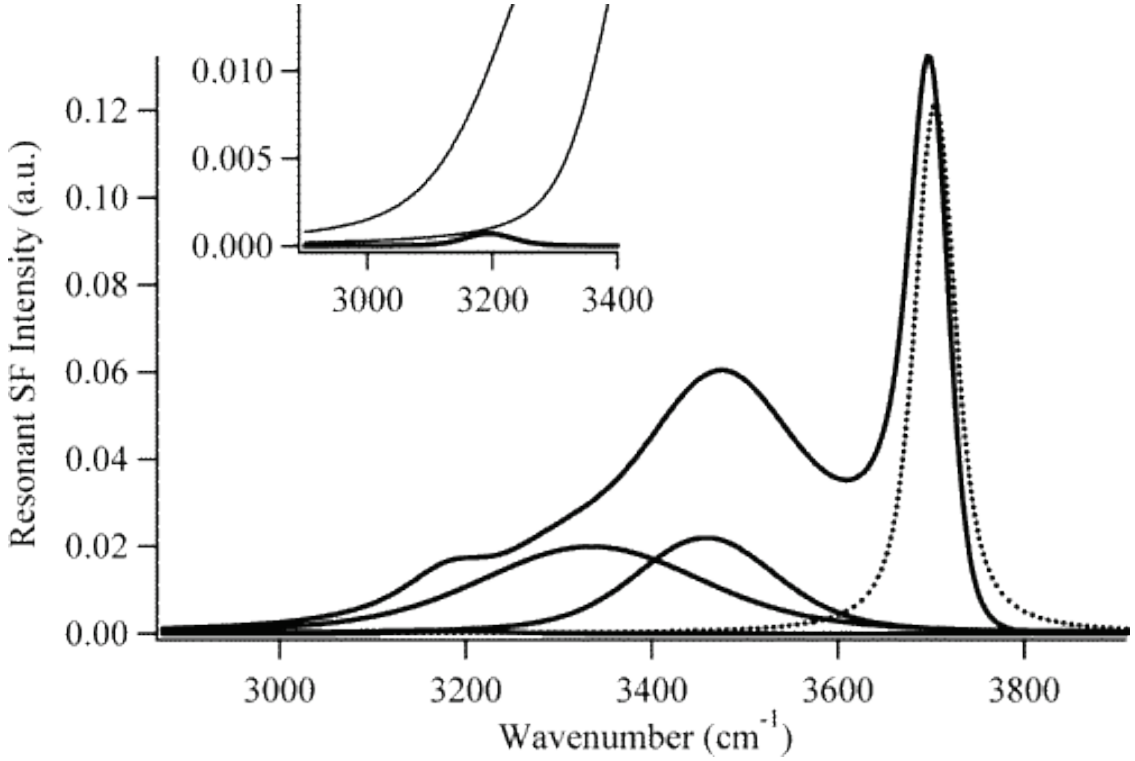

Figure 1.1- The vibrational sum-frequency (VSFG) spectrum of the neat water interface in the OH stretching region (enveloping function), and Gaussian deconvolution of its component vibrational modes. The free OH stretching peak is denoted by the dotted line, its sharpness and blue-shift characteristic of a highly oriented gas-phase-like vibrational mode. The remainder of the peaks are attributed to sub-surface water molecules exhibiting net-broken orientational inversion symmetry. *Reprinted in part with permission from* Raymond, E.A. and G.L. Richmond, *J. Phys. Chem. B*, **108**, 5051 (2004). *Copyright 2004 American Chemical Society.*

1.1. The Neat Water Interface

A reasonable amount of information is known about the microscopic structure and extent of the neat water interface. Early surface potential measurements attempted to determine the average orientation of the dipoles at the air/water interface, although the results often conflicted in both sign and magnitude, making such studies inconclusive as a whole ([3] and references therein). X-ray absorption spectroscopy of liquid water microjets, interpreted via molecular dynamics based simulated spectra, made some progress in addressing this molecule-sized region[4-6]. These studies determined a reduced water density near the liquid water surface, and made some assignment of the types of hydrogen bonds present there. However, it wasn't until the advent of vibrational sum-frequency generation (VSFG) spectroscopy of liquid water surfaces that the development of the microscopic description flourished[7-9]. The key finding of the VSFG spectrum of the OH stretching region of the neat water interface is the

unique, narrow, intense peak at 3705 cm^{-1}; absent in Raman spectrum of the bulk liquid but apparent in the IR spectrum of small water clusters; it is assigned to the free OH stretch of a dangling (broken) hydrogen bond (Figure 1.1)[8, 10]. When compared to the hydrophilic interface of quartz, this feature vanishes as the quartz hydrogen bond terminates the surface water structure[11]. In the VSFG spectra of water-hydrophobe interfaces, this feature remains[9, 12]. The two broad features at 3454 cm^{-1} and 3325 cm^{-1} (including 3200 cm^{-1}) are similar to the Raman spectrum of liquid water: The lower energy peak(s) are taken to be the OH stretching frequency of tetrahedrally coordinated water ('ice-like'), often taken as in indication of enhanced order, where the higher energy peak is an indication of a more loosely ordered structure similar to the bulk liquid ('liquid-like')[11]. As temperature is increased, the liquid-like feature of the VSFG spectrum increases in intensity at the expense of the ice-like feature, also observed in the bulk IR spectrum[8]. While some of the specific assignments remain controversial[13-16], the assignment of the free OH stretch remains undisputed. Analysis of the dilution of the dangling OH moiety by methanol has

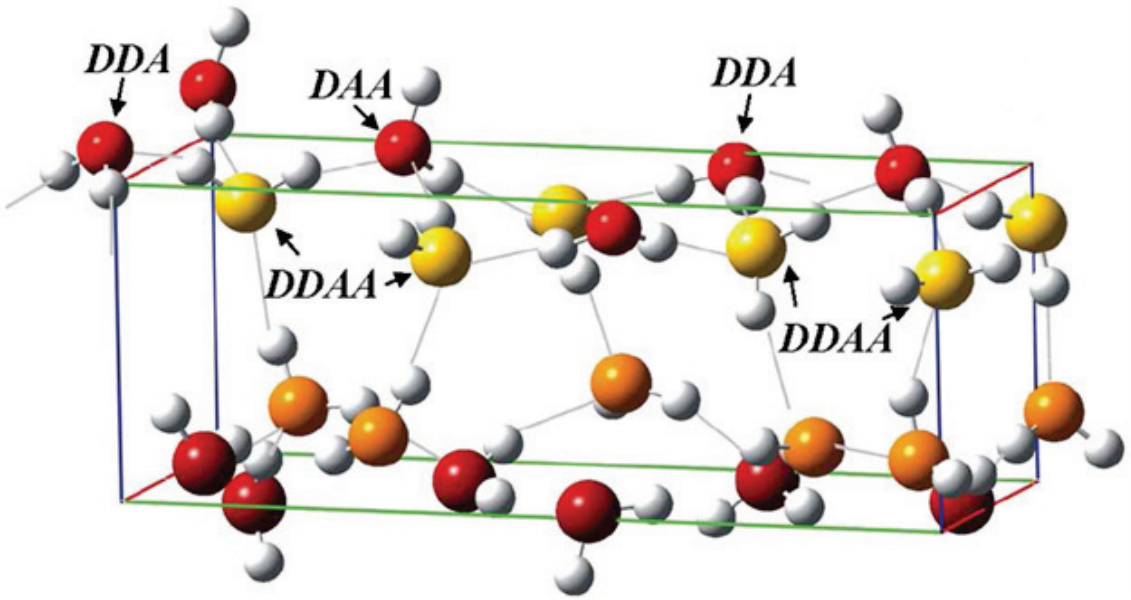

Figure 1.2- Cartoon of the neat water interface (interface is up). The interface comprises two dominant moieties: donor-acceptor-acceptor (DAA) for which a free OH protrudes into the vapor phase above the surface, and a donor-donor-acceptor (DDA) which tends to hydrogen bond to the second water layer with both hydrogens. The second layer (yellow) adopts a somewhat constrained hydrogen bond network and is responsible for the 'ice-like' features of the neat water VSFG spectrum. The third layer (orange) is considered 'water-like' and represents the deepest layer considered observed by VSFG spectra. *Reprinted in part with permission from* Ji, N., V. Ostroverkhov, *et al.*, *Phys. Rev. Lett.*, **100**, 096102 (2008). *Copyright 2008 American Physical Society.* http://link.aps.org/doi/10.1103/PhysRevLett.100.096102

led to the conclusion that the free OH moiety comprises approximately 25% of the water monolayer[8].

Orientational analysis by VSFG has suggested that the dangling OH group points out of the interface at 33°±1° from the surface normal with a very tight distribution (<15°), and even suggests the existence of a second type of free OH moiety at the interface[13]. In total, the current description of the air-water interface (neglecting the spectroscopic assignment exceptions mentioned previously) is described by the cartoon of Figure 1.2[17], which depicts the overall description gleaned from phase-sensitive VSFG and molecular dynamics simulations. The outermost layer of neat water comprises predominately two moieties. The single-donor, double-acceptor (DAA) moiety has one OH group pointing out of the interface and the water dipole oriented slightly into the bulk (on average), forming one hydrogen bond with the second layer. This is the moiety responsible for the dangling OH peak present in the VSFG spectrum. The other surface moiety is a double-donor, single-acceptor (DDA) moiety for which both hydrogen atoms tend to hydrogen bond with the second layer and has the potential to accept a hydrogen bond from this layer. Although not shown in the cartoon there has also been evidence of a significant population of acceptor-only (AA) moieties based on near-edge X-ray absorption fine spectroscopy results and subsequent *ab intio* simulations, which may corroborate the existence of the second type of free OH postulated by Gan, *et al.*[5, 13, 18].

Simulations also suggest that the neat water interface has a net asymmetric structure through the first two molecular layers (~7 Å), the second layer forming a constrained hydrogen bond network between the fluid bulk phase and the oriented molecules of the surface proper. This structure satisfies the need to maximize hydrogen bonds at the surface, coupled with the tendency to bury any partial charge towards the higher dielectric of the condensed phase[2].

No consideration of the water interface would be complete, however, without also considering auto-ionization in the interface region, and lately this topic has engendered vigorous debate[19-21]. Bubbles in water have long been known to travel towards the positive electrode in electrophoresis measurements[22], recently yielding a zeta potential of -65 mV at pH=7 [23]. Similarly, the pH of water is found to decline measurably when emulsified with oils, low-dielectric analogues to air, and isoelectric points determined for such systems are often below pH=5 ([19] and references therein). The recent first-principles molecular dynamics simulation of Mundy *et al.* has placed the

stabilization energy of hydroxide ions at the interface at ~k_BT[24]. Surface tension measurements of surfactant-stabilized thin films also suggests preferential hydroxide adsorption, and simultaneous consideration of surface active hydroxide and inductive forces allow for quantitative reproduction of the surface tensions of surfactant/salt systems up to 4 M, as well as describe the zeta potential of bubbles to good effect[25]. The negative zeta potential, the drop in pH on generation of hydrophobic interfaces, and pH dependence of the isoelectric points of such systems is widely attributed to the preferential adsorption of hydroxide to the boundaries of water and low-dielectric media. Recently Enami, *et. al.* have directly probed the presence of hydronium at the air/water interface of electrospray droplets using gaseous trimethylamine, effectively as a titrant, avoiding the subject of potential measurements altogether[26]. Their results indicate that no significant presence of hydronium appears at the interface above a bulk pH of 5.

In spite of this longstanding interpretation, recent simulations have suggested the possibility of specific adsorption of hydronium to, and/or the repulsion of hydroxide from, the interface ([27] and references therein). Some spectroscopic evidence corroborates these studies. The second-harmonic generation (SHG) work of Petersen and Saykally concludes that the Langmuir-modeled adsorption of iodide in acidic media is enhanced over alkali-halide salt solutions[28], inferring that the increase is due to an increased preference of hydronium over that of sodium and potassium in the interface. A mechanism invoked to explain this describes hydronium being expelled to the surface as a defect in the bulk hydrogen bond network[29]. Subsequent SHG measurements of alkali hydroxides conclude that hydroxide is, at most, not strongly attracted to the interface[21]. VSFG spectra of halide acids are characterized by a decrease in the free-OH stretch, the appearance of a weak, broad response on the red end of the spectrum, and by an increase of the ice-like feature intensity[30, 31]. These features are attributed to the appearance of hydronium in the interface. In contrast, the vibrational surface spectrum of hydroxide solutions appear predominately unchanged from that of neat water.

The nature of the acid/base quality of the air/water interface seems to be a reopened book, and currently is following the same historical path as that concerning the presence of ions in the interface: longstanding evidence for a traditional view based largely on macroscopic observations being challenged by the advent of experimental and simulation methodologies that probe the system

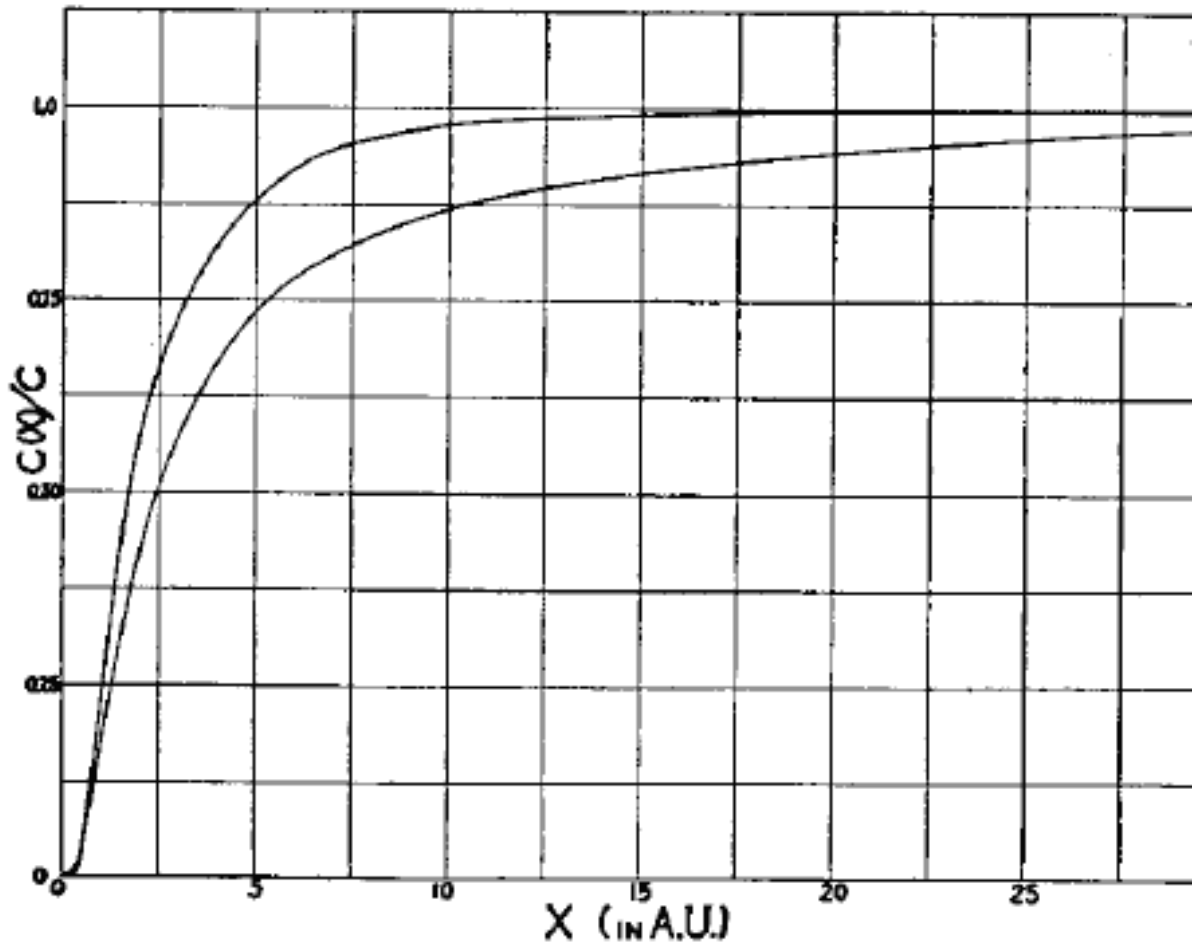

Figure 1.3- Plot of the normalized concentration of a 1:1 electrolyte at 0.1 M (upper) and 10^{-3}M as a function of depth from the surface of a dielectric continuum. The depletion of ions near the interface agrees with the trend of decreasing surface tension with increasing electrolyte concentration. *Reprinted with permission from* Onsager, L. and N.N.T. Samaras, *J. Chem. Phys.*, **2**, 528 (1934). *Copyright 1934 American Institute of Physics.*

on a molecular scale. The discussion now shifts to explicitly consider air/aqueous electrolyte interfaces.

1.2. Aqueous Electrolyte Interfaces

The "textbook" description of the aqueous electrolyte interface, based on continuum electrostatic models developed by Wagner, Onsager, and Samaras[32, 33], describes the interface as an ion-depleted (or even ion-free) region of water (see Figure 1.3). The theory is simplistic, considering the ions to act as point charges embedded in a dielectric continuum. The charges are repelled from the interface with lower dielectrics through the induction of a like-signed image charge. The screening of the image charge by the ionic atmosphere of the solute allows for a close but finite approach to the surface. This theory was advanced to

explain the observed increase in surface tension upon the increase of electrolyte concentration[32, 34]. By the Gibbs surface adsorption equation this observation demands a relative depletion of solute in the interface relative to that of the bulk, the depletion being described by the Gibbs surface excess[35].

$$\left(\frac{\partial\gamma}{\partial[J]}\right)_{T,[i\neq J]} = -\frac{RT\,\Gamma_J}{[J]} \tag{1.1}$$

While the initial theory significantly underestimates surface tensions at molar concentrations, the most notable failing of the model is that it does not capture the specific-ion effects observed in such measurements (Figure 1.4). In treating cation and anion equivalently, the theory already failed to account for the contemporary observation that surface potential grew more negative with increasing alkali-halide concentrations, implying that the anion approached the surface more closely than did the cation, perhaps even penetrating into the 'region of ion-depletion'[36]. Similarly, the model does not explain the tendency of inorganic acids to *decrease* surface tension. Nonetheless, subsequent refinements have extended the success of this theory in describing the molar-concentration electrolyte surface tensions, notably doing so by explicitly incorporating the effect of an ion-depleted region in the consideration of the screening length near the interface[37-40].

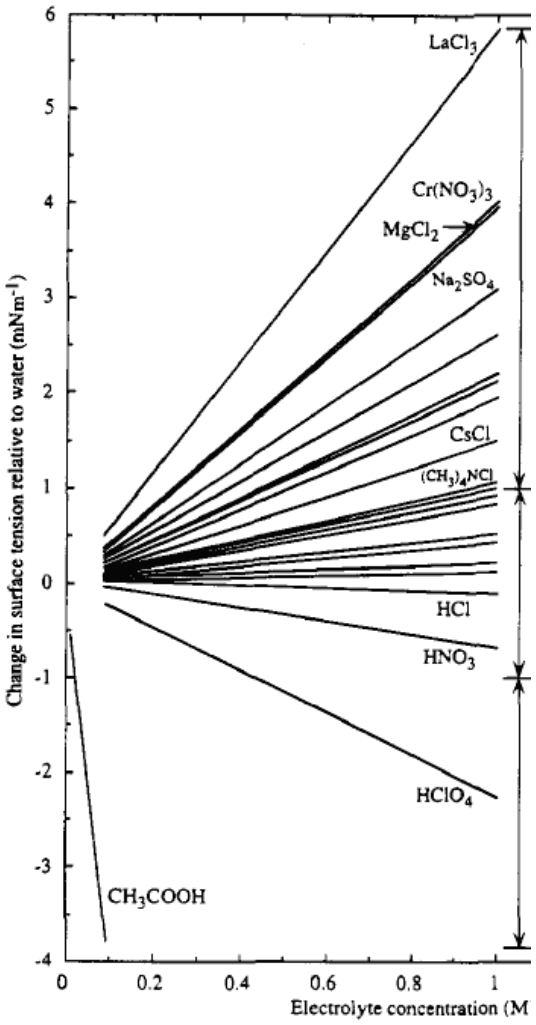

Figure 1.4- The change in surface tension of a selection of electrolyte and inorganic acid solutions as a function of concentration. Electrolytes tend to increase surface tension linearly with concentration above ~100 mM, while acids tend to engender a decrease. *Reprinted with permission from* Weissenborn, P.K. and R.J. Pugh, *Langmuir*, **11**, 1422 (1995). *Copyright 1995 American Chemical Society.*

However, even in the dilute electrolyte regime there has been

evidence that this theory is fundamentally inadequate. As early as 1935, Jones and Ray reported a *decrease* in surface tension with respect to concentration for several electrolytes, suggesting that these ions must then be concentration-enhanced in the interface[41]. In spite of this evidence, and its subsequent replication by Dole and Swartott in 1940 [42], widespread exploration into the possibility of electrolyte concentration enhancement in the interface didn't begin in earnest until the findings of Hu, *et. al.* suggested that interfacial halide reactions were responsible for the observed uptake rates of molecular halogens in aerosols[43, 44].

Observations of gas-aerosol chemistry, and related simulations, continue to suggest the presence and importance of significant concentrations of halogens in aerosol interfaces[45-48]. Some water/halide cluster spectroscopy also indicate that large halides reside at the surface of such clusters, the largest of which could be considered small aerosols[49-52]. Photoelectron spectroscopy measurements of deliquescing KI and KBr found that iodide and bromide partition closer to the interface than their counter-ion[53], while the hard electrolyte KF in an aqueous microjet appears to maintain equal proportions of K^+ and F^- as a function of interfacial depth[54]. In this manner the traditional description of monotonic electrolyte partitioning in the interface has begun to be supplanted by a one of complex partitioning within the interface.

Resonant surface SHG measurements of the iodide charge-transition-to-solvent (CTTS) bands in sodium iodide solutions confirm, within the framework of a Langmuir adsorption model, the interfacial enhancement of iodide concentrations in the Jones-Ray (mM) bulk concentration regime, determining a strong affinity of iodide for the surface (-25 $kJ \cdot mol^{-1}$)[55]. Similar studies also continue to support exergonic anion surface adsorption for other anions[21, 55-59]. Some small anions seem not to exhibit this behavior, even iodide mitigating its affinity at molar bulk concentrations[60, 61]. This concentration-dependent change of affinity for iodide is in qualitative agreement with the simulation of Ishiyama and Morita[62]. VSFG experiments have also directly probed the interface hydrogen bond structure of electrolytic solutions. The VSFG spectra of sub-molar sodium halide solution interfaces reveal an intensity increase in the liquid-like region of the spectra for bromide and iodide, a negligible effect for chloride, and a decrease for fluoride[10]. Based on the frequency shifts of both the ice-like and liquid-like regions with respect to halide size, this study concluded that these ions were present in the interfacial region, interacting with the

hydrogen bond network in a manner consistent with the respective structure-making/breaking character of these ions.

In efforts to explain this behavior, molecular dynamics simulations of sodium halide interfacial affinity in a water-slab initially observed that (only) when ions were imbued with polarizable potentials would they be adsorbed to the surface[63], and that surface affinity correlated with the polarizability (size) of the anion in the series $F^- < Cl^- < Br^- < I^-$, while the relatively unpolarizable cations partitioned closer to the bulk[64, 65]. This ordering also agrees with the change in surface potential along the halide series[36], and is in agreement with the usual Hofmeister ordering of halides[66]. The simulations also offer an explanation for the apparent contradiction of interfacial concentration enhancement with positive surface tension increments in the molar regime: the microscopic partitioning allows for a net interfacial depletion of ions while maintaining a localized concentration enhancement near the surface proper. In interesting contrast, where the enhanced interface concentration of ions could explain the decrease in surface tensions observed by Jones, Ray and Dole[42, 67], the model of Karraker and Radke successfully explains these minima (partly on the basis of including polarizability in its treatment of the modified Poison-Boltzmann distribution) without invoking a net surface concentration enhancement of anions at all[25].

In further efforts to consider the mechanism for these phenomena, Noah-Vanhoucke and Geissler's simulations found that the fluctuations of the interface geometry can result in an interfacial region where electrostatic costs can be unpaid while cavity-expulsion benefits are still realized[68], achieving huge concentration enhancements of non-polarizable ions when suitable size and charge parameters were selected for the ion. Horinek, *et al.* have also demonstrated that well chosen empirical parameters, rather than polarizable force fields, are sufficient to demonstrate anionic surface concentration enhancements, highlighting the delicate balance of hydration and electrostatic forces at play in the interface[69].

Thus, aqueous electrolyte interface studies suggest that ions are present to differing degrees in the interfacial region depending on identity, sometimes even in higher concentrations than in the bulk. Interfacial affinity seems tied to either polarizability or ionic size, or both, and may play a key role in overcoming the simple electrostatic arguments for repulsion engendered by a charge approaching a lower-dielectric boundary. Finally, ion-specific microscopic partitioning *within*

the interfacial region is a necessary requirement to rationalize thermodynamic and macroscopic observables, the most prevalent theme being the selective adsorption of anions over cations in electrolyte solutions, and the double-layer structure that this engenders.

1.3. UV SHG Studies of Concentrated Aqueous Electrolyte Interfaces

It is clear that progress on understanding the interfacial air/aqueous system has been astounding over the past 10 years. Even over the short period of this study, tremendous leaps have been made in the nonlinear optical theory of SHG/VSFG surface spectroscopy, the modeling power and theoretical tools available to tackle such problems, and even the sheer amount of research being published in this growing field. In the following chapters I discuss the surface SHG studies my colleagues and I have performed, beginning with a brief introduction of the fundamentals of SHG, how it has been applied to aqueous interface studies, and some of the experimental developments made on the apparatus itself. This chapter also considers the nature and application of the Langmuir model in more detail, identifying how to use the model itself as a diagnostic of the mechanism of the adsorption of these ions into the interface. In particular I highlight the important distinction between *surface* (*viz*. outermost liquid layer) and *interface*, and do not use these terms interchangeably. Chapter 3 follows in the footsteps of Petersen[70], applying the Langmuir/SHG methodology to the sodium nitrate and nitrite systems and the mechanistic diagnostic developed in Chapter 2. In Chapter 4, I present an examination of some of the photochemistry observed while performing SHG studies of the thiocyanate ion, as well as the results of the temperature dependence of the Langmuir/SHG response of potassium thiocyanate. Chapter 5 discusses a somewhat abortive attempt at interfacial electronic spectroscopy with SHG, discussing the observed SHG spectrum of the CTTS transition of sodium iodide at the air/solution interface as well as some of the oxidation chemistry that was evident in these solutions. Chapter 6 concludes with a brief summary of the results presented herein, and presents some directions to expand studies into the future.

1.4. References

1) Atkins, P.W., "*Physical Chemistry*," 1031 (1994)

2) Fan, Y., X. Chen*, et al.*, *J. Phys. Chem. B*, "*On the Structure of Water at the Aqueous/Air Interface*," **113**, 11672 (2009)

3) Paluch, M., *Adv. Colloid Interface Sci.*, "*Electrical properties of free surface of water and aqueous solutions*," **84**, 27 (2000)

4) Wilson, K.R., B.S. Rude*, et al.*, *J. Phys. Chem. B*, "*X-ray Spectroscopy of Liquid Water Microjets*," **105**, 3346 (2001)

5) Wilson, K.R., M. Cavalleri*, et al.*, *J. Phys.: Condens. Matter*, "*Characterization of Hydrogen Bond Acceptor Molecules at the Water Surface using Near-edge X-ray Absorption Fine-structure Spectroscopy and Density Functional Theory*," **14**, L221 (2002)

6) Cappa, C.D., J.D. Smith*, et al.*, *J. Phys.: Condens. Matter*, "*Revisiting the Total Ion Yield X-ray Absorption Spectra of Liquid Water Microjets*," **20**, 205105 (2008)

7) Shen, Y.R. and V. Ostroverkhov, *Chem. Rev.*, "*Sum-Frequency Vibrational Spectroscopy on Water Interfaces: Polar Orientation of Water Molecules at Interfaces*," **106**, 1140 (2006)

8) Du, Q., R. Superfine*, et al.*, *Phys. Rev. Lett.*, "*Vibrational spectroscopy of water at the vapor/water interface*," **70**, 2313 LP (1993)

9) Du, Q., E. Freysz*, et al.*, *Science*, "*Surface Vibrational Spectroscopic Studies of Hydrogen Bonding and Hydrophobicity*," **264**, 826 (1994)

10) Raymond, E.A. and G.L. Richmond, *J. Phys. Chem. B*, "*Probing the Molecular Structure and Bonding of the Surface of Aqueous Salt Solutions*," **108**, 5051 (2004)

11) Du, Q., E. Freysz*, et al.*, *Phys. Rev. Lett.*, "*Vibrational spectra of water molecules at quartz/water interfaces*," **72**, 238 LP (1994)

12) Scatena, L.F., M.G. Brown*, et al.*, *Science*, "*Water at hydrophobic surfaces: Weak hydrogen bonding and strong orientation effects*," **292**, 908 (2001)

13) Gan, W., D. Wu*, et al.*, *J. Chem. Phys.*, "*Polarization and experimental configuration analyses of sum frequency generation vibrational spectra, structure, and orientational motion of the air/water interface*," **124**, 114705 (2006)

14) Sovago, M., R.K. Campen*, et al.*, *Phys. Rev. Lett.*, "*Vibrational Response of Hydrogen-Bonded Interfacial Water is Dominated by Intramolecular Coupling*," **100**, 173901 (2008)

15) Tian, C.S. and Y.R. Shen, *Phys. Rev. Lett.*, "*Comment on "Vibrational Response of Hydrogen-Bonded Interfacial Water is Dominated by Intramolecular Coupling"*," **101**, 139401 (2008)

16) Sovago, M., R.K. Campen*, et al.*, *Phys. Rev. Lett.*, "*Sovago et al. Reply:*," **101**, 139402 (2008)
17) Ji, N., V. Ostroverkhov*, et al.*, *Phys. Rev. Lett.*, "*Characterization of Vibrational Resonances of Water-Vapor Interfaces by Phase-Sensitive Sum-Frequency Spectroscopy*," **100**, 096102 (2008)
18) Wick, C.D., I.-F.W. Kuo*, et al.*, *J. Chem. Theory Comput.*, "*The Effect of Polarizability for Understanding the Molecular Structure of Aqueous Interfaces*," **3**, 2002 (2007)
19) Beattie, J.K., A.M. Djerdjev*, et al.*, *Faraday Discuss.*, "*The surface of neat water is basic*," **141**, 31 (2009)
20) Buch, V., A. Milet*, et al.*, *Proc. Natl. Acad. Sci. USA*, "*Water surface is acidic*," **104**, 7342 (2007)
21) Petersen, P.B. and R.J. Saykally, *Chem. Phys. Lett.*, "*Is the liquid water surface basic or acidic? Macroscopic vs. molecular-scale investigations*," **458**, 255 (2008)
22) Quincke, G., *Ann. Phys. Chem.*, **113**, 513 (1861)
23) Graciaa, A., G. Morel*, et al.*, *J. Colloid Interface Sci.*, "*The ζ-Potential of Gas Bubbles*," **172**, 131 (1995)
24) Mundy, C.J., I.-F.W. Kuo*, et al.*, *Chem. Phys. Lett.*, "*Hydroxide anion at the air-water interface*," **481**, 2 (2009)
25) Karraker, K.A. and C.J. Radke, *Adv. Colloid Interface Sci.*, "*Disjoining pressures, zeta potentials and surface tensions of aqueous non-ionic surfactant/electrolyte solutions: theory and comparison to experiment*," **96**, 231 (2002)
26) Enami, S., M.R. Hoffmann*, et al.*, *J. Phys. Chem. Lett.*, "*Proton Availability at the Air/Water Interface*," **1**, 1599 (2010)
27) Vacha, R., D. Horinek*, et al.*, *Phys. Chem. Chem. Phys.*, "*Hydronium and hydroxide at the interface between water and hydrophobic media*," **10**, 4975 (2008)
28) Petersen, P.B. and R.J. Saykally, *J. Phys. Chem. B*, "*Evidence for an Enhanced Hydronium Concentration at the Liquid Water Surface*," **109**, 7976 (2005)
29) Petersen, M.K., S.S. Iyengar*, et al.*, *J. Phys. Chem. B*, "*The Hydrated Proton at the Water Liquid/Vapor Interface*," **108**, 14804 (2004)
30) Mucha, M., T. Frigato*, et al.*, *J. Phys. Chem. B*, "*Unified Molecular Picture of the Surfaces of Aqueous Acid, Base, and Salt Solutions*," **109**, 7617 (2005)
31) Tarbuck, T.L., S.T. Ota*, et al.*, *J. Am. Chem. Soc.*, "*Spectroscopic Studies of Solvated Hydrogen and Hydroxide Ions at Aqueous Surfaces*," **128**, 14519 (2006)

32) Wagner, C., *Phys. Z.*, "*The surface tension of diluted electrolyte solutions*," **25**, 474 (1924)
33) Onsager, L. and N.N.T. Samaras, *J. Chem. Phys.*, "*The Surface Tension of Debye-Hückel Electrolytes*," **2**, 528 (1934)
34) Heydweiller, A., *Ann. Phys. (Leipzig)*, "*Concerning the physical characteristics of solutions in correlation. II. Surface tension and electronic conductivity of watery salt solutions*," **33**, 145 (1910)
35) Gibbs, J.W., *Scientific Papers of J. Willard Gibbs*. 1st ed. Vol. 1. 1906, London: Longmans, Green, and Co.
36) Frumkin, A., *Z. Phys. Chem. (Muenchen, Ger.)*, "*Phase interface powers and adsorption on the segregative surface air - Solution of an organic electrolyte*," **109**, 34 (1924)
37) Nichols III, A.L. and L.R. Pratt, *J. Chem. Phys.*, "*Salt effects on the surface tensions of dilute electrolyte solutions: The influence of nonzero relative solubility of the salt between the coexisting phases*," **80**, 6225 (1984)
38) Levin, Y., *J. Chem. Phys.*, "*Interfacial tension of electrolyte solutions*," **113**, 9722 (2000)
39) Ohshima, H. and H. Matsubara, *Surface tension of electrolyte solutions*, in *Colloid & Polymer Science*. 2004, Springer Berlin / Heidelberg.
40) Dean, D.S. and R.R. Horgan, *Phys. Rev. E*, "*Field theoretic calculation of the surface tension for a model electrolyte system*," **69**, 061603 (2004)
41) Jones, G. and W.A. Ray, *J. Am. Chem. Soc.*, "*The Surface Tension of Solutions*," **57**, 957 (1935)
42) Dole, M. and J.A. Swartout, *J. Am. Chem. Soc.*, "*A Twin-Ring Surface Tensiometer. I. The Apparent Surface Tension of Potassium Chloride Solutions*," **62**, 3039 (1940)
43) Hu, J.H., Q. Shi*, et al.*, *J. Phys. Chem.*, "*Reactive Uptake of $Cl_{2(g)}$ and $Br_{2(g)}$ by Aqueous Surfaces as a Function of Br^- and I^- Ion Concentration: The Effect of Chemical Reaction at the Interface*," **99**, 8768 (1995)
44) Garrett, B.C., *Science*, "*Ions at the Air/Water Interface*," **303**, 1146 (2004)
45) Foster, K.L., R.A. Plastridge*, et al.*, *Science*, "*The Role of Br_2 and BrCl in Surface Ozone Destruction at Polar Sunrise*," **291**, 471 (2001)
46) Clifford, D. and D.J. Donaldson, *J. Phys. Chem. A*, "*Direct Experimental Evidence for a Heterogeneous Reaction of Ozone with Bromide at the Air-Aqueous Interface*," **111**, 9809 (2007)

47) Hunt, S.W., M. Roeselová*, et al.*, *J. Phys. Chem. A*, "*Formation of Molecular Bromine from the Reaction of Ozone with Deliquesced NaBr Aerosol: Evidence for Interface Chemistry*," **108**, 11559 (2004)
48) Knipping, E.M., M.J. Lakin*, et al.*, *Science*, "*Experiments and Simulations of Ion-Enhanced Interfacial Chemistry on Aqueous NaCl Aerosols*," **288**, 301 (2000)
49) Choi, J.-H., K.T. Kuwata*, et al.*, *J. Phys. Chem. A*, "*Vibrational Spectroscopy of the $Cl^-(H_2O)_n$ Anionic Clusters, n = 1-5*," **102**, 503 (1998)
50) Markovich, G., S. Pollack*, et al.*, *J. Chem. Phys.*, "*Photoelectron spectroscopy of Cl^-, Br^-, and I^- solvated in water clusters*," **101**, 9344 (1994)
51) Koch, D.M. and G.H. Peslherbe, *Chem. Phys. Lett.*, "*On the transition from surface to interior solvation in iodide-water clusters*," **359**, 381 (2002)
52) Finlayson-Pitts, B.J., *Phys. Chem. Chem. Phys.*, "*Reactions at surfaces in the atmosphere: integration of experiments and theory as necessary (but not necessarily sufficient) for predicting the physical chemistry of aerosols*," **11**, 7760 (2009)
53) Ghosal, S., J.C. Hemminger*, et al.*, *Science*, "*Electron Spectroscopy of Aqueous Solution Interfaces Reveals Surface Enhancement of Halides*," **307**, 563 (2005)
54) Brown, M.A., R. D'Auria*, et al.*, *Phys. Chem. Chem. Phys.*, "*Ion spatial distributions at the liquid-vapor interface of aqueous potassium fluoride solutions*," **10**, 4778 (2008)
55) Petersen, P.B., J.C. Johnson*, et al.*, *Chem. Phys. Lett.*, "*Direct experimental validation of the Jones-Ray effect*," **397**, 46 (2004)
56) Petersen, P.B. and R.J. Saykally, *Chem. Phys. Lett.*, "*Confirmation of enhanced anion concentration at the liquid water surface*," **397**, 51 (2004)
57) Petersen, P.B. and R.J. Saykally, *J. Am. Chem. Soc.*, "*Adsorption of Ions to the Surface of Dilute Electrolyte Solutions: The Jones-Ray Effect Revisited*," **127**, 15446 (2005)
58) Onorato, R.M., D.E. Otten*, et al.*, *J. Phys. Chem. C.*, "*Measurement of Bromide Ion Affinities for the Air/Water and Dodecanol/Water Interfaces at Molar Concentrations by UV Second Harmonic Generation Spectroscopy*," **114**, 13746 (2010)
59) Petersen, P.B., R.J. Saykally*, et al.*, *J. Phys. Chem. B*, "*Enhanced Concentration of Polarizable Anions at the Liquid Water Surface: SHG Spectroscopy and MD Simulations of Sodium Thiocyanide*," **109**, 10915 (2005)

60) Petersen, P.B. and R.J. Saykally, *J. Phys. Chem. B*, "*Probing the Interfacial Structure of Aqueous Electrolytes with Femtosecond Second Harmonic Generation Spectroscopy*," **110**, 14060 (2006)
61) Otten, D.E., P.B. Petersen*, et al.*, *Chem. Phys. Lett.*, "*Observation of nitrate ions at the air/water interface by UV-second harmonic generation*," **449**, 261 (2007)
62) Ishiyama, T. and A. Morita, *J. Phys. Chem. C.*, "*Molecular Dynamics Study of Gasâˆ’Liquid Aqueous Sodium Halide Interfaces. I. Flexible and Polarizable Molecular Modeling and Interfacial Properties*," **111**, 721 (2006)
63) Jungwirth, P. and D.J. Tobias, *J. Phys. Chem. B*, "*Ions at the Air/Water Interface*," **106**, 6361 (2002)
64) Jungwirth, P. and D.J. Tobias, *J. Phys. Chem. B*, "*Molecular Structure of Salt Solutions: A New View of the Interface with Implications for Heterogeneous Atmospheric Chemistry*," **105**, 10468 (2001)
65) Dang, L.X., *J. Phys. Chem. B*, "*Computational Study of Ion Binding to the Liquid Interface of Water*," **106**, 10388 (2002)
66) Collins, K.D. and M.W. Washabaugh, *Q. Rev. Biophys.*, "*The Hofmeister effect and the behaviour of water at interfaces*," **18**, 323 (1985)
67) Jones, G. and W.A. Ray, *J. Am. Chem. Soc.*, "*The Surface Tension of Solutions of Electrolytes as a Function of the Concentration. I. A Differential Method for Measuring Relative Surface Tension*," **59**, 187 (1937)
68) Noah-Vanhoucke, J. and P.L. Geissler, *Proc. Natl. Acad. Sci. USA*, "*On the fluctuations that drive small ions toward, and away from, interfaces between polar liquids and their vapors*," **106**, 15125 (2009)
69) Horinek, D., A. Herz*, et al.*, *Chem. Phys. Lett.*, "*Specific ion adsorption at the air/water interface: The role of hydrophobic solvation*," **479**, 173 (2009)
70) Petersen, P.B. and R.J. Saykally, *Annu. Rev. Phys. Chem.*, "*On the nature of ions at the liquid water surface*," **57**, 333 (2006)

Chapter 2 - The Study of Aqueous Electrolyte Surfaces by SHG

This chapter endeavors to put the relevant components second harmonic generation on a concise theoretical footing, followed by a more thorough discussion of the Langmuir models applied in our studies, and specifically, their interpretation. It concludes with a technical description of our implementation of SHG used to probe the air/solution interface, including some of the experimental obstacles and the methods developed to overcome them.

2.1. SHG as a Surface Probe

Second harmonic generation (SHG) is a second-order nonlinear process that transfers the energy of two photons into a single photon of twice the energy, the result of the nonlinear polarization of a medium induced by an electric driving field. Under a sufficiently strong driving field, the dipole polarization of a medium can be expressed as a perturbation of the usual linear response of a medium[1]

$$\begin{aligned}\vec{P} &= \vec{\chi}^{(1)} \cdot \vec{E} + \vec{\chi}^{(2)} : \vec{E}\vec{E} + \vec{\vec{\chi}}^{(3)}\vec{E}\vec{E}\vec{E} + \ldots \\ &\equiv \vec{P}^{(1)} + \vec{P}^{(2)} + \vec{P}^{(3)} + \ldots \end{aligned} \quad , \qquad (2.1)$$

where the induced polarization of a given order of perturbation is described by the macroscopic susceptibility tensor (χ), a material constant of the system. The n^{th} order nonlinear polarization of the medium can take on frequencies that are the sums of *n* (positive and negative) frequency components of the driving field. In the case of a single, monochromatic driving field, the total second-order polarization the medium is described by

$$\vec{P}^{(2)} = \vec{\vec{\chi}}\left(\Omega = \omega - \omega\right) : \vec{E}\left(\omega\right)\vec{E}\left(-\omega\right) + \vec{\vec{\chi}}\left(\Omega = \omega + \omega\right) : \vec{E}\left(\omega\right)\vec{E}\left(\omega\right) , \qquad (2.2)$$

where the notation $\chi\left(\Omega = \omega \pm \omega\right)$ indicates that the susceptibility tensor is specifically defined for the polarization of the system oscillating at frequency Ω due to the combination of frequencies $\omega \pm \omega$. Thus, the allowed second-order polarization frequencies for a monochromatic driving field of frequency ω are $\Omega = 0$ (optical rectification) and $\Omega = 2\omega$ (second harmonic).

The utility of SHG as a surface probe lies in its forbidden nature within centro-symmetric media, under the dipole approximation[2]. The susceptibility tensor is a direct reflection of the properties of the material and obeys the same symmetry that the material itself possesses. In the case of a centro-symmetric

material, this indicates that the tensor must be invariant over any rotation and inversion. Applying inversion symmetry to the system (in the dipole approximation) then reveals that a second-order polarization, like any other even-ordered dipolar process, is forbidden in a centro-symmetric medium.

$$\begin{aligned} P_i^{(2)} &= \chi_{ijk}^{(2)} E_j E_k \\ P_{-i}^{(2)} &= \chi_{-i-j-k}^{(2)} E_{-j} E_{-k} \\ \chi_{ijk}^{(2)} &= \chi_{-i-j-k}^{(2)} \qquad \text{by symmetry} \\ -P_i^{(2)} &= \chi_{ijk}^{(2)} \left(-E_j\right)\left(-E_k\right) = \chi_{ijk}^{(2)} E_j E_k \\ -P_i^{(2)} &= P_i^{(2)} = 0 \\ \therefore \chi_{ijk}^{(2)} &= 0 \end{aligned} \tag{2.3}$$

At the air/water interface, this symmetry is necessarily broken, and the second-order response is then entirely due to the properties of the boundary region where the symmetry remains broken. This is selective to a very natural definition of the air/water interface: the region for which the symmetry of the system is no longer centro-symmetric. For a rotationally isotropic surface, such as the air/water interface, the susceptibility components of the interface are reduced by symmetry to seven components of which only three are independent[3]:

$$\begin{gathered} \chi_{xxz}^{(2)} = \chi_{xzx}^{(2)} = \chi_{yzy}^{(2)} = \chi_{yyz}^{(2)} \\ \chi_{zxx}^{(2)} = \chi_{xyy}^{(2)} \\ \chi_{zzz}^{(2)} \end{gathered} \tag{2.4}$$

Here the normal of the interface is taken to be in the $\hat{z}$ direction.

The macroscopic susceptibility of the system is the sum of the responses of its component oscillators (*i.e.* molecular induced dipole oscillations), and can be decomposed into the sum of the individual responses as,

$$\vec{\vec{\chi}}^{(2)} = \sum_J N_J \left\langle \vec{\vec{\beta}}_J \right\rangle_{Orientation} \equiv \sum_J N_J \beta_{J,eff} \tag{2.5}$$

,

where $\vec{\vec{\beta}}_J$ is the molecular second-order susceptibility (hyper-polarizability) of species J. The second-order hyperpolarizability tensor is defined in the reference frame of the molecules themselves, the average over orientation reflecting the transformation from the molecular frame to the lab frame. The molecular susceptibility tensor is subject to the same symmetry requirements (*i.e.* selection-rules) as the macroscopic susceptibility tensor. The hyper-polarizability tensor can be derived from third-order time-dependent perturbation theory as a sum-over states expression, and for SHG, this is[4]:

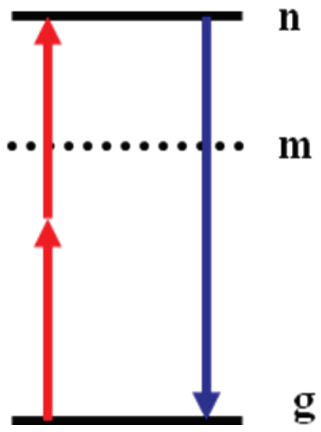

Figure 2.1- Schematic representation of two photon resonance between the ground (g) and excited (n) states for second harmonic described in equation **2.6**. Two photons of frequency ω (red) are converted to a single photon of energy 2ω (blue).

$$\beta_{ijk}\left(2\omega=\omega+\omega\right)\propto\sum_{mn}\frac{\mu_{gn}^{i}\left(\mu_{nm}^{j}\mu_{mg}^{k}+\mu_{nm}^{k}\mu_{mg}^{j}\right)}{\left(2\omega-\omega_{ng}+i\gamma_{ng}\right)\left(\omega-\omega_{mg}+i\gamma_{mg}\right)}+\frac{\mu_{mg}^{i}\left(\mu_{gn}^{j}\mu_{nm}^{k}+\mu_{gn}^{k}\mu_{nm}^{j}\right)}{\left(2\omega+\omega_{mg}+i\gamma_{mg}\right)\left(\omega+\omega_{ng}+i\gamma_{ng}\right)}-\frac{\mu_{nm}^{i}\left(\mu_{mg}^{j}\mu_{gn}^{k}+\mu_{mg}^{k}\mu_{gn}^{j}\right)}{\left(\omega+\omega_{ng}+i\gamma_{ng}\right)\left(\omega+\omega_{mg}+i\gamma_{mg}\right)} \quad (2.6)$$

Here μ_{gn} is the dipole transition moment between states n and g. γ is a damping parameter, usually interpreted as the dipole dephasing time[5]. It is clear that the first and second term can be under either one- or two- photon resonance (as the complex driving field includes both positive and negative frequency contributions), while the third term can only contribute to one-photon resonance (Figure 2.1). This forms the basis of species selectivity in surface second harmonic via the observation of resonance enhancement.

Second-order spectroscopy of the liquid water surface models the dipolar response of the interface as an oscillating polarization sheet of thickness much smaller than a wavelength[6], and the radiated second harmonic of this sheet in the reflected direction is given by[7],

$$I_{2\omega} = \frac{8\pi^3 (2\omega)^2 \sin^2(\theta)}{c^3 \left(\varepsilon_{2\omega}^{\alpha}\right)^{\frac{1}{2}} \varepsilon_{\omega}^{\alpha}} \left| \gamma(2\omega) : \vec{\vec{\chi}}_{eff}^{(2)} : \gamma(\omega)\gamma(\omega) \right|^2 I_{\omega}^2, \tag{2.7}$$

where I_{Ω} is the intensity of the incident field ($\Omega = \omega$) or reflected second harmonic ($\Omega = 2\omega$), θ is the angle of the reflected second harmonic with respect to the surface normal and $\varepsilon_{\Omega}^{\alpha}$ is the dielectric constant for frequency Ω of the medium (α) of incidence (*e.g.* air). The susceptibility $\vec{\vec{\chi}}_{eff}^{(2)}$ is an effective susceptibility which we assume to be entirely due to the surface sheet, and $\gamma(\Omega) = \vec{L}(\Omega) \cdot \hat{e}(\Omega)$ is the tensor product of the Fresnel factor and the polarization vector for frequency Ω. The Fresnel factor effectively accounts for the fact that the oscillators in the polarization sheet experience an electric field strength that is altered in the dielectric medium of the sheet itself, due to the electric fields transmission across the sheet/air dielectric boundary. For second harmonic studies after which this study is modeled ([8, 9] and references therein), the Fresnel factors are neglected and the experimental configuration is unchanged throughout an experiment. In this case the above expression can simply be reduced to

$$I_{2\omega} \propto \left| \chi_{eff}^{(2)} \right|^2 I_{\omega}^2. \tag{2.8}$$

For a two-component system of water and a resonant solute, substitution of Equation 2.5 with rearrangement gives

$$\frac{I_{2\omega}}{I_{\omega}^2} \propto \left| N_{water} \beta_{water}^{eff} + N_{solute} \beta_{solute}^{eff} \right|^2, \tag{2.9}$$

which is the spectroscopic basis for the determination of the surface concentration of solute with respect to changing bulk composition used in published SHG studies of electrolyte interface affinities[8-19]. For the wavelengths used herein, water is considered to be entirely non-resonant, while the solute may be in resonance. As such, the solute hyperpolarizability is complex-valued relative to the real response of water, and taking the modulus of (the complex-valued) Equation 2.9 gives the functional form of the second harmonic response of the air/electrolyte solution interface[9]:

$$\begin{aligned} \frac{I_{2\omega}}{I_{\omega}^2} &\propto \left(N_{water} \beta_{water}^{eff} + N_{solute} \operatorname{Re}\left[\beta_{solute}^{eff} \right] \right)^2 + \left(N_{solute} \operatorname{Im}\left[\beta_{solute}^{eff} \right] \right)^2 \\ &= \left(\mathrm{A} N_{water} + \mathrm{B} N_{solute} \right)^2 + \left(\mathrm{C} N_{solute} \right)^2 \end{aligned} \tag{2.10}$$

Here the effective molecular the susceptibilities are assumed to be constants of the system.

2.2. Langmuir Modeling of Aqueous Interfacial Adsorption

2.2.1. ***The 1:1 Exchange Model***

In previous similar studies, the adsorption of ions to the interface has been described by an adapted Langmuir model (hereafter exchange model) whereby the anion competes with water molecules for surface sites[8, 9, 12-19]. It models the effective equilibrium of bulk solvated anions and surface bound water (X^-, $S\mathrm{W}$) with surface bound anions ($S\mathrm{X}^-$) and bulk water (W):

$$S\mathrm{W} + \mathrm{X}^- \rightleftarrows \mathrm{W} + S\mathrm{X}^- \tag{2.11}$$

$$\mathrm{K}_{\mathrm{ads}} = \frac{\left[S\mathrm{X}^-\right]\left[\mathrm{W}\right]}{\left[S\mathrm{W}\right]\left[\mathrm{X}^-\right]} = \frac{\left[S\mathrm{X}^-\right]\left[\mathrm{W}\right]}{\left(\left[S_{\max}\right]-\left[S\mathrm{X}^-\right]\right)\left[\mathrm{X}^-\right]}, \tag{2.12}$$

where S is one of $S_{\max}$ surface sites (all occupied by water molecules in the neat water interface). The usual Langmuir adsorption assumptions of non-interacting adsorbates and conservation of surface sites apply. It deserves to be mentioned that in previous applications of this model[8, 9, 12-19], the standard states for the bulk and surface species are considered to be identical: 55.5 M for bulk water and surface water, 1 M for bulk and surface solute. This defines S_{max} to be 55.5 M. Rearrangement of Equation 2.12 provides the number of surface anions in terms of the bulk concentrations of water and anion:

$$\left[S\mathrm{X}^-\right] = \left[S_{\max}\right]\frac{\left[\mathrm{X}^-\right]}{\left(\left[\mathrm{W}\right]\mathrm{K}_{\mathrm{ads}}^{-1} + \left[\mathrm{X}^-\right]\right)} \tag{2.13}$$

When substituted into Equation 2.10, we resolve a functional form of the expected intensity of second harmonic as a function of bulk concentration of water and anion,

$$\frac{I_{2\omega}}{I_{\omega}^2} = \left(\mathrm{A} + \mathrm{B}'\frac{\left[\mathrm{X}^-\right]}{\left(\left[\mathrm{W}\right]\mathrm{K}_{\mathrm{ads}}^{-1} + \left[\mathrm{X}^-\right]\right)}\right)^2 + \left(\mathrm{C}'\frac{\left[\mathrm{X}^-\right]}{\left(\left[\mathrm{W}\right]\mathrm{K}_{\mathrm{ads}}^{-1} + \left[\mathrm{X}^-\right]\right)}\right)^2. \tag{2.14}$$

The fit of the SHG intensity as a function of bulk solute concentration and four unknown parameters allows for the determination of $\mathrm{K}_{\mathrm{ads}}$. Although the

application of this model has been very successful in a variety of previous studies, the adapted model contains one explicit and one implicit assumption over the usual Langmuir assumptions: an explicit assumption of a 1:1 exchange of anion and water, and the implicit assumption that the cation is irrelevant in describing the processes.

2.2.2. ***The Effect of Water Exchange in the Exchange Model***

Considering first the nature of water exchange, this begs the question of how many water molecules *would* be displaced in the interface if an ion partitioned there. There are a couple of means to approach this problem. Using partial molar volumes as a rough guide[20], it is clear that in bulk solution even atomic anions effectively rival or exceed the volumetric dimensions of a water molecule (Table 2.1). For adsorption to a surface that is two-dimensional on the scale of an individual molecule, we expect that the replacement of water would scale roughly as the $\frac{2}{3}$ power of its volume. Other parameters, such as ionic radii, or effective hydrated radii might also help make some useful approximations, but fundamentally the exchange model always demands that we choose a number before we examine the system in this fashion.

Fortunately, the consequences of choosing a particular number of waters to displace are appreciable only if the concentration of water can change appreciably over a Langmuir isotherm. Choosing zero (requiring empty surface sites for neat water) is tantamount to holding the concentration of water fixed, albeit now the value of S_{max} is not predefined. In some early works[8, 10-12, 16], the concentration of water was assumed to be constant at its pure value in the application of the Langmuir isotherm. While appropriate for low concentration studies, such as those performed in the Jones-Ray concentration regime[8, 10, 12], the water concentration in concentrated electrolyte solutions can deviate strongly from its pure value. For example, measurements of sodium nitrate solution densities demonstrate a linear trend that effectively conserves the number of species in a given volume (water + anion + cation=55M),

Species	Partial Molar Volume (ml/mol)	Volume Relative to Water
H_2O	18	1.00
H^+	-5.4	-0.30
Na^+	-7.4	-0.41
K^+	3.4	0.19
F^-	3.3	0.18
Cl^-	23.7	1.32
Br^-	30.2	1.68
I^-	41.4	2.30
NO_3^-	34.8	1.93

Table 2.1- Partial molar volumes of selected anions and cations from Ref [20.]

leading to a 20% decrease in water concentration in the case of 5.5 M sodium nitrate[21]. The effect of excluding the decreased concentration of water as a function of increased solute concentration is to make the adsorption process appear more favorable than the model implies by a ratio of

$$\frac{\mathrm{K}^{(actual)}\left(\left[\mathrm{X}_B\right]\right)}{\mathrm{K}^{(observed)}} = \frac{\left[\mathrm{W}_B\left(\left[\mathrm{X}_B\right]\right)\right]}{\left[\mathrm{W}_B\right]^{o}} \tag{2.15}$$

at any given bulk concentration. This suggests that the fitting process would attribute the concentration of surface solute at high concentrations to a more favorable thermodynamic process by discounting the effect of the reduction of bulk water molecules competing for surface sites. The SHG/Langmuir fit is nonlinear in $\mathrm{K}_{\mathrm{ads}}$ and the bias is dependent on the concentration that the Langmuir expression is evaluated at (fit to) such that no general correction factor can be applied to results interpreted under the constant water concentration approximation. However, the bias is monotonic in bulk solute concentration and an upper limit can be determined by taking at the highest concentration measured. Assuming a 20% decrease in water concentration, this upper limit amounts to a relatively modest ~0.5 kJ·mol^{-1} negative shift in the observed value from the model value.

It is easy to demonstrate that the equilibrium constants for the other 1:*n* water replacements relate by

$${}^{1:n}\mathrm{K}_{\mathrm{ads}} = {}^{1:1}\mathrm{K}_{\mathrm{ads}} \frac{\left[\mathrm{W}\right]^{n-1}}{\left(\left[S_{\max}\right]-\left[S\mathrm{X}\right]\right)^{n-1}}. \tag{2.16}$$

While the bias would clearly be more pronounced if more than one water molecule is chosen to be displaced, for low concentrations of solute (wherein the constant water concentration approximation is valid) *and* somewhat weak adsorption of the solute, these values are roughly indistinguishable. If the concentration of water is made to vary significantly, it is conceivable that the relative displacement of water could be deduced by applying the various fits for each order of replacement.

If different integer replacements (or rational fraction) exchanges are then assumed, the expression for the surface solute concentration dependence on bulk concentration dependence remains analytical, albeit more complicated:

$$
\begin{aligned}
^{1:1}[SX] &= \frac{[S_{max}][X]}{[W]K_{ads}^{-1}+[X]} \\
^{1:2}[SX] &= 2[S_{max}]+\frac{[W]^2-[W]\sqrt{[W]^2+4K_{ads}[S_{max}][X]}}{2K_{ads}[X]} \\
^{1:3}[SX] &= [S_{max}]+[W]^2\sqrt[3]{\frac{2}{27K_{ads}^2[S_{max}][X]^2+3\sqrt{3K_{ads}^3[X]^3\left(4[W]^3+27K_{ads}^2[S_{max}]^2[X]\right)}}} \\
&\quad -[W]\sqrt[3]{\frac{9K_{ads}^2[S_{max}][X]^2+\sqrt{3K_{ads}^3[X]^3\left(4[W]^3+27K_{ads}^2[S_{max}]^2[X]\right)}}{18K_{ads}^3[X]^3}}
\end{aligned}
\tag{2.17}
$$

Along with the added complexity, notion of an integer replacement of water in the interface is non-intuitive. Due to the limited resolution of the SHG studies presented here, this effect is not explored herein.

Of course, the volume of the interface is finite and the argument above is then somewhat pedantic when one considers that a surface site in a finite volume interface is a fictitious concept. Similarly, SHG probe depth is the entirety of this region of broken symmetry, and in the case of electrolyte solutions this may extend to greater depths than that of neat water[1, 22]. From here forward, we treat the interface as a finite volume, consistent with both the natural notion of a continuous transition between the bulk phases and the effective probe region of second-order spectroscopies. In this sense we make a complete distinction between the *surface* (*viz*. outermost layer of liquid density) and the *interface*.

2.2.3. ***Langmuir Adsorption to an Interfacial Volume***

If the interface volume was treated ideally, one would simply define a partition coefficient for the adsorption of ions into the interface

$$
K_{ads} = \frac{\left[X_{(\sigma)}\right]}{\left[X_{(aq)}\right]}, \tag{2.18}
$$

where $\left[X_{(\sigma)}\right]$ is the concentration of the adsorbate in the surface region (σ). However, the system is not ideal, and if there is a significant population of solute in the interface, the surface species will eventually crowd each other due to the restricted volume available. This is reflected in previous SHG studies of strongly adsorbing anions through the saturation of signal observed at high concentrations (Figure 2.2)[11, 13, 16]. Allowing the volume of the interface *available* to

adsorbates be a function of the size and number of the interfacial molecules, we adopt:

$$\left[\mathrm{X}_{(\sigma)}\right]_{eff} = \frac{N_{X_{(\sigma)}}}{V_{Int} - \sum_{J} b_J N_{J_{(\sigma)}}} \tag{2.19}$$

Here $N_{J_{(\sigma)}}$ is the number of the interfacial species $J_{(\sigma)}$ with an empirical effective exclusion volume of b_J, and V_{Int} is the actual volume of the interface region. This expression has its analogy in the Van der Waals expression for a real gas[23], where the b coefficient reflects a Van der Waals gas molecule's exclusion volume. Borrowing further from ideal gas theory we will assume that only solutes exclude volume, allowing water to effectively act as a non-interacting background (ideal) gas. As is usual when dealing with non-ideal systems, we can always include the effect of water through the application of an activity coefficient if necessary. Rewriting this expression for a single species and multiplying the interface volume to both numerator and denominator, we find that we recover the usual form of the Langmuir adsorption isotherm:

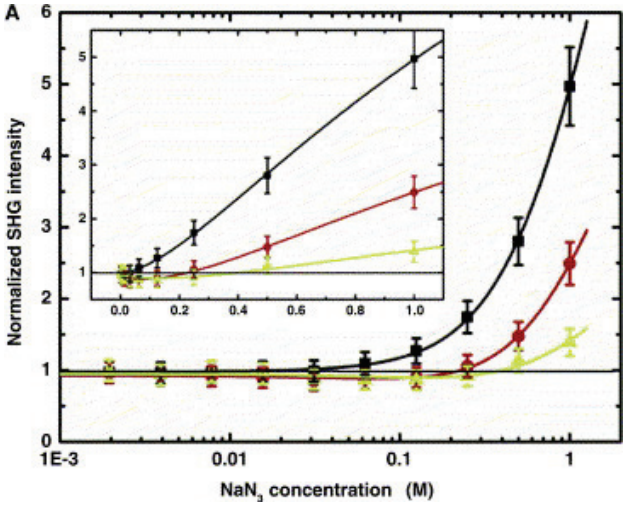

Figure 2.2- The second harmonic signal profile of aqueous NaN_3 as determined by resonant SHG at (largest to smallest) 200 nm, 225 nm, and 250 nm. At high bulk concentrations (inset) the surface begins to saturate, as is evidenced by the sub-second-order dependence of SHG on concentration. *Reprinted in part from Chem. Phys. Lett.,* **397**, Petersen, P.B. and R.J. Saykally, "*Confirmation of enhanced anion concentration at the liquid water surface,*" p51, *Copyright 2005, with permission from Elsevier.*

$$\mathrm{K}_{\mathrm{ads}} = \frac{\left[\mathrm{X}_{(\sigma)}\right]_{eff}}{\left[\mathrm{X}_{(aq)}\right]} = \frac{\left[\mathrm{X}_{(\sigma)}\right]}{\left(1 - b_{\mathrm{X}_{(\sigma)}}\left[\mathrm{X}_{(\sigma)}\right]\right)\left[\mathrm{X}_{(aq)}\right]} \tag{2.20}$$

$$\begin{aligned}\left[\mathrm{X}_{(\sigma)}\right] &= \frac{\left[\mathrm{X}_{(aq)}\right]\mathrm{K}_{\mathrm{ads}}}{1+b_{\mathrm{X}_{(\sigma)}}\mathrm{K}_{\mathrm{ads}}\left[\mathrm{X}_{(aq)}\right]} \\ &= \frac{b_{\mathrm{X}_{(\sigma)}}^{-1}\left[\mathrm{X}_{(aq)}\right]}{b_{\mathrm{X}_{(\sigma)}}^{-1}\mathrm{K}_{\mathrm{ads}}^{-1}+\left[\mathrm{X}_{(aq)}\right]} \\ &= \frac{\left[S_{\max}\right]\left[\mathrm{X}_{(aq)}\right]}{\left[S_{\max}\right]\mathrm{K}_{\mathrm{ads}}^{-1}+\left[\mathrm{X}_{(aq)}\right]}\end{aligned} \tag{2.21}$$

This approach avoids the issue of considering water replacement altogether by allowing such effects to be characterized by either the effective exclusion volume and/or activity coefficient. Comparison with Equation 2.13 demonstrates that the exchange model and this model are equivalent when the same assumptions are applied; in this case the exchange ratio is 1:1, and surface water is assumed to have the same concentration as bulk water in its standard state.

$$\frac{\left[S_{\max}\right]\left[\mathrm{X}_{(aq)}\right]}{\left[S_{\max}\right]\mathrm{K}_{\mathrm{ads}}^{-1}+\left[\mathrm{X}_{(aq)}\right]} \cong \frac{\left[S_{\max}\right]\left[\mathrm{X}^{-}\right]}{\left(\left[\mathrm{W}\right]\mathrm{K}_{\mathrm{ads}}^{-1}+\left[\mathrm{X}^{-}\right]\right)} \tag{2.22}$$

In this regard we have validated applying the exchange model to a volume, recognizing that we are not making any more assumptions than were already present in the usual exchange model.

To explicitly account for a true *competitive* equilibrium of water and solute, one would also model the adsorption of water to the interface. The argument set out above leads to

$$\begin{aligned}\left[\mathrm{X}_{(\sigma)}\right] &= \frac{\mathrm{K}_{\mathrm{ads}}\left[\mathrm{X}_{(aq)}\right]}{1+b_{\mathrm{W}}\mathrm{K}_{\mathrm{W}_{(\sigma)}}\left[\mathrm{W}_{(aq)}\right]+\mathrm{K}_{\mathrm{ads}}b_{\mathrm{X}}\left[\mathrm{X}_{(aq)}\right]} \\ &= \frac{\left[\mathrm{X}_{(\sigma)\max}\right]\left[\mathrm{X}_{(aq)}\right]}{\mathrm{K}_{\mathrm{ads}}^{-1}\left[\mathrm{X}_{(\sigma)\max}\right]\left(\ 1+b_{\mathrm{W}}\mathrm{K}_{\mathrm{W}_{(\sigma)}}\right)\left[\mathrm{W}_{(aq)}\right]+\left[\mathrm{X}_{(aq)}\right]}\end{aligned}, \tag{2.23}$$

where $\mathrm{K}_{\mathrm{W}_{(\sigma)}}$ is the effective adsorption of water to the interface, and presumably would model the density of water in the interfacial volume (that an adsorbate can partition to) at zero solute concentration. This expression is equivalent to the usual Langmuir isotherm for *competitive* adsorption to surface sites[24].

Unfortunately, this expression also directly couples the desired $\mathrm{K}_{\mathrm{ads}}$ to unknown parameters;

$$\left[\mathrm{X}_{(\sigma)}\right]=\frac{\left[\mathrm{X}_{(\sigma)\max}\right]\left[\mathrm{X}_{(aq)}\right]}{\gamma\left[\mathrm{W}_{(aq)}\right]+\left[\mathrm{X}_{(aq)}\right]}, \tag{2.24}$$

where

$$\gamma=\mathrm{K}_{\mathrm{ads}}^{-1}\left[\mathrm{X}_{(\sigma)\max}\right]\left(1+b_{\mathrm{W}}\mathrm{K}_{\mathrm{W}_{(\sigma)}}\right); \tag{2.25}$$

and cannot be used to fit the SHG response.

Thus, in judicious application of Ockham's razor, we retain the 1:1 exchange model for its simplicity in use, the ability to compare with other like-modeled systems, and its success in previously modeling the concentration dependence of the SHG signal. However, we recognize that the energies it describes for the adsorption process are only relevant when compared to equivalently modeled systems and, at minimum, discounts some of the water desorption free energy that would be present for >1:1 replacements.

2.2.4. ***Langmuir Adsorption Modeling Including Cations***

While this discussion has focused thus far on the nature of water desorption in the interface region, and consideration of the Langmuir adsorption model against a volume, another concern is the issue of the cations in the interface. By the electroneutrality condition, if an anion adsorbs to the interface region a cation must also be absorbed, although the microscopic partitioning depth with respect to the Gibb's dividing surface is likely be unique to each[25-29]. In related SHG studies previously mentioned, this is generally disregarded, as the model takes no account of cations and the signal observed is only resonant with the anion. However, those studies that do explicitly consider cation dependence suggest a relatively weak effect[10, 19]. Nonetheless, in order for an anion to adsorb into the interface, the process must not only have sufficient free energy for the anion to do so, but it must have also enough in excess to bring a cation into this vicinity such that electroneutrality is maintained. Uneven partitioning may mean that the necessary excess energy is negligible, but this effect is still easily captured for a 1:1 electrolyte under a slight revision to the exchange model:

$$\mathrm{W}S^{(+)} + \mathrm{M}^+ \rightleftarrows \mathrm{W} + S^{(+)}\mathrm{M}^+ \tag{2.26}$$

$$\mathrm{K}_{\mathrm{ads}}^{+} = \frac{\left[S^{(+)}\mathrm{M}^+\right]\left[\mathrm{W}\right]}{\left[S^{(+)}\mathrm{W}\right]\left[\mathrm{M}^+\right]} = \frac{\left[S^{(+)}\mathrm{M}^+\right]\left[\mathrm{W}\right]}{\left(\left[S_{\max}\right] - \left[S^{(+)}\mathrm{M}^+\right]\right)\left[\mathrm{M}^+\right]} \tag{2.27}$$

Here we have allowed the surface sites to be distinct from those of the anion, to reflect that for preferential anion adsorption the cations partition into a deeper region of the interface than that of the anion[22, 26, 27, 29]. The restriction of electroneutrality for a 1:1 electrolyte gives,

$$\left[S^{(-)}\mathrm{X}^-\right] = \left[S^{(+)}\mathrm{M}^+\right], \tag{2.28}$$

and the overall adsorption constant is then:

$$\begin{aligned}\mathrm{K}_{\mathrm{U}} = \mathrm{K}_{\mathrm{ads}}^{+}\mathrm{K}_{\mathrm{ads}}^{-} &= \frac{\left[S^{(-)}\mathrm{X}^-\right]^2\left[\mathrm{W}\right]^2}{\left(\left[S_{\max}^{(-)}\right] - \left[S^{(-)}\mathrm{M}^-\right]\right)\left(\left[S_{\max}^{(+)}\right] - \left[S^{(-)}\mathrm{X}^-\right]\right)\left[\mathrm{X}^-\right]^2} \\ &= \frac{\left[S^{(+)}\mathrm{X}^-\right]\left[\mathrm{W}\right]^2}{\left(\left[S_{\max}^{-}\right] - \left[S^{(-)}\mathrm{X}^-\right]\right)^2\left[\mathrm{X}^-\right]^2}\end{aligned} \tag{2.29}$$

Here we have assumed, as in the 1:1 exchange model, that the maximum number of surface sites for both species are equal (to the concentration of water in the neat interface). Consideration of same-site competition merely leads to a factor of two in the difference in the denominator. The net result is isomorphic to that of simple anion adsorption by 1:1 exchange, only now the total energy of adsorption is recognized to be divided between both the cation and anion (but not necessarily evenly). In this model, the cation and anion are still free to explore independently their respective interfacial volumes, but electroneutrality is conserved explicitly. While this conclusion is not necessarily new or striking, it forms the basis for considering the co-adsorption of cation and anion to a single surface site:

$$\mathrm{K}_{\mathrm{B}} = \frac{\left[\mathrm{M}^+S\mathrm{X}^-\right]\left[\mathrm{W}\right]}{\left(\left[S_{\max}\right] - \left[\mathrm{M}^+S\mathrm{X}^-\right]\right)\left[\mathrm{X}^-\right]\left[\mathrm{M}^+\right]} = \frac{\left[\mathrm{M}^+S\mathrm{X}^-\right]\left[\mathrm{W}\right]}{\left(\left[S_{\max}\right] - \left[\mathrm{M}^+S\mathrm{X}^-\right]\right)\left[\mathrm{X}^-\right]^2} \tag{2.30}$$

In this expression, the translational partition functions of the two surface species are coupled as the ions are 'bonded' to the same surface site, and is reflective of ion-pairing in the interface. The fundamental difference is that now the observed surface concentration will be identifiably second-order in bulk concentration. This can act as a distinguishing characteristic between two possible mechanisms for bringing anions to the interface, one in which the anion has an intrinsic propensity for the interface, and the other where charge neutralization by its paired cation helps it overcome the usual electrostatic costs associated with such partitioning.

2.3. Implementation

While the use of SHG as a surface probe is theoretically well-established and experimentally proven ([2] and references therein), actual implementation entails details that mandate discussion, especially if the equipment available to perform the experiments allow only for sub-optimal experimental conditions. In this section, we present the design of experimental methods used herein and highlight some of the tangible aspects of, and obstacles to, implementing a femtosecond surface SHG experiment, including some of the developed methodologies to help overcome such obstacles.

2.3.1. ***Chemicals and Glassware***

The water used for solutions and rinsing was generated by a Millipore Milli-Q A-10 system, yielding 18.2 MΩ impedance water of <4 ppb total organic content. All handling of glassware was done with nitrile gloves, thoroughly scrubbed under flowing deionized water to remove lotions and powders added by the manufacturer. At any opportunity for cross-contamination, this was repeated. All glassware used was soaked in a solution of Nochromix inorganic oxidizer in concentrated sulfuric acid for at least one hour, and thoroughly rinsed (with vigorous agitation) under flowing Millipore water.

Sodium Nitrate and Nitrite Studies (Chapter 3)

The various concentrations of sodium nitrate and nitrite studied were generated by successive volumetric dilutions of either stock 6 M or 1 M solutions. The stock solutions were prepared fresh each day from >99% purity sodium nitrate and nitrite, dissolved in Millipore water sparged with nitrogen for at least 1 hour before use. The samples themselves are contained in a 5 cm diameter Petri dish during analysis and kept in a nitrogen atmosphere at atmospheric pressure and room temperature for the duration of measurement. Between

measurements, the samples are kept (covered) in a hood under positive nitrogen pressure, but no accommodation for environmental control could be made for the transfer of solutions from hood to apparatus.

Potassium and Sodium Thiocyanate Studies (Chapter 4)

Sodium thiocyanate used was of >99.99% purity (metals basis), and potassium thiocyanate of >99%. All solutions and dilutions were prepared gravimetrically and stored for no more than 24-hours in air-tight, ambered or opaque glass containers, cleaned as previously described. Solutions of potassium thiocyanate were passed by syringe through a 0.22 μm filter (Millipore, Durapore GVWP02500) that had been previously rinsed thrice with water and then thrice with the solution of interest. Failure to rinse with an electrolyte solution resulted in an SHG signal increase at 193 nm on the order of ½ the water signal when measuring electrolyte solutions. An ion-exchange type residue is presumed to be present in the filters as supplied. The filtration itself mainly had the tendency to reduce noise in measurements rather than change the measurement value itself, probably owing to particulate effects previously observed in other SHG liquid surface studies[30].

Sodium Iodide Studies (Chapter 5)

Stock sodium iodide solutions were prepared gravimetrically from >99% reagents as supplied by the vendor. Other aspects follow that described for sodium nitrate and nitrite, except that the room was darkened during preparation and measurement to reduce possible photochemical interactions in the iodide solutions.

2.3.2. ***Optical Design***

Incident Beam

The laser system used for the studies herein is identical to that previously described by Petersen, *et. al.*[8], consisting of an OPA (TOPAS, Quantronix) pumped by a regeneratively amplified femtosecond system (Spitfire, Spectra Physics), capable at specification of outputting ~70 fs pulses at 800 nm with powers of 2 mJ·pulse^{-1} when operated at 1 kHz. The amplifier is seeded by a home-built Ti:sapphire oscillator and the OPA is outfitted with two *BBO* motorized mixing crystals, yielding a total tuning range from ~2400 nm to 290 nm. For the experiments described herein, only the visible and near ultraviolet range was used, generally providing <10 μJ per pulse with a beam radius of ~2 mm.

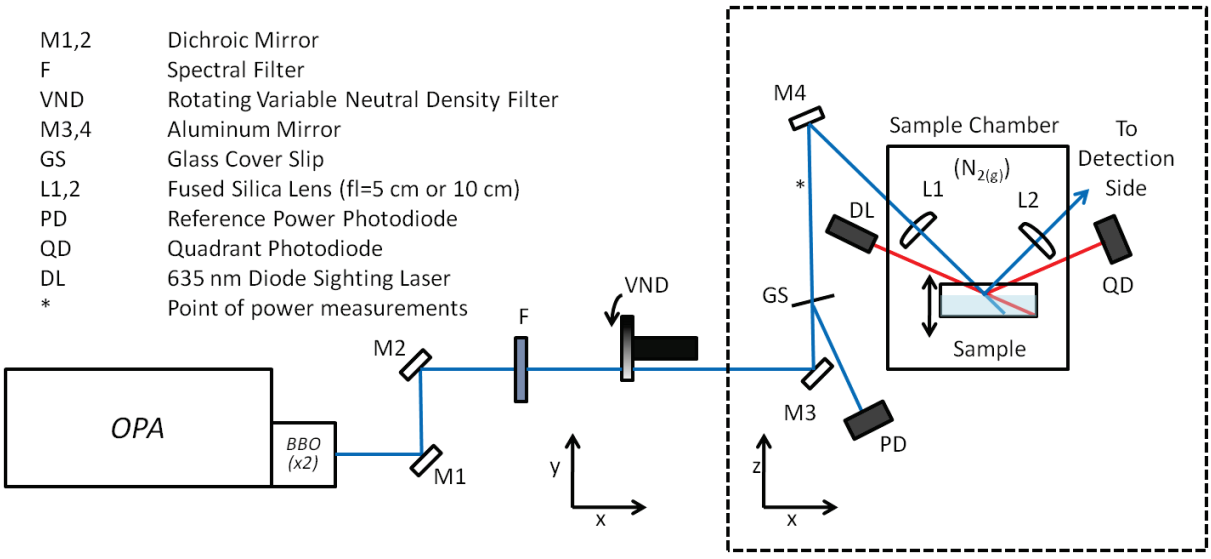

Figure 2.3- Schematic of the experimental design of the incident optical system. M1,2 and F were used to spectrally purify the incident beam of the extraneous frequencies generated by the OPA. VND was either manually adjusted or rotated continually by electric motor to modulate the incident power. The dashed box indicates a change in lab coordinates of the schematic. Incident power was measured by PD, calibrated to the power measured at (*). In some experiments the height of the sample surface was determined by the location of a diode laser (DL) reflection onto QD. The sample chamber was purged with nitrogen gas, humidified in some experiments.

The optical design for the incident beam is presented in Figure 2.3. The direct output of the OPA contains significant extraneous wavelengths as a result of undesired wave-mixing processes, which are spectrally filtered by steering the beam with appropriate dichroic mirrors and (sometimes) with the use of filters when dichroics provide insufficient spectral purity. The spectral purity is verified both by examination with a fiber coupled spectrometer (Ocean Optics, SD200), and by observation of the correct second-order power dependence of the second harmonic signal from water.

In some experiments, the incident power was manually controlled by a variable neutral density filter wheel (OD ~0.1-3), and in other experiments the power was continuously modulated by motorized rotation of the same (discussed below). A glass cover-slip pickoff is used to direct ~5-10% of the available intensity to a photodiode, the photodiode current being used to measure the relative incident power applied to the sample. Absolute power measurements were made using a calibrated photodiode with wavelength correction (OP2-Vis photodiode, 3Sigma meter, both Coherent) directly before the final turning mirror prior to the sample. The power measurements are used to calibrate the photodiode response. The exception is for 386 nm power measurements, which

were measured with a thermoelectric detection head (PS10, Coherent). No correction is made for losses from the final incident mirror or incident focusing lens. The incident beam is focused onto the sample by either a nominal 10 cm (Chapters 3,5) or 5 cm (Chapter 4) focal length fused silica biconvex lens. The second harmonic signal is collimated in the reflected direction by a matching lens, positioned at a slightly closer distance from the sample to correct for the different focal length of the second harmonic. This distance is determined by maximizing the collected intensity at the detector (below). The incident beam is angled at 45° for the experiments with sodium nitrate and nitrite (Chapter 3) but was changed to 60° for the remaining experiments to maximize the response due to the angular dependence of the Fresnel factors.

Detection-Side Steering Mirrors

The detection side optical train varied for the studies presented in each chapter. For Chapters 3 and 5 the (second harmonic) signal is steered by three stock high-reflectance laser-line mirrors, optimized for un-polarized light, and are chosen for optimal reflection of the second harmonic wavelength. The fundamental wavelength is largely transmitted by these mirrors, and provides the majority of spectral filtering necessary to separate the weak second harmonic signal from the incident beam. Reflection bandwidths of UV mirrors such as these are generally on the order of 5 nm and had to be changed frequently to perform the spectroscopy presented in Chapter 5. For the experiments presented in Chapter 4, these mirrors have been replaced with broadband UV enhanced aluminum mirrors to allow for wavelength changes without the overhead of significant realignment.

Detection-Side Filtering and Detection

Aside from any filtering garnered from the use of specific steering mirrors, the signal is further separated from the fundamental by spatial filtering. In Chapters 3 and 5, this is accomplished by a fused silica prism and a solar-blind photomultiplier tube (PMT) (Hamamatsu, R7154PHA) is placed in the path of the signal beam. In Chapters 4 and 5, the signal is focused by a 15 cm focal length calcium fluoride lens into a monochromator (Acton, SpectraPro 2150i) equipped with a 1200 lpi grating with a blaze angle optimized for 300 nm. No effort was made to consider resolution, as the signal and fundamental are separated by large energies. In Chapter 4, the use of broadband detection-side mirrors necessitated the use of a calcium fluoride Pellin-Broca prism (geometrically cut for optimal 193 nm performance) prior to focusing into the monochromator. The

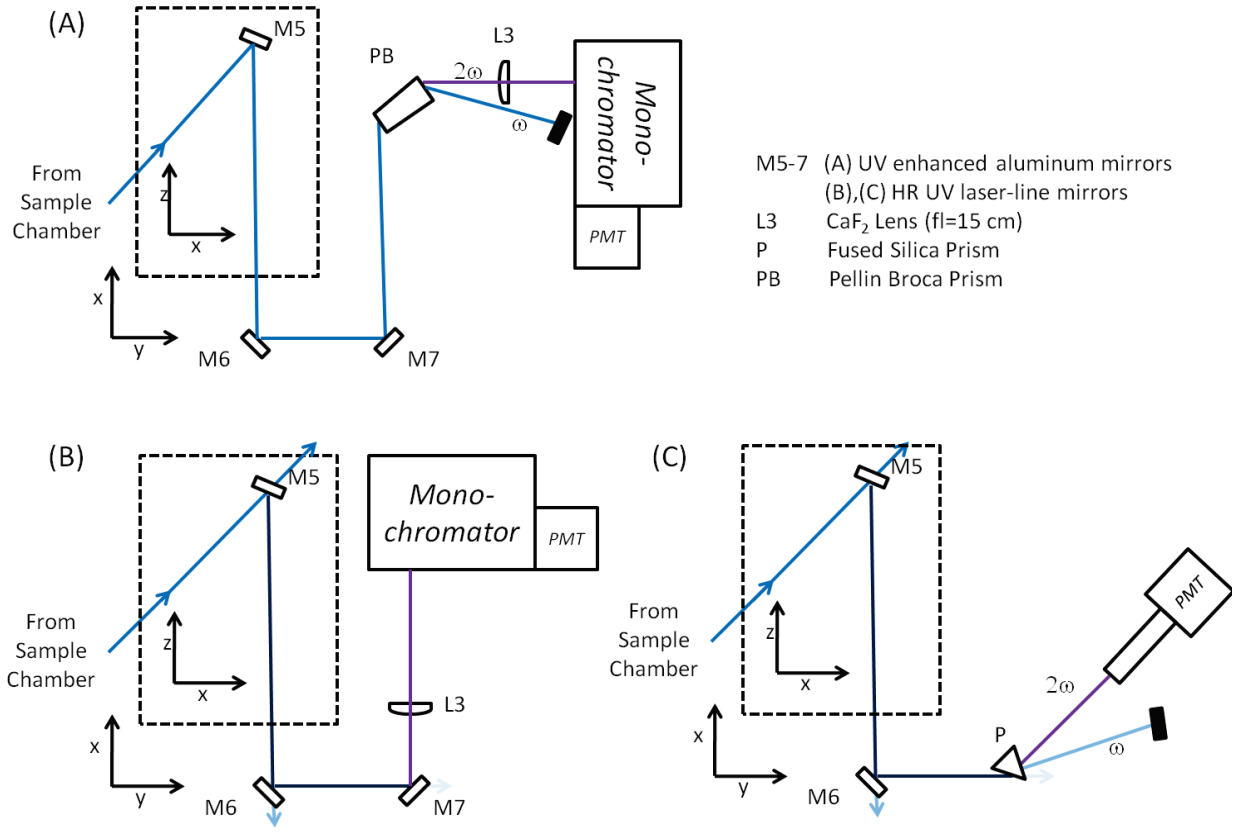

Figure 2.4- Schematic of the detection-side configurations used. (A) Chapter 4: Spectral filtering of the second harmonic from the fundamental is handled by a Pellin-Broca prism and monochromator. (B) Chapter 5: Spectral filtering is handled by stock high reflectance (HR) laser line mirrors that transmit the fundamental, and is further purified by a monochromator. (C) Chapter 3: Spectral filtering is achieved by using the HR mirrors and a fused silica prism, the signal collected by positioning the solar-blind PMT in the second harmonic beam path.

currents from both the PMT and photodiode were integrated by gated integrators (Stanford Research Systems, SR250) and individual pulse integrations were collected by computer. Custom programs written in Labview 5.3, and 8.0-8.5 (National Instruments) handled data acquisition and pre-processing of the data.

2.3.3. ***Sample Normalization Methodology***

As experimental conditions could vary day-to-day (and even minute to minute in the worst cases), absolute measurements of SHG intensity was generally an unreliable indicator of the surface susceptibility. Thus, in general, the SHG response of a given sample was immediately preceded and followed by a measurement of neat water as a reference. The fundamental unit of measurement used throughout this work is the sample signal normalized by the average of the bracketing water measurements. This measurement technique is susceptible to experimental changes that occur with frequencies on the order of minutes.

Neat water, the reference used herein, has a weak non-resonant second harmonic response. Depending on the experimental conditions the signal collected can sometimes be on the order of $1/1000$ photons per pulse, although ~ $1/100$ can be consistently achieved. Other reference systems can be, and have been employed, such as a dodecanol-monolayer on water[18, 19]. At room temperature the dodecanol-monolayer generates approximately three times more signal (at 193nm) than that of the neat water interface. However, it was found to also be highly variant when exposed to flowing nitrogen and has the potential for significant structural changes as a function of temperature[31, 32]. For the studies herein, all normalization was done directly against water samples. To help overcome some of the difficulties in optimizing such a weak signal, several modifications were made to the apparatus over the course of the study to enhance both reproducibility and signal, discussed below.

2.3.4. ***Sample Positioning***

The second harmonic response is fundamentally dependent on the local power density applied at the sample surface, and reproducibly overlapping the focal volume of the beam with the surface is critical. The samples themselves are contained in 5 cm diameter Petri dishes, prepared as described previously. Overlap of sample surface with the focal plane of the incident beam was implemented using a vertically oriented translation stage, the sample dish held on a horizontal Plexiglas platform with a cutout for reproducible positioning of the Petri dish. For the temperature dependent measurements of Chapter 4, the platform/cutout was constructed of an aluminum block attached to a Peltier thermoelectric stack (x2) (Custom Thermoelectric, TEC127) to control the temperature of the sample.

For the experiments described in Chapters 3, the height alignment of the sample was performed by manual adjustment of a micrometer, judging the peak intensity by eye. For signal strengths in a photon-counting regime, this is difficult to accomplish in practice. The only defense against misalignment is to take many measurements to randomize this effect, and even then, one is guaranteed a low-signal bias due to the single-tailed nature of the error this produces. By this method, in instances of low signal, one is more likely to sample non-optimal heights as the maximum of signal intensity is difficult to gauge for weak signals, thus biasing weak signals to appear even weaker against stronger samples for which the correct height is more easily identified. When using the weak response of water as a reference, this may introduce a systematic bias in normalized

measurements, wherein large signals (being easier to optimize) will appear amplified over weak signals. The opportunity for operator bias can be a real concern in these situations.

Figure 2.5 shows the second harmonic response of a neat water surface observed as a function of sample height. There is some structure evident in the profile itself; the shoulders and peaks are reproducible features which are likely attributable to the secondary and tertiary Airy disc maxima in the focal region. When the focal volume is located within the bulk, the slope of the response changes less rapidly than when it is in the adjoining air, which may be evidence of self-focusing through the focal volume causing a more rapidly diverging beam after the focal point. Under the conditions of this setup the vertical depth of focus for linear optics is calculated to be 370 μm. We take the square-root of this as an approximation of the second harmonic depth-of-focus, determined to be roughly 19 μm. This is in surprisingly good agreement with the observed 20 μm window of relatively stable response. We also note that the response varies strongly outside of this region, declining by ~1% per μm when the focus is outside the condensed phase, and about half that when the focus is within. This rapid variation has critical implications for how the second harmonic experiment is conducted, and was identified as a point to improve for further experiments. Personal estimates of reproducibility in manual adjustment of the sample height using the sighting laser (below) were around ±15 μm standard error. No estimate is available for comparison of the intensity-by-eye optimization discussed initially in this section.

To aid in sample alignment, a diode sighting laser (Thorlabs, CPS180, 1mW, 635 nm) was employed, reflecting the beam off the surface to a home-built calibrated quadrant photodiode functioning as an alignment target. This had the tangible effect of reducing the standard deviation of repeated measurements from approximately 20% to 10% in the case of water. It ensured that any change in conditions (such as incident beam alignment drift) were systematically introduced to both sample and reference and could be conveniently normalized away. This technique was used in the experiments of Chapter 5. While there was some small issue with the stability of the sighting laser and positioning of the quadrant photodiode, it eventually became apparent that there could be a new systematic bias introduced by this method that could not be carried over from one measurement to the next.

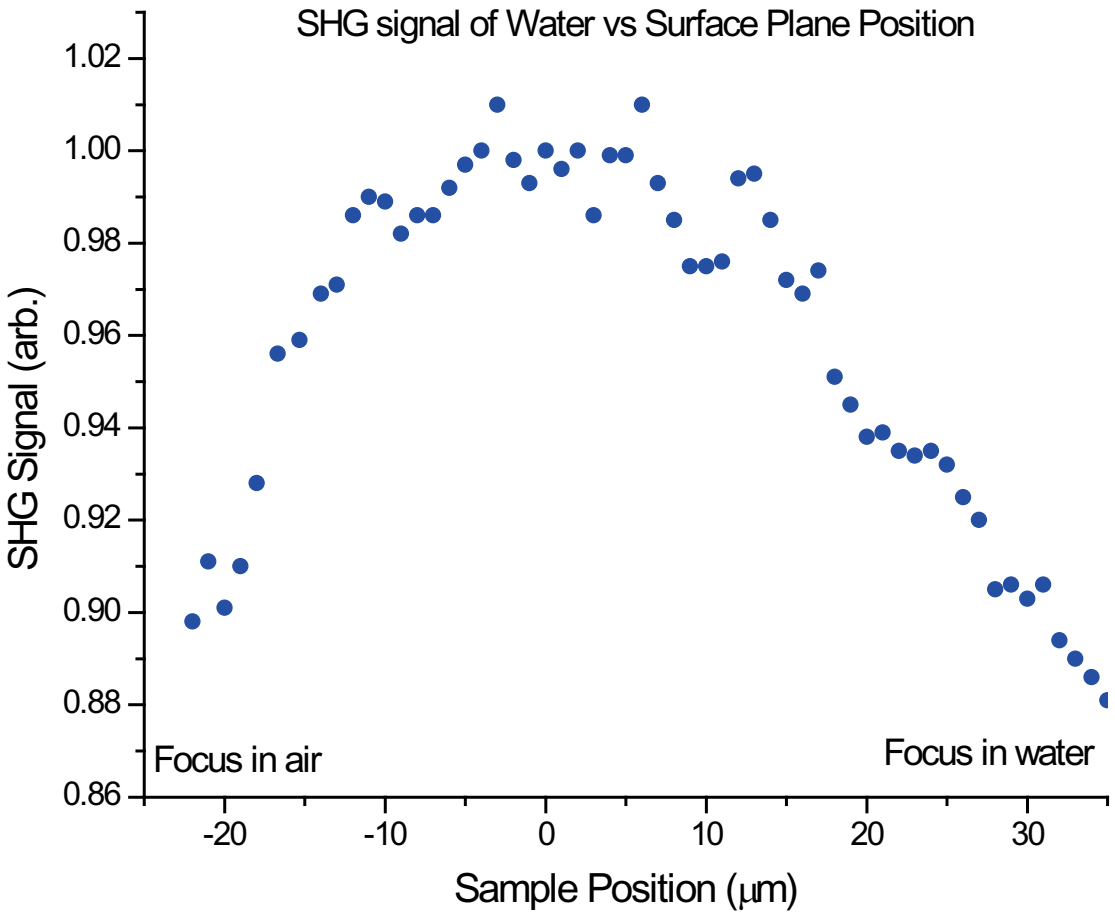

Figure 2.5- SHG response at 193 nm of a neat water surface as a function of focal plane distance from the interface. Experimental parameters were: 60° angle of incidence, 386 nm incident wavelength, 2 mm collimated beam diameter and a 5.5 mm focal length. The SHG focal volume is observed to be ~20 μm in the vertical direction. Structure on this profile was generally reproducible and is attributed to the maxima of the Airy disc profile of the beam. The differing rate of change in the signal when the focus is in air versus water is attributed to self-focusing of the beam as it passes through its focal point, resulting in greater divergence before reaching the sample.

The Petri-dishes used to contain the samples come with a range of small size variations, with diameters differing by as much as a millimeter. As positioning of the dish in the sample chamber (in an effort to reproducibly place the meniscus) was often done by pushing one side of the dish against the fixed wall of the cutout described above, the meniscus placement is then a characteristic of a given dish. While the reflected *signal* beam alignment was determined to be largely unaffected by this (the collection window from sample to detector was sufficiently wide), it had a significant effect on the pointing of the *sighting* beam. Thus, the sighting beam had a characteristic change in pointing for a given dish, and an individual dish could then be systematically placed at a

differing height than another dish. The resulting difference in signal could be as much as 10% in extreme cases. Often, many samples were discarded as contaminated, whereas the problems were most likely due to this effect. Randomization of dishes would help to alleviate this, requiring more measurements but making the errors random rather than systematic. However, due to cross-contamination concerns between water and samples, water samples would often be restricted to one or two dishes in a given experimental day.

Matching of dishes could also be done by determining the signal vs. height profile for a given dish and then comparing this profile against a second dish, using the sighting laser as an absolute reference. In general, a specific dish could be found to generate reproducibility on the order of 5-10%, depending on the stability of the sighting laser, and the fluctuations of the surface itself. For our studies employing dodecanol monolayers[18, 19] and the sighting laser, this may have had a significant impact. To generate a dodecanol monolayer, a small crystal of dodecanol is floated on the surface of water and positioned to the edge of the Petri-dish to remain adhered to both the dish and the water by surface tension. This has a profound effect on the meniscus shape (as observed by the variation of the sighting laser direction).

In the final analysis, it seemed the most reliable method was to actually scan the sample height along the z-axis to identify the acceptable focal plane, effectively generating a signal vs. height profile for every measurement. To perform this, a motorized micrometer was installed to provide reproducible, small step sizes (Figure 2.5 was generated under this method). Although tedious, the methodology often proved to provide standard errors of less than 3%, provided that the stability of the laser was longer than the timescale of three measurements (enough to bracket a single sample with two reference samples, see above). In practice, this timescale was on the order of 5 minutes. Stable conditions could last for hours, but similarly could change on the order of minutes. This still necessitated three to five sample measurements to ensure good averaging when laser fluctuations did break into a given measurement bracket, but also revealed exactly how the stability of the laser could dramatically change measurement values, as these fluctuations were now decoupled from height misalignment (sometimes as much as 50% over an hour time period). This methodology is employed in Chapter 4 and a comparison of the error bars of between the SHG signals of Chapter 3 and 4 demonstrate its success.

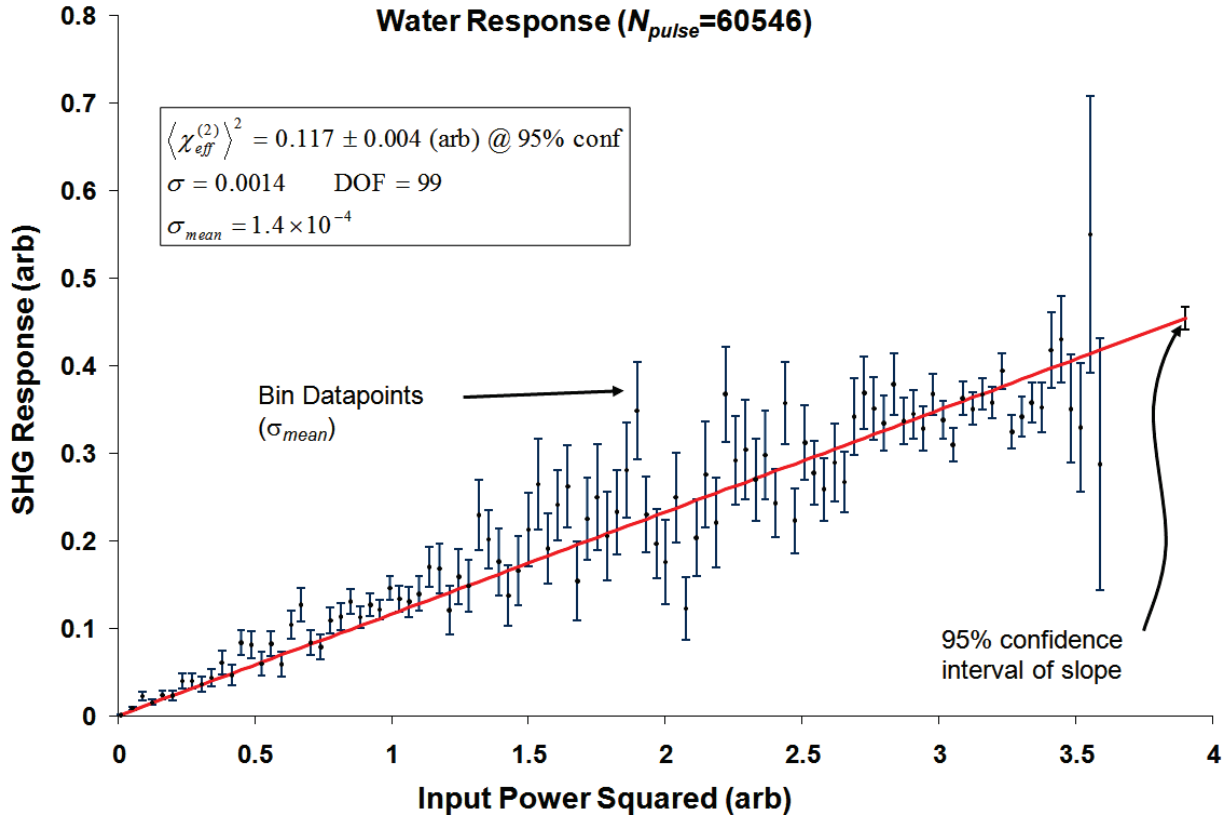

Figure 2.6- A representative continuous power modulation profile of neat water using the photon counting and real-time curve fitting algorithms developed (described in the text). The weighted regression fit of 60k pulses (~1 min @ 1kHz) is shown as a red line. Statistical moments are explicitly presented in the graph. The effective susceptibility of the sample is proportional to the slope of the fitted line.

2.3.5. ***Signal Processing and Power Normalization***

The measurements presented in Chapter 3 are processed using the software written by P. Petersen in Labview 5.0 (National Instruments) while performing his doctoral studies[14] on this apparatus. Incident power and signal power are each collected independently as the average of 500 pulses. These sub-measurements are then averaged over 20k pulses (100 sub-measurements) and the average incident power is squared and used as a normalization value for the averaged signal to generate a single measurement. This measurement scheme is simple, but has the disadvantage of expressing the normalization value as $\langle I_\omega \rangle^2$ while the signal is actually proportional to $\langle I_\omega^2 \rangle$, and under situations of large incident power fluctuations this can introduce significant error into the measurement. At later stages in the other studies presented herein, this became a significant issue, as our equipment performance began to deteriorate and power fluctuations became an unavoidable occurrence. Also, as previously

mentioned, the signal strength is usually on the order of 10^{-2} photons per pulse . Signal collection by this method was originally based on the intensity observed from the PMT and therefore the majority of collected pulses were measurements of baseline noise.

A complete rewrite of the software was undertaken, written in Labview 8.0-8.5 (National Instruments), in order to improve the visibility and processing accuracy of the information being collected in real-time. To remove the electronic noise of the detection setup, photon-counting methodology was employed. A processing algorithm was developed to discriminate photon signals from baseline, the number of null counts was used as the primary measurement, and average signal intensity was determined from an assumed Poissonian distribution of photon counts. This relationship is

$$I_{2\omega} \propto \langle k \rangle = -\ln\left[\frac{N_{k=0}^{pulse}}{N^{pulse}}\right], \qquad 2.31$$

where the intensity of second harmonic, $I_{2\omega}$, is proportional to the average number of photons, $\langle k \rangle$, per pulse. The signal from individual pulses (being binary: photon or no photon) were assigned to one of 100 bins by the square of the incident power measured for the pulse, and each bin kept a running average of the number of null-shots (signal), the variance of the signal, and the average of the square of the incident power and its variance. Dark counts were virtually undetectable ($<10^{-5}$ pulse^{-1}) due to the gated integration (duty cycle ~10^{-8}), spectral and spatial filtering of the signal, and the solar-blind character of the PMT.

By modulating the incident power with a motorized rotating (~1 Hz) variable neutral density filter this processing methodology also allowed for the real-time collection of the power dependence profile, taken as a variance weighted linear fit of the second harmonic power versus the square of the incident power. This yields a line described by

$$I_{2\omega} = \left|\chi_{eff}^{(2)}\right|^2 {I_\omega}^2, \qquad (2.32)$$

where the slope is the measure of the susceptibility of the sample. An example of the type of line and information collected is presented in Figure 2.6. The weighting was found to be especially necessary to help discount the effect of

poorly sampled bins, especially in early time domains of the measurement. This methodology of signal acquisition and processing was used in Chapter 5 and also for the photochemistry work mentioned in Chapter 4. For the temperature-dependent study in Chapter 4, the power was not modulated to decrease the time of measurements, and the processing scheme was rewritten to utilize the photon-counting algorithm for measurements at a single incident power.

2.3.6. ***SHG/Langmuir Fitting***

Fits of the SHG/Langmuir expressions (2.14 and related) were performed using the nonlinear curve fitting tool of Origin 7.03 (Origin Labs). The fitting tool utilizes the Levenberg-Marquardt regression algorithm and the fits were performed with sample weighting of the inverse variance of the measurements. Reported errors by this algorithm are based on the weighted variance of the data points and their dependence on the parameters for which the error relates, and were scaled by χ^2/DoF. The default optimization parameters of the tool were used. For unimolecular fits, all fitting parameters were set to +1 for initial conditions, while bimolecular fits used a ΔG value of either -20000 or -40000 to avoid a local minimum in the fitting process that clearly did not replicate the data.

2.4. References

1) Boyd, R.W., *Nonlinear Optics*. Second ed. 2003, San Diego: Academic Press.

2) Shen, Y.R., *Surf. Sci.*, "*Surfaces probed by nonlinear optics*," **299-300**, 551 (1994)

3) Shen, Y.R., *Annu. Rev. Phys. Chem.*, "*Optical Second Harmonic Generation at Interfaces*," **40**, 327 (1989)

4) Morita, A. and J.T. Hynes, *J. Phys. Chem. B*, "*A Theoretical Analysis of the Sum Frequency Generation Spectrum of the Water Surface. II. Time-Dependent Approach*," **106**, 673 (2001)

5) Neipert, C., B. Space*, et al.*, *J. Phys. Chem. C.*, "*Generalized Computational Time Correlation Function Approach: Quantifying Quadrupole Contributions to Vibrationally Resonant Second-Order Interface-Specific Optical Spectroscopies*," **111**, 8749 (2007)

6) Heinz, T.F., *Dissertation: Nonlinear Optics of Surfaces and Adsorbates*, in *Department of Physics*. 1982, University of California, Berkeley: Berkeley.

7) Shen, Y.R., *Applied Physics B*, "*Surface contribution versus bulk contribution in surface nonlinear optical spectroscopy*," **68**, 295 (1998)

8) Petersen, P.B. and R.J. Saykally, *J. Phys. Chem. B*, "*Probing the Interfacial Structure of Aqueous Electrolytes with Femtosecond Second Harmonic Generation Spectroscopy*," **110**, 14060 (2006)

9) Petersen, P.B., *Dissertation: Surface Structure of Aqueous Electrolyte Solutions Probed by UV Second Harmonic Generation*, in *Department of Chemistry*. 2005, University of California, Berkeley: Berkeley.

10) Petersen, P.B., J.C. Johnson*, et al.*, *Chem. Phys. Lett.*, "*Direct experimental validation of the Jones-Ray effect*," **397**, 46 (2004)

11) Petersen, P.B. and R.J. Saykally, *Chem. Phys. Lett.*, "*Confirmation of enhanced anion concentration at the liquid water surface*," **397**, 51 (2004)

12) Petersen, P.B. and R.J. Saykally, *J. Am. Chem. Soc.*, "*Adsorption of Ions to the Surface of Dilute Electrolyte Solutions: The Jones-Ray Effect Revisited*," **127**, 15446 (2005)

13) Petersen, P.B. and R.J. Saykally, *J. Phys. Chem. B*, "*Evidence for an Enhanced Hydronium Concentration at the Liquid Water Surface*," **109**, 7976 (2005)

14) Petersen, P.B. and R.J. Saykally, *Annu. Rev. Phys. Chem.*, "*On the nature of ions at the liquid water surface*," **57**, 333 (2006)

15) Petersen, P.B. and R.J. Saykally, *Chem. Phys. Lett.*, "*Is the liquid water surface basic or acidic? Macroscopic vs. molecular-scale investigations*," **458**, 255 (2008)

16) Petersen, P.B., R.J. Saykally*, et al.*, *J. Phys. Chem. B*, "*Enhanced Concentration of Polarizable Anions at the Liquid Water Surface: SHG Spectroscopy and MD Simulations of Sodium Thiocyanide*," **109**, 10915 (2005)
17) Otten, D.E., P.B. Petersen*, et al.*, *Chem. Phys. Lett.*, "*Observation of nitrate ions at the air/water interface by UV-second harmonic generation*," **449**, 261 (2007)
18) Onorato, R.M., D.E. Otten*, et al.*, *J. Phys. Chem. C.*, "*Measurement of Bromide Ion Affinities for the Air/Water and Dodecanol/Water Interfaces at Molar Concentrations by UV Second Harmonic Generation Spectroscopy*," **114**, 13746 (2010)
19) Onorato, R.M., D.E. Otten*, et al.*, *Proc. Natl. Acad. Sci. USA*, "*Adsorption of thiocyanate ions to the dodecanol/water interface characterized by UV second harmonic generation 10.1073/pnas.0904800106*," **106**, 15176 (2009)
20) Zana, R. and E. Yeager, *J. Phys. Chem.*, "*Ultrasonic vibration potentials and their use in the determination of ionic partial molal volumes*," **71**, 521 (1967)
21) Söhnel, O. and P. Novontný, *Densities of Aqueous Solutions of Inorganic Substances*. Physical Sciences Data, ed. J. Nývlt. Vol. 22. 1985, New York: Elsevier.
22) Allen, H.C., N.N. Casillas-Ituarte*, et al.*, *Phys. Chem. Chem. Phys.*, "*Shedding light on water structure at air-aqueous interfaces: ions, lipids, and hydration*," **11**, 5538 (2009)
23) Atkins, P.W., "*Physical Chemistry*," 1031 (1994)
24) Adamson, A.W.G., Alice P., *Physical Chemistry of Surfaces*. 6th ed. 1997, New York: John Wiley & Sons, Inc.
25) Minofar, B., R. Vácha*, et al.*, *J. Phys. Chem. B*, "*Propensity for the Air/Water Interface and Ion Pairing in Magnesium Acetate vs Magnesium Nitrate Solutions: Molecular Dynamics Simulations and Surface Tension Measurements*," **110**, 15939 (2006)
26) Ghosal, S., J.C. Hemminger*, et al.*, *Science*, "*Electron Spectroscopy of Aqueous Solution Interfaces Reveals Surface Enhancement of Halides*," **307**, 563 (2005)
27) Noah-Vanhoucke, J. and P.L. Geissler, *Proc. Natl. Acad. Sci. USA*, "*On the fluctuations that drive small ions toward, and away from, interfaces between polar liquids and their vapors*," **106**, 15125 (2009)
28) Salvador, P., J.E. Curtis*, et al.*, *Phys. Chem. Chem. Phys.*, "*Polarizability of the nitrate anion and its solvation at the air/water interface*," **5**, 3752 (2003)

29) Jungwirth, P. and D.J. Tobias, *J. Phys. Chem. B*, "*Ions at the Air/Water Interface*," **106**, 6361 (2002)
30) Feng, R.-r., Y.-y. Xu*, et al.*, *Phys. Chem. Chem. Phys.*, "*Increased interfacial thickness of the NaF, NaCl and NaBr salt aqueous solutions probed with non-resonant surface second harmonic generation (SHG)*," **10**, 4920 (2008)
31) Vollhardt, D., V.B. Fainerman*, et al.*, *J. Phys. Chem. B*, "*Dynamic and Equilibrium Surface Pressure of Adsorbed Dodecanol Monolayers at the Air/Water Interface*," **104**, 8536 (2000)
32) Vollhardt, D. and V.B. Fainerman, *Adv. Colloid Interface Sci.*, "*Characterisation of phase transition in adsorbed monolayers at the air/water interface*," **154**, 1 (2010)

Chapter 3 - Interfacial Properties of Aqueous Sodium Nitrate and Sodium Nitrite Solutions

3.1. Introduction

This chapter discuses the surface second-harmonic generation (SHG) study of interfacial aqueous nitrate and nitrite anions that, like chloride, bromide and sulfate, are among the most abundant charged species present in atmospheric aerosols and terrestrial water sources[1]. Understanding the chemistry of the NO_x cycle in the stratosphere and troposphere has long been a subject of vigorous research, and current consideration of aqueous interfacial reactions and solvation on aerosols have expanded on this[1-9]. In daylight, the tropospheric ozone is directly produced by gas phase NO_x while indirectly initiating chain processes, such as the generation of hydroxyl radicals, that tend to deplete ozone[10-13]. At night, these species are the dominate initiators of such chain processes[14].

In aqueous systems, ammonium nitrate acts as a liquid phase reservoir for gas phase nitric acid and ammonia, with nitrate also acting as a liberator of halides from the aqueous phase[2]. Approximately half of the ~80 Tg/year (N_2) of fertilizers applied world-wide is actually fixed by crops, the remaining half is distributed in surface waters or bind to minerals in the form of ammonium, nitrate and nitrite[15]. Nitrate is also known to displace chloride in sea-salt particles in the marine atmosphere, also freeing halogens to escape into the gas phase[10]. Nitrate and nitrite in ice acts as a chlorine reservoir by binding chlorine as $ClONO_2$, and nitrous acid similarly acts as a reservoir for hydroxyl radicals[8]. On solid substrates such as ice the formation of nitrous (nitric) acids from NO_2 (NO_3) occur readily in the presence of water[1, 13].

Nitrate and nitrite chemistry at the air-water interface has been a somewhat unexplored arena, especially that of nitrite. As such, surface accommodation rates for these species (and many others) suffer from significant uncertainty in the literature, hindering atmospheric and ecosystem modeling of the surface chemistry of these species[16]. The vibrational sum-frequency generation (VSFG) of Schnitzer, *et al.*[17], and the mass-spectrometric/electro-spray study of Cheng, *et al.*[18], indicate a minimal presence of nitrate in the interface, yet observe a noticeable effect on interface structure. Photoelectron spectroscopy on liquid microjets of 3 M sodium nitrate and nitrite solutions have recently established the relative depletion of these species in the interface via

depth-profiling[19]. Two polarizable MD simulations have produced conflicting results concerning the propensity of the nitrate anion to the interface[9, 20]. Dang, *et al.*'s model suggests low surface affinity, with nitrate ions being concentration-enhanced below the surface proper, while Salvador, *et al.*'s model suggests a much higher propensity. The differing results are possibly attributable to the different localization and magnitudes of polarizable centers used in the two simulations[20].

A more recent simulation by Thomas, *et al.* concludes that the nitrate ion resides primarily in the bulk, but when fluctuations do bring it to the solution surface it adopts a parallel orientation[5]. This surface solvation motif is consistent with the asymmetric solvation of small nitrate-water clusters, where waters tend to locate on a single side of the plane of the molecule[21, 22]. The work of Pegram and Record establishes a relative scale of ion-independent partition coefficients for anions and cations, and nitrate is expected to have a surface affinity somewhere between that of bromide and iodide[23]. This position correlates with the position of nitrate in the ordering of the Jones-Dole viscosity B coefficients of anions, and its usual assignment as a weaker chaotrope[24]. These all suggest that nitrate should be surface active, but perhaps not strongly so.

This chapter discusses a direct probe the relative number density of the aqueous nitrate and nitrite anions in the interfacial region as a function of bulk concentration via electronically resonant SHG. Special focus is directed, not on the apparent energies of adsorption, but to the relative order of bulk concentration dependence that describe adsorption process, in an attempt to elucidate mechanistic information from these profiles. The focus is also explicitly on the SHG active interfacial *region* (viz. region of broken inversion symmetry), as distinct from the interface *surface* (viz. outermost layer of liquid density). This focus is a necessity for consideration of the partitioning of ions in the finite volume of the interface region with respect to the observed response.

3.2. Experimental

The second harmonic response of 0 M to 6 M solutions was observed at 255 nm, 247 nm, and 200 nm, generated by incident wavelengths of 510 nm, 485 nm, and 400 nm. The wavelengths were chosen largely by experimental convenience as the anticipated surface resonance can be shifted from their bulk values[25]. These wavelengths are found to be (two-photon) resonant at 255 nm

and 247 nm for the nitrate anion, and 247 nm only for the nitrite anion. For comparison, the observed responses of 6 M solutions are plotted along with their linear absorption spectrum in Figure 3.1, normalized such that the largest signal observed of a given 6 M solution is 1, and the signal of water is zero. The preparation methods, normalization methods, laser system and optical setup are described in Chapter 2. Average pulse energies ranged from 0.2 µJ to 5 µJ·pulse^{-1} and the appropriate second order dependence of the SHG signal on input power was confirmed. Focusing onto the sample resulted in a diffraction-limited spot diameter at the sample surface of ~140 µm, with average power densities generally ranging from 1 to 30 mJ·cm^{-2} per pulse.

The SHG responses collected are plotted versus concentration in Figure 3.2. A given data point is an average of at least three different days of collection, distributed over three months, normalized to the response of neat water collected and processed identically. Error bars presented in Figure 3.2 represent the standard deviation of the power-normalized values for a given solution, pooled over each day of collection. The error is propagated from both the neat water signal and the solution signal in the formulation of the water-normalized

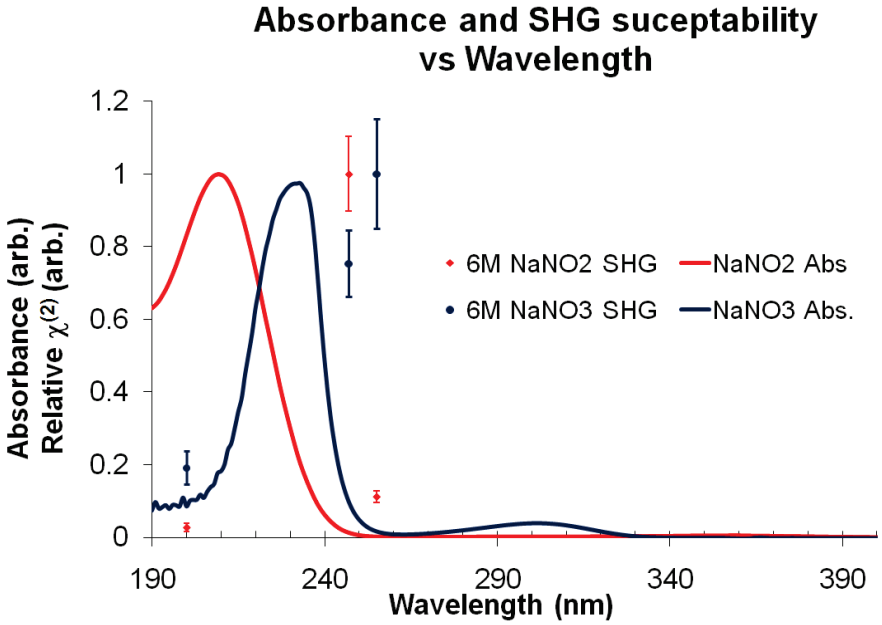

Figure 3.1- The linear absorption spectra of sodium nitrate (blue) and nitrite (red) scaled to their maximum observed value. The overlaid data points are second harmonic responses observed at 6 M concentrations, normalized such that 1 is the largest signal observed for that species and 0 is signal observed from water. Error bars are of one standard deviation. The resonances for both species are clearly shifted from the bulk, but there is insufficient data to determine the direction of the shift or approximate location of the resonance maxima.

signal. The large error of the high-magnitude signals mainly originates from uncertainty of the water signal.

3.3. Results

Figure 3.1 depicts the observed SHG responses overlaid on the linear absorption spectrum for each species. The resonant responses of nitrate and nitrite are clearly shifted from their observed bulk absorption energies, but there is not enough spectral information to determine the magnitude or direction of the shift. The minimum SHG signals observed are at wavelengths that would normally be resonant in the bulk, however. This spectral character establishes that the species probed are unique from those observed in the bulk, while the resonance enhancement itself distinguishes the response of the analyte from the non-resonant response of water.

In a similar study, the SHG spectrum has been found to bathochromically shift with respect to the linear spectrum by nearly 40 nm, and is attributed to the decreased polarity of the interfacial region[25]. The comparison of the linear absorption spectrum against the observed SHG resonances seems to suggest two possibilities: a more modest bathochromic shift (~20 nm) of the $\pi^* \leftarrow \pi$ band (nitrite ~205 nm, nitrate ~230 nm), or a strong (~50 nm) hypsochromic shift of $\pi^* \leftarrow n$ band (nitrite ~355 nm, nitrate ~305 nm). The shifts are presently unquantifiable due to the lack of a complete spectrum. The strength of the response and previous indications of surface induced bathochromic shifts suggest that the former case is most likely.

The observed resonant response of nitrite is strong, rivaling even that observed for sodium thiocyanate[26]. Such a strong resonance enhancement is not observed for nitrate, although the SHG response maximum can only be determined by further measurements as a function of wavelength. At concentrations exceeding 4 M, the nitrite SHG signal declines as a function of concentration, a trend previously unreported for molar concentrations of electrolytes studied by SHG in the literature. This likely indicates that the symmetry of the observed interface is becoming more inversion symmetric, and is discussed in the next section.

In previous similar studies, the adsorption of ions to the interface has been described by an adapted Langmuir model (exchange model, see Chapter 2)

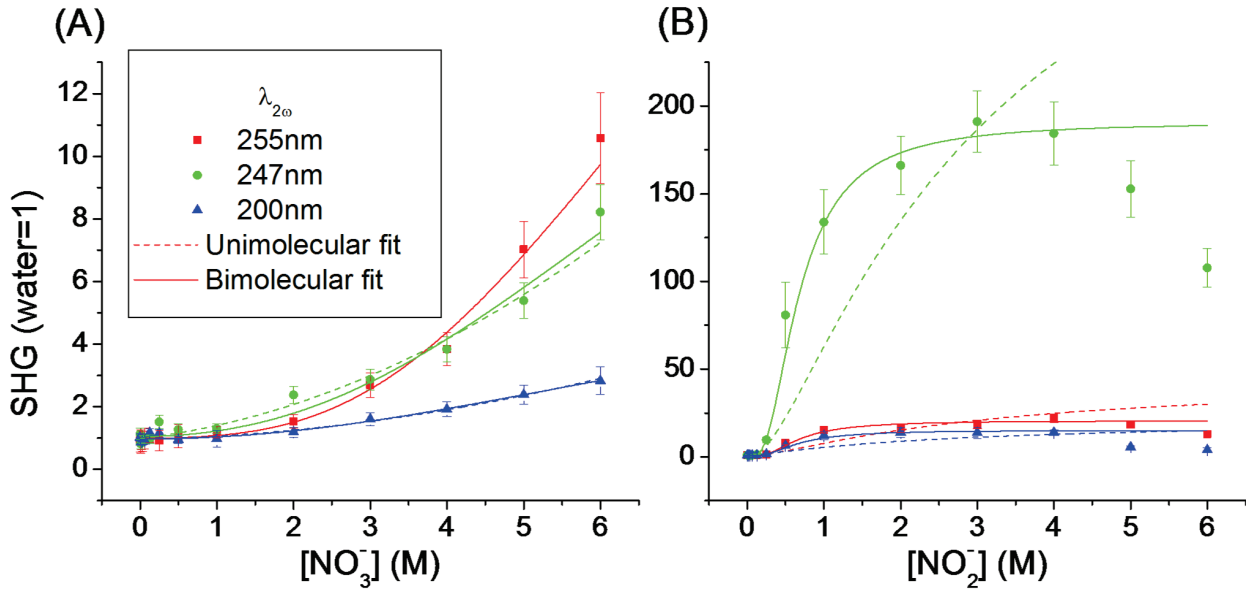

Figure 3.2- The second harmonic response of sodium nitrate (Panel A) and nitrite (Panel B) as a function of concentration. Error bars represent the pooled standard deviations of the underlying normalized data. Fits are against the unimolecular (dashed line) and bimolecular (solid line) models. The fit for the unimolecular model for sodium nitrate does not converge but is stable as shown (see text). The 200 nm and 255 nm unimolecular fits for sodium nitrate are indistinguishable from their respective bimolecular fits. The fits for sodium nitrite do not include values >4 M. Fit parameters and errors are presented in Table 3.1.

whereby the anion competes with water molecules for surface sites[4, 26-34]. It models the effective equilibrium:

$$\mathrm{W}S + \mathrm{X}^- \rightleftarrows \mathrm{W} + S\mathrm{X}^- \tag{3.1}$$

$$\mathrm{K}_\mathrm{U} = \frac{[S\mathrm{X}^-][\mathrm{W}]}{[S\mathrm{W}][\mathrm{X}^-]} = \frac{S\mathrm{X}^-[\mathrm{W}]}{(S_{\max} - S\mathrm{X}^-)[\mathrm{X}^-]}, \tag{3.2}$$

where S is one of $S_{\max}$ surface sites (all occupied by water molecules in the neat water interface). The usual simple Langmuir adsorption assumptions of non-interacting adsorbates and conservation of surface sites apply. As the interface is electroneutral, the cation must also be considered to adsorb to the interface region, although it is assumed to partition independently within this region, and the exchange model for a 1:1 electrolyte in aqueous solution can then be expressed as:

$$\mathrm{K_U} = \mathrm{K_U^{(+)}K_U^{(-)}} = \left(\frac{S\mathrm{X^-}\left[\mathrm{W}\right]}{\left(S_{\max} - S\mathrm{X^-}\right)\left[\mathrm{X^-}\right]} \right)^2 . \tag{3.3}$$

Here the surface sites for anion and cation are assumed to be independent, but the maximum number of surface sites are assumed to be equal for both. Rearrangement of 3.3 provides the number of surface anions in terms of the bulk concentrations of water and anion:

$$S\mathrm{X^-} = S_{\max} \frac{\left[\mathrm{X^-}\right]}{\left[\mathrm{W}\right]\mathrm{K_U^{-½}}\left[\mathrm{X^-}\right]} \tag{3.4}$$

The SHG signal as a function of bulk concentration of solute by this model is then[25]

$$\frac{I_{2\omega}}{I_{\omega}^2} = \left(A + B\frac{\left[\mathrm{X^-}\right]}{\left[\mathrm{W}\right]\mathrm{K_U^{-½}}\left[\mathrm{X^-}\right]} \right)^2 + \left(C\frac{\left[\mathrm{X^-}\right]}{\left[\mathrm{W}\right]\mathrm{K_U^{-½}}\left[\mathrm{X^-}\right]} \right)^2 , \tag{3.5}$$

where $\frac{I_{2\omega}}{I_{\omega}^2}$ is the intensity of the second-harmonic response normalized by the square of the incident intensity. The parameters A, B, and C, are proportional to the wavelength-dependent molar second-harmonic susceptibility of water, and the real and imaginary molar susceptibility components of the anion, respectively. The concentration of water is assumed to be constant at its neat value, 55.5 M. Equation 3.5 is then fit to the observed signal as a function of anion concentration with the four parameters A, B, C, and $\mathrm{K_U}$ as unknowns, allowing for the determination of the free energy of adsorption for the processes described by Equation 3.1.

For a bimolecular adsorption process, wherein two adsorbates are assumed to adsorb to the same surface site, this exchange model is expressed as:

$$\mathrm{W}S + \mathrm{X^-} + \mathrm{M^+} \rightleftarrows \mathrm{W} + \mathrm{M^+}S\mathrm{X^-} \tag{3.6}$$

$$\mathrm{M^+}S\mathrm{X^-} = S_{\max} \frac{\left[\mathrm{X^-}\right]\left[\mathrm{M^+}\right]}{\left[\mathrm{W}\right]\mathrm{K_B^{-1}} + \left[\mathrm{X^-}\right]\left[\mathrm{M^+}\right]} . \tag{3.7}$$

The SHG fit can be modified accordingly.

Table 3.1- Fit parameters for the data presented in Figure 3.2. The unimolecular model applied to NO_3^- does not converge.

Species		NO_3^-	Na^+ x NO_3^-	NO_2^-	Na^+ x NO_2^-
Model		Unimolecular	Bimolecular	Unimolecular	Bimolecular
χ^2/DoF		N/A	0.80	4.97	0.59
R^2		N/A	0.94	0.84	0.98
ΔG (kJ/mole)		N/A	-0.4 ± 1.0	-17.5 ± 1.4	-13.7 ± 0.2
255 nm	A	N/A	0.99 ± 0.04	0.95 ± 0.07	0.96 ± 0.02
	B	N/A	1.7 ± 2.0	-0.8 ± 2.0	-1.5 ± 0.5
	C	N/A	5.9 ± 1.3	6.9 ± 0.8	4.5 ± 0.1
247 nm	A	N/A	1.02 ± 0.02	1.04 ± 0.09	0.97 ± 0.02
	B	N/A	3.9 ± 1.1	-12.8 ± 3.5	-4.7 ± 1.4
	C	N/A	0*	17.4 ± 4.0	13.3 ± 0.5
200 nm	A	N/A	0.98 ± 0.02	0.84 ± 0.06	0.94 ± 0.02
	B	N/A	1.5 ± 1.0	3.8 ± 1.0	-0.5 ± 0.4
	C	N/A	0.6 ± 5.1	0*	3.9 ± 0.1

*Constrained to 0

The fits of these two models are presented in Figure 3.2 for sodium nitrate (Panel A) and nitrite (Panel B) at 293 K, the unimolecular fit as a dotted line, the bimolecular fit as a solid line. For nitrite the fits extend only to 4 M because of the marked decrease observed in the SHG signal thereafter, which clearly deviates from the model (discussed in the next section). For sodium nitrate, the unimolecular fit does not converge, a consequence of exceedingly weak adsorption on the SHG fit[4]:

$$\frac{I_{2\omega}}{I_{\omega}^2} \approx \left(A + B'[\mathrm{X}^-]\right)^2 + \left(C'[\mathrm{X}^-]\right)^2 \qquad [\mathrm{W}]\cdot \mathrm{K}_{\mathrm{U}}^{-1/2} >> [\mathrm{X}^-] \tag{3.8}$$

In such instances, the equilibrium constant becomes highly coupled to the other fit parameters, and cannot be determined by the intensity fit alone. For a few parameters, it was necessary to artificially constrain them to zero, as the fitting algorithm had difficulty converging when these values approached very small magnitudes ($<1\times10^{-6}$). The fit parameters generated can be found in Table 3.1. For all but the sodium nitrite bimolecular model, the reported errors in many of the parameters are very large.

To consider the possibility that the conjugate acid of nitrite played some role in the adsorption process, a unimolecular fit against calculated concentrations of $HONO$ was attempted, assuming a pK_a of 2.3 [35], and 3.3 [36]. The pH curve calculated for $pK_a = 3.3$ is reproduced in Figure 3.3. Similarly, the bimolecular fit against every combination of NO_2^- with HNO_2, H_3O^+, and OH^- was also attempted. These fits all failed to describe the data. An example of the failure of the unimolecular model to fit the nitrite concentration is reported in Figure 3.2 (dashed line).

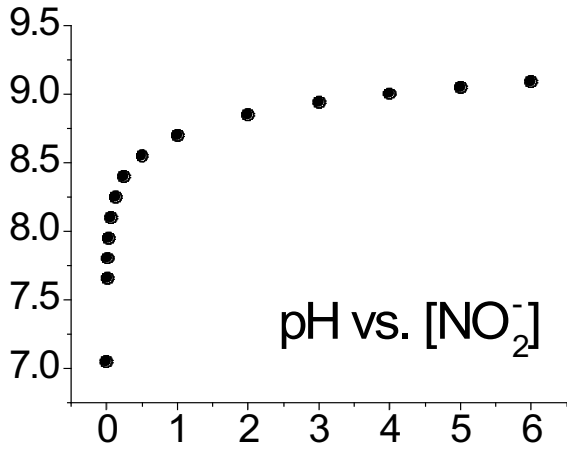

Figure 3.3- pH versus nitrate concentration for pK_a=3.3, used in attempts to model the possible effect of hydronium concentration of nitrite interface adsorption.

3.4. Discussion

The resonant detection of both nitrate and nitrite at molar bulk concentrations is strong evidence that these species are abundant in the interfacial region, although a bulk quadrupole response cannot be entirely ruled out[37]. In some previous resonant SHG studies of electrolytes[25, 30, 33, 38], the evidence favoring surface specificity of the signal was twofold: both the solvated analytes themselves and the bulk environment were inversion-symmetric. This indicated that, for a given molecule to become SHG active, it required the interface to break its molecular/electronic symmetry, as in the case for iodide and azide[25, 38, 39]. However, nitrate and nitrite are both inversion-asymmetric and the restriction for an SHG response is reduced entirely to the requirement of an anisotropic orientational distribution[40]. This is the same reason that water (also inversion-asymmetric) is VSFG responsive through two to three layers[41].

Whether concentration enhancement of these solutes at the outermost layer of liquid water is effected or not, it is clear from simulations and experiment that a strong gradient of nitrate concentration exists in the interfacial region, in some cases suggesting the stratification of anion/cation typical of that of alkali halide solutions (Figure 3.4)[5, 6, 19, 20, 42]. Schnitzer, *et. al.* attribute the

change in free-OH VSFG spectral intensity of 0.2*x* $NaNO_3$ solutions to an enhanced electric field at the interface due to stratified partitioning of the sodium and nitrate moieties below the interface[17]. This evidence suggests that the likely origin of the SHG resonant response of nitrate is from a buried surface layer, SHG active due to orientational ordering imposed by the nearby interface or by the electric field gradient resulting from stratified partitioning of the cation and anion. Unfortunately, there is little such simulation or experimental literature available for the consideration of interfacial nitrite, excepting that Brown, *et.al.* have determined that nitrite and nitrate appear to have similar interfacial distributions (Figure 3.5)[19]. Our probe depth for these inversion-asymmetric ions would extend through the region for which such net structure may exist. Based on the resonant wavelength shift observed for both nitrate and nitrite, it is clear that the electronic environments of the interfacial NO_x^- moieties probed are significantly different than those in bulk solution, although this shift cannot be quantified without a full spectrum of the SHG response.

As discussed in Chapter 2, interpretation of the adsorption free energies is suspect, except when compared against similarly modeled systems. However, consideration of the mechanism, based on the relative reactant order of the process, can provide more reliable information. The nitrite data was only reproduced by fitting to the bimolecular adsorption model, and only when Na^+ and NO_2^- were the species of adsorption. Models that considered hydronium-nitrite pairs, nitrous acid, and hydronium adsorption did not reproduce the data. These two experimental observations are convincing evidence that the adsorption nitrite to the interface is coupled to the adsorption of sodium in a concerted manner.

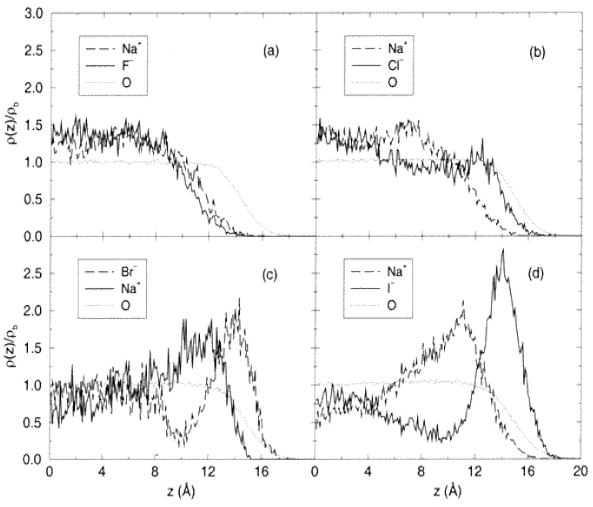

Figure 3.4- Density profiles from molecular dynamics simulations of 1.2 M sodium halides. Both anion and cation demonstrate a structured partitioning in the interface, with highly polarizable ions being adsorbed closer to the outermost layer of liquid density. *Reprinted with permission from* Jungwirth, P. and D.J. Tobias, *J. Phys. Chem. B*, **106**, 6361 (2002). *Copyright 2002 American Chemical Society.*

This result can be thought of in two ways: either anion adsorption to the interface requires concomitant cation adsorption (albeit, probably

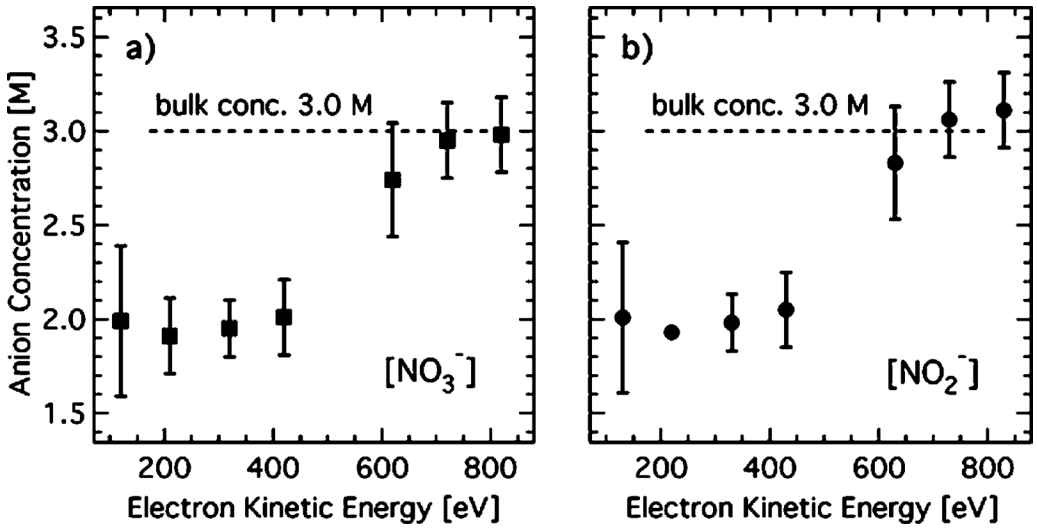

Figure 3.5- Photo-electron spectroscopy depth profiles of 3 M sodium nitrate and nitrite solutions in a liquid microjet. Electron kinetic energy reflects the relative depth of the originating NO_x^- species indicating a depletion of these ions near the interface. *Reprinted with permission from* Brown, M.A., B. Winter*, et al.*, *J. Am. Chem. Soc.*, **131**, 8354 (2009). *Copyright 2009 American Chemical Society.*

unevenly partitioned) due to electroneutrality of the interface, or the anion is explicitly paired with its cation in doing so. The difference is not semantic. In the former case, the anion may be uncorrelated with respect to its counter-ion, merely required to present in the interface but free to sample the roughly two-dimensional volume. However, the SHG data would then fit the unimolecular model which describes the independent adsorption of anion and cation. The latter mechanism requires a strong correlation of the anion and cation location, effectively treating it as a single species within the interface. This bimolecular model thus implicitly assumes the ion-pairing mechanism, *viz*. ions are assumed to adsorb to the same 'surface-site' and act statistically as a single species with respect to their translational partition function(s).

It is well established that in bulk solutions ion-pairing is generally enhanced in low-dielectric solvents[43]. In a lower dielectric medium, such as that of the interface[44], the effect of the dielectric reaction field is weakened and oppositely charged ions are more strongly attracted by Columbic forces. The stabilization of ion pairs of NaCl at the dichloroethane/water and air/water interfaces has been demonstrated in simulation[45, 46]. While image forces can still result in a net repulsion of an ion pair from the interface, these forces will also be reduced by the local charge neutralization, the image charges effectively being reduced to a large image dipole. While the results presented here do not necessarily indicate a

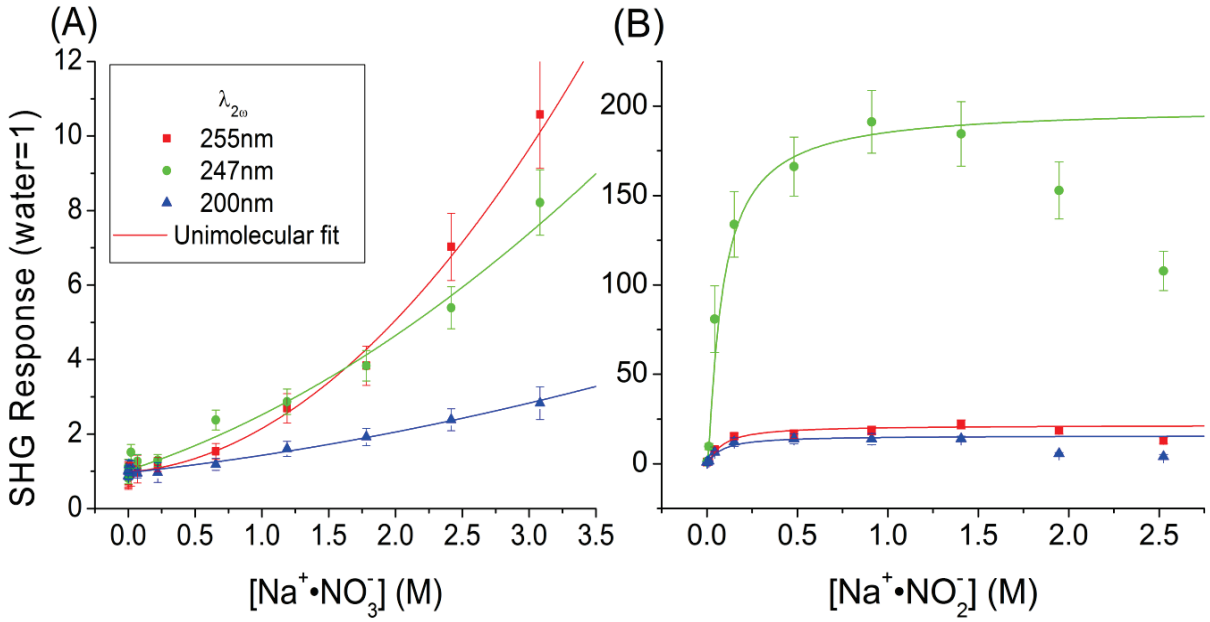

Figure 3.6- Unimolecular fits of ion-pair concentrations as calculated by the association constants of Simonin *et al.* presented in the text [47]. Fit parameters are found in Table 3.2. Otherwise as Figure 3.2**.**

net interfacial concentration enhancement (Chapter 2), they do seem to indicate that at molar concentrations of sodium nitrite, ion-pair interfacial solvation strongly dominates independent-ion interfacial solvation.

In the case of nitrate, this argument is less rigorous without a statistically meaningful unimolecular fit to compare with. Although the fit did not converge using the unimolecular model, the non-convergent fit is qualitatively very similar to the bimolecular fit. Nonetheless, the error in the parameters of the bimolecular fit is significant. This suggests that the apparent success of the bimolecular fit for nitrate is probably due to the weak dependence of the change in signal on bulk concentration even under this model, similar to the coupling described by Equation 3.8. Imposing a second order dependence on concentration is just enough to prevent complete coupling of the fit parameters to K_B^{-1} while still being strongly covariant. In fact, the simulations of Minofar, *et. al.* have examined the interfacial partitioning of the $Mg(NO_3)_2$, specifically looking considering ion-pairing at the interface for nitrate[6]. They find that the nitrate anion has a weak interface propensity and a negligible tendency for the ions to pair throughout their simulation slab.

Simonin *et al.* have semi-empirically calculated the association constants for both of these solutes in water under the mean spherical approximation[47].

For sodium nitrite the value is 0.209, while for sodium nitrate it is 0.362, nearly double that of nitrite. Using these association constants, the isotherms of Figure 3.2 were refit to unimolecular model using the calculated ion-pair concentrations for both systems, the results presented in Figure 3.6 and Table 3.2. The error in the parameters for the nitrate model continues to be large, and indicates that this fit is still not conclusive in spite of convergence. Alternatively, the nitrite model demonstrates excellent agreement and suggests the strongest free energy of adsorption yet observed for simple electrolytes[4, 25-28, 30-34, 38]. However, as discussed in Chapter 2, this value is only meaningful when compared between like modeled systems, and we have explicitly recognized that the *interfacial* adsorption described here does not imply the surface adsorption implied in earlier studies. Nonetheless, this result further supports the postulate that nitrite is adsorbing to the interface via ion-pairing.

The decline in SHG response at concentrations of >4 M suggests the development of greater inversion symmetry of the interfacial environment at high concentrations. The strong adsorption of sodium nitrite pairs to the interface, as well as the observed saturation of signal, also suggests that the population of adsorbate has likely reached capacity at ~4 M. At such saturations the development of the quaternary complexes of ions is probable, and would likely be quadrupolar in arrangement. Such arrangements could exhibit inversion symmetry (on a molecular level) which would effectively quench the SHG signal as these complexes are formed.

The results for nitrate under every scenario examined are consistent with studies that do not conclude strong interface adsorption, but do suggest a significant (*i.e.* observable) presence of nitrate in the interface[5, 6, 17, 18, 20]. This also agrees with

Table 3.2- Fit parameters for the data presented in Figure 3.6.

Species Model		$Na^+ \bullet NO_3^-$ Unimolecular	$Na^+ \bullet NO_2^-$ Unimolecular
χ^2/DoF		0.68	0.69
R^2		0.95	0.9791
ΔG (kJ/mole)		7 ± 50	-36.6 ± 0.4
255 nm	A	0.99 ± 0.04	0.97 ± 0.02
	B	30± 340	-1.6 ± 0.5
	C	204 ± 2000	4.6 ± 0.1
247 nm	A	1.02 ± 0.02	0.98 ± 0.03
	B	100 ± 1300	-5.6 ± 1.5
	C	0*	13.4 ± 0.6
200 nm	A	0.98 ± 0.02	0.95 ± 0.02
	B	40 ± 440	-0.6 ± 0.5
	C	50 ± 440	4.0± 0.1

*Constrained to 0

Brown, *et. al.*'s photoelectron depth profiling experiments which did observe molar concentrations of the nitrate but did not observe a local maximum of concentration near the surface[19].

The question arises as to why these two ostensibly very similar species may behave so differently. The results are ambiguous concerning the mechanistic order of adsorption of nitrate anions to the interface, while being strongly indicative of bimolecular adsorption for nitrite. In many studies[7, 28, 42, 48-50], the polarizability of the anion is found to be an order parameter for ion-specific interfacial adsorption. Marcus gives rough guides for the polarizability of these anions based on literature molar refractivity[51], with nitrate being 4.13 $Å^3$ and nitrite being 3.4 $Å^3$; although general agreement is that the polarizability of nitrate is larger than this and that its anisotropic nature is relevant to interface partitioning[5, 9, 52]. It seems reasonable, therefore, to suggest that the nitrate anion may be more likely than nitrite to partition independently to the interface, and less inclined rely ion-pairing to stabilize its approach towards the lower dielectric of the vapor phase.

3.5. Conclusions

The adsorption of nitrate to the air/solution interface appears to be weak but detectable by SHG in the interfacial region at molar bulk concentrations. The interfacial nitrate and nitrite anions exhibit an unquantified shift resonance enhancement that indicate that these interfacial species are in a different electronic environment than in the bulk. Considering the ubiquitous presence of these species in atmospheric aerosols and terrestrial water bodies, these ions may engender significant, yet presently unrecognized interfacial chemistry in aqueous systems. Similar surface-active halogens have already been shown to have dramatic effects on aqueous molecular bromine and chlorine production rates on aerosol surfaces in the presence of ozone[53, 54].

The apparent bimolecular adsorption mechanism of nitrite provides compelling evidence that the uppermost layer of sodium nitrite in solutions are likely ion-pairs, even at nominal bulk concentrations as low at 100 mM. These ions are likely to be preferentially adsorbed relative to individually solvated ions, owing to the zero net charge of the pair and the weaker dielectric of the interfacial region, but partitioning to the interfacial *surface* is unlikely based on the evidence from VSFG data[19]. This finding also suggests that simulations that do not consider the cation as a specific entity may not capture important effects

of a real electrolytic interface; the cation is apparently a critical component in the mechanism of sodium nitrite adsorption to the interface region at molar concentrations and may be the case for other systems as well.

3.6. References

1) Finlayson-Pitts, B.J. and J.M.J. Pitts, *Chemistry of the Upper and Lower Atmosphere*. 2000, San Diego: Academic Press.

2) Finlayson-Pitts, B.J., *Phys. Chem. Chem. Phys.*, "*Reactions at surfaces in the atmosphere: integration of experiments and theory as necessary (but not necessarily sufficient) for predicting the physical chemistry of aerosols*," **11**, 7760 (2009)

3) Xu, M., R. Spinney*, et al.*, *J. Phys. Chem. B*, "*Water Structure at the Air-Aqueous Interface of Divalent Cation and Nitrate Solutions*," **113**, 4102 (2009)

4) Otten, D.E., P.B. Petersen*, et al.*, *Chem. Phys. Lett.*, "*Observation of nitrate ions at the air/water interface by UV-second harmonic generation*," **449**, 261 (2007)

5) Thomas, J.L., M. Roeselova*, et al.*, *J. Phys. Chem. A*, "*Molecular Dynamics Simulations of the Solution-Air Interface of Aqueous Sodium Nitrate*," **111**, 3091 (2007)

6) Minofar, B., R. Vácha*, et al.*, *J. Phys. Chem. B*, "*Propensity for the Air/Water Interface and Ion Pairing in Magnesium Acetate vs Magnesium Nitrate Solutions: Molecular Dynamics Simulations and Surface Tension Measurements*," **110**, 15939 (2006)

7) Jungwirth, P. and D.J. Tobias, *J. Phys. Chem. B*, "*Molecular Structure of Salt Solutions: A New View of the Interface with Implications for Heterogeneous Atmospheric Chemistry*," **105**, 10468 (2001)

8) Tolbert, M.A., M.J. Rossi*, et al.*, *Geophys. Res. Lett.*, "*Heterogeneous interactions of chlorine nitrate, hydrogen chloride, and nitric acid with sulfuric acid surfaces at stratospheric temperatures*," **15**, 847 (1988)

9) Salvador, P., J.E. Curtis*, et al.*, *Phys. Chem. Chem. Phys.*, "*Polarizability of the nitrate anion and its solvation at the air/water interface*," **5**, 3752 (2003)

10) Finlayson-Pitts, B.J. and J.C. Hemminger, *J. Phys. Chem. A*, "*Physical Chemistry of Airborne Sea Salt Particles and Their Components*," **104**, 11463 (2000)

11) Hauglustaine, D.A., F. Hourdin*, et al.*, *J. Geophys. Res.*, "*Interactive chemistry in the Laboratoire de Météorologie Dynamique general circulation model: Description and background tropospheric chemistry evaluation*," **109**, D04314 (2004)

12) Cicerone, R.J., *Science*, "*Changes in Stratospheric Ozone*," **237**, 35 (1987)

13) Stutz, J., B. Alicke*, et al.*, *J. Geophys. Res.*, "*Nitrous acid formation in the urban atmosphere: Gradient measurements of NO2 and HONO over grass in Milan, Italy*," **107**, 8192 (2002)
14) Zafiriou, O.C. and R. Bonneau, *Photochem. Photobiol.*, "*WAVELENGTH-DEPENDENT QUANTUM YIELD OF OH RADICAL FORMATION FROM PHOTOLYSIS OF NITRITE ION IN WATER*," **45**, 723 (1987)
15) Nevison, C. and E.A. Holland, *J. Geophys. Res., [Atmos.]*, "*A reexamination of the impact of anthropogenically fixed nitrogen on atmospheric N2O and the stratospheric O3 layer*," **102**, 25519 (1997)
16) Davidovits, P., C.E. Kolb*, et al.*, *Chem. Rev.*, "*Mass Accommodation and Chemical Reactions at Gas-Liquid Interfaces*," **106**, 1323 (2006)
17) Schnitzer, C., S. Baldelli*, et al.*, *J. Phys. Chem. B*, "*Sum Frequency Generation of Water on NaCl, $NaNO_3$, $KHSO_4$, HCl, HNO_3, and H_2SO_4 Aqueous Solutions*," **104**, 585 (2000)
18) Cheng, J., C.D. Vecitis*, et al.*, *J. Phys. Chem. B*, "*Experimental Anion Affinities for the Air/Water Interface*," **110**, 25598 (2006)
19) Brown, M.A., B. Winter*, et al.*, *J. Am. Chem. Soc.*, "*Spatial Distribution of Nitrate and Nitrite Anions at the Liquid/Vapor Interface of Aqueous Solutions*," **131**, 8354 (2009)
20) Dang, L.X., T.-M. Chang*, et al.*, *J. Phys. Chem.*, "*On NO_3^-–H_2O interactions in aqueous solutions and at interfaces*," **124**, 066101.1 (2006)
21) Wang, X.-B., X. Yang*, et al.*, *J. Chem. Phys.*, "*Photodetachment and theoretical study of free and water-solvated nitrate anions, $NO_3^-(H_2O)_n$ (n = 0-6)*," **116**, 561 (2002)
22) Goebbert, D.J., E. Garand*, et al.*, *J. Phys. Chem. A*, "*Infrared Spectroscopy of the Microhydrated Nitrate Ions $NO_3(H_2O)_{1-6}$*," **113**, 7584 (2009)
23) Pegram, L.M. and M.T. Record, *J. Phys. Chem. B*, "*Thermodynamic Origin of Hofmeister Ion Effects*," **112**, 9428 (2008)
24) Collins, K.D., *Biophys. J.*, "*Charge density-dependent strength of hydration and biological structure*," **72**, 65 (1997)
25) Petersen, P.B., J.C. Johnson*, et al.*, *Chem. Phys. Lett.*, "*Direct experimental validation of the Jones-Ray effect*," **397**, 46 (2004)
26) Petersen, P.B., R.J. Saykally*, et al.*, *J. Phys. Chem. B*, "*Enhanced Concentration of Polarizable Anions at the Liquid Water Surface: SHG Spectroscopy and MD Simulations of Sodium Thiocyanide*," **109**, 10915 (2005)

27) Petersen, P.B. and R.J. Saykally, *J. Phys. Chem. B*, "*Probing the Interfacial Structure of Aqueous Electrolytes with Femtosecond Second Harmonic Generation Spectroscopy*," **110**, 14060 (2006)
28) Petersen, P.B. and R.J. Saykally, *Annu. Rev. Phys. Chem.*, "*On the nature of ions at the liquid water surface*," **57**, 333 (2006)
29) Petersen, P.B. and R.J. Saykally, *J. Phys. Chem. B*, "*Evidence for an Enhanced Hydronium Concentration at the Liquid Water Surface*," **109**, 7976 (2005)
30) Petersen, P.B. and R.J. Saykally, *J. Am. Chem. Soc.*, "*Adsorption of Ions to the Surface of Dilute Electrolyte Solutions: The Jones-Ray Effect Revisited*," **127**, 15446 (2005)
31) Petersen, P.B., *Dissertation: Surface Structure of Aqueous Electrolyte Solutions Probed by UV Second Harmonic Generation*, in *Department of Chemistry*. 2005, University of California, Berkeley: Berkeley.
32) Petersen, P.B. and R.J. Saykally, *Chem. Phys. Lett.*, "*Is the liquid water surface basic or acidic? Macroscopic vs. molecular-scale investigations*," **458**, 255 (2008)
33) Onorato, R.M., D.E. Otten*, et al.*, *J. Phys. Chem. C.*, "*Measurement of Bromide Ion Affinities for the Air/Water and Dodecanol/Water Interfaces at Molar Concentrations by UV Second Harmonic Generation Spectroscopy*," **114**, 13746 (2010)
34) Onorato, R.M., D.E. Otten*, et al.*, *Proc. Natl. Acad. Sci. USA*, "*Adsorption of thiocyanate ions to the dodecanol/water interface characterized by UV second harmonic generation*," **106**, 15176 (2009)
35) das Graças Gomes, M., S. da S.S. Borges*, et al.*, *Anal. Chim. Acta*, "*UV-visible spectrum of nitrous acid in solution: pKa determination and analytical applications*," **282**, 81 (1993)
36) Wetters, J.H. and K.L. Uglum, *Anal. Chem.*, "*Direct spectrophotometric simultaneous determination of nitrite and nitrate in the ultraviolet*," **42**, 335 (1970)
37) Shen, Y.R., *Applied Physics B*, "*Surface contribution versus bulk contribution in surface nonlinear optical spectroscopy*," **68**, 295 (1998)
38) Petersen, P.B. and R.J. Saykally, *Chem. Phys. Lett.*, "*Confirmation of enhanced anion concentration at the liquid water surface*," **397**, 51 (2004)
39) Petersen, M.K., S.S. Iyengar*, et al.*, *J. Phys. Chem. B*, "*The Hydrated Proton at the Water Liquid/Vapor Interface*," **108**, 14804 (2004)
40) Boyd, R.W., *Nonlinear Optics*. Second ed. 2003, San Diego: Academic Press.

41) Allen, H.C., N.N. Casillas-Ituarte*, et al.*, *Phys. Chem. Chem. Phys.*, "*Shedding light on water structure at air-aqueous interfaces: ions, lipids, and hydration*," **11**, 5538 (2009)
42) Jungwirth, P. and D.J. Tobias, *J. Phys. Chem. B*, "*Ions at the Air/Water Interface*," **106**, 6361 (2002)
43) Marcus, Y. and G. Hefter, *Chem. Rev.*, "*Ion Pairing*," **106**, 4585 (2006)
44) Benjamin, I., *Chem. Rev.*, "*Static and Dynamic Electronic Spectroscopy at Liquid Interfaces*," **106**, 1212 (2006)
45) Schweighofer, K. and I. Benjamin, *J. Chem. Phys.*, "*Ion pairing and dissociation at liquid/liquid interfaces: Molecular dynamics and continuum models*," **112**, 1474 (2000)
46) Wick, C.D., *J. Phys. Chem. C.*, "*NaCl Dissociation Dynamics at the Airâˆ’Water Interface*," **113**, 2497 (2009)
47) Simonin, J.-P., O. Bernard*, et al.*, *J. Phys. Chem. B*, "*Real Ionic Solutions in the Mean Spherical Approximation. 3. Osmotic and Activity Coefficients for Associating Electrolytes in the Primitive Model*," **102**, 4411 (1998)
48) Dang, L.X., *J. Phys. Chem. B*, "*Computational Study of Ion Binding to the Liquid Interface of Water*," **106**, 10388 (2002)
49) Ghosal, S., J.C. Hemminger*, et al.*, *Science*, "*Electron Spectroscopy of Aqueous Solution Interfaces Reveals Surface Enhancement of Halides*," **307**, 563 (2005)
50) Ishiyama, T. and A. Morita, *J. Phys. Chem. C.*, "*Molecular Dynamics Study of Gasâˆ’Liquid Aqueous Sodium Halide Interfaces. I. Flexible and Polarizable Molecular Modeling and Interfacial Properties*," **111**, 721 (2006)
51) Marcus, Y. and G. Hefter, *Chem. Rev.*, "*Ion Pairing*," **2006**, 4585 (2006)
52) Netz, R.R., *Curr. Opin. Colloid Interface Sci.*, "*Water and ions at interfaces*," **9**, 192 (2004)
53) Knipping, E.M., M.J. Lakin*, et al.*, *Science*, "*Experiments and Simulations of Ion-Enhanced Interfacial Chemistry on Aqueous NaCl Aerosols*," **288**, 301 (2000)
54) Hunt, S.W., M. Roeselová*, et al.*, *J. Phys. Chem. A*, "*Formation of Molecular Bromine from the Reaction of Ozone with Deliquesced NaBr Aerosol: Evidence for Interface Chemistry*," **108**, 11559 (2004)

Chapter 4 - Surface Adsorption and Photochemistry of Aqueous Alkali Thiocyanates

4.1. Introduction

The liquid-vapor interface of water is expected to be a region of reduced dielectric constant, owing to the restricted geometries of interfacial water and the decrease in density attending evolution into the vapor phase[1-6]. The process of moving a charged species from regions of high to low dielectric necessarily involves the expenditure of work, implying an increase in potential energy of the system[7, 8]. The considerable recent evidence supporting the concept of small anion partitioning into the interface has motivated efforts to elucidate the mechanism for the apparent spontaneity of this process. The major driving force is currently believed to be volume exclusion from the hydrogen-bond network, augmented by inductive forces unique to the interface[3, 5, 9-13].

Previous investigations have demonstrated the exergonic behavior of anion adsorption to the air/water interface under the assumption of a Langmuir-type adsorption model, wherein the anion is assumed to partition to the interface in a competitive equilibrium with water molecules for a conserved number of surface sites[14-22]. In this chapter, we extend these studies to examine the temperature dependence of the free energy of adsorption for potassium thiocyanate determined in this manner. This initial candidate species has two key characteristics which facilitate the present study: a) thiocyanate is already known to be quite strongly adsorbed to aqueous solution interfaces, and b) the thiocyanate anion is found to have the strongest second-harmonic (SH) charge-transition-to-solvent (CTTS) response of any anion studied thus far by this method[3, 5, 9-13]. The observed SH susceptibility for molar bulk concentrations of thiocyanate exceeds 100 times that of the neat water surface. Thus, we can expect that the temperature dependence of the surface concentration will be detectable over a meaningful range of temperatures that can be accessed with the experiments employed here.

Although this study was initiated with the aim to observe the temperature dependence of thiocyanate adsorption to the solution interface, it was found that molar concentrations of sodium and potassium thiocyanate suffered from initially unexplained changes in SH response as a function of time. The first section describes the diagnostics undertaken to determine the origin of these changes,

and the determination of the necessary experimental parameters to execute the temperature dependent study in light of this observation. We then follow with the report of the results of the temperature dependent study itself.

4.2. Ultraviolet Photochemistry of Thiocyanates

When molar concentrations of sodium and potassium thiocyanate were probed herein at 410 nm and 386 nm (205 nm and 193 nm SH), photochemical products were evident to the naked eye. At low concentrations (>0.5 M), a white suspension formed along the transmitted beam path in the solutions and, at higher concentrations (>5 M), this suspension phase-separated into white droplets that would descend through the solution to settle at the base of the Petri dish. When the sighting laser was operational (see Chapter 2), the suspension was observable to the naked eye even in the millimolar regime as it readily scattered the visible 635 nm light. This effect was not observed in studies employing a lower energy probe wavelength of 532 nm, and was unreported at higher energies used in other studies of similar systems[15, 23].

A turbid solution generated in such a manner was preserved for weeks, protected only by the Petri dish cover but otherwise exposed to the ambient conditions of the laboratory environment. In such conditions, the turbidity slowly decreased and eventually disappeared. The white dispersion is attributed to the formation of sulfur oligimers and elemental sulfur, as the observations reported here are consistent with those reported by Dogliotti and Haydon in their flash photolysis study of thiocyanate solutions[24]. In their work, solutions of <~10^{-4} M became turbid after exposure to deep ultraviolet flashes of an oxygen flash lamp. They also noted that the solution gave off the smell of $H_2S_{(g)}$ which we also observed when the sample was removed from the sample chamber in the absence of nitrogen purging. After Dogliotti and Haydon's observations, Luria and Treinin subsequently followed up with a study of this photochemistry of thiocyanate in aqueous solution, determining the reaction scheme[25]:

$$SCN^- \overset{h\nu}{\rightleftharpoons} SCN^{-*} \quad SCN^- \overset{h\nu}{\rightleftharpoons} SCN^{-*} \tag{4.1}$$

$$SCN^{-*} \longrightarrow \left(CN^- + S\right)_{cage} \quad SCN^{-*} \longrightarrow \left(CN^- + S\right)_{cage} \tag{4.2}$$

$$SCN^- + \left(S + CN^-\right)_{cage} \longrightarrow 2CN^- + S_2 \quad SCN^- + \left(S + CN^-\right)_{cage} \longrightarrow 2CN^- + S_2 \tag{4.3}$$

$$nS_2 \longrightarrow S_{2n} \quad nS_2 \longrightarrow S_{2n}\,, \tag{4.4}$$

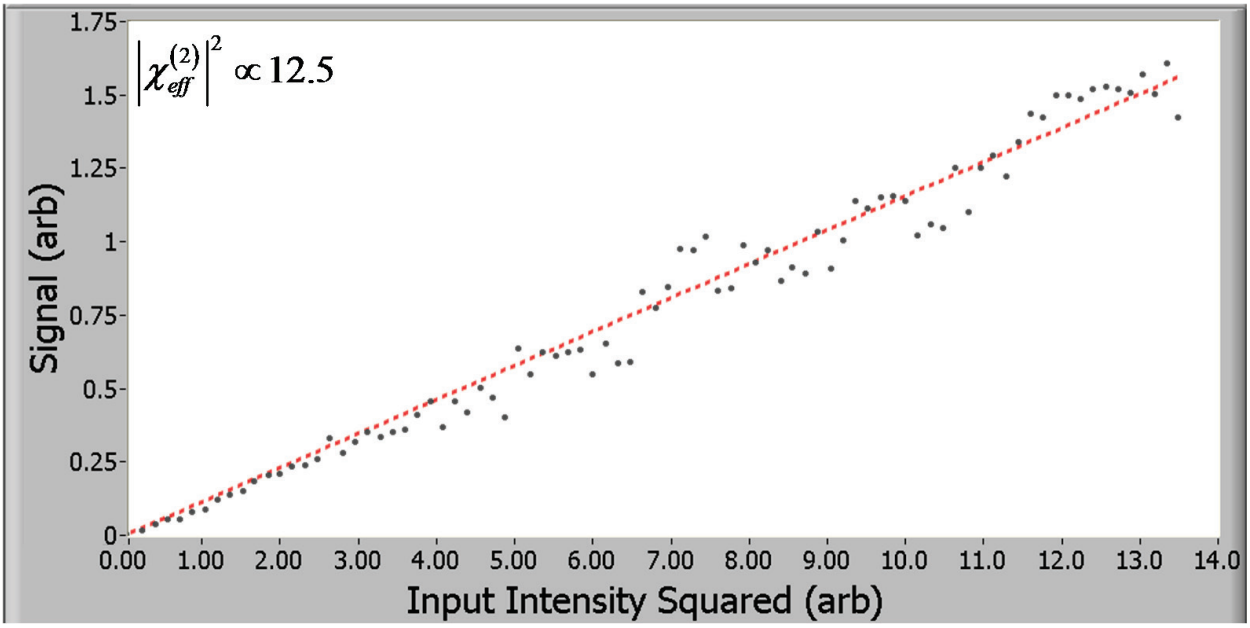

Figure 4.1- Initial power dependence profile (t=0 minutes) of 4.7 NaSCN at 205 nm. The proper second order power dependence is observed (red, dashed line). Selected observations of this solution over time can be found in Figure 4.2, and the complete data for the series is plotted in Figure 4.3.

where the parenthesis indicate that the products are still within their solvent cage. The reverse reaction to regenerate SCN^- is slow, especially in polar solvents, and is hindered by the formation of elemental S_8 in the form of a strong ring structure[26].

To examine this further, power dependence profiles were collected as a function of time for a 4.7 M NaSCN solution. These profiles are collected using the power modulation scheme described in Chapter 2. Briefly, they entail modulating the incident intensity cyclically at a repetition rate of ~1 Hz, and the response is collected over a period of 3 minutes. Figure 4.1 is an example of a typical profile for 410 nm irradiation of fresh NaSCN solutions (4.7 M, 205 nm SH), characterized by the correct second-order power dependence of the signal. A few selected profiles are presented as a series in time for this solution in Figure 4.2. KSCN solutions were found to behave similarly.

It is clear from Figure 4.2 that over a period of minutes the second harmonic was no longer second-order in incident power. The profiles can be effectively split into two domains that *are* second-order, in which the susceptibility (defined by the slope of the linear portions of the profile) is constant as a function of the square of intensity (x-axis). These have been indicated in the figures by black lines. We refer to these domains as a high-intensity domain (HID)

and a low-intensity domain (LID). Over time it is evident that the LID increases its intensity domain, and over the period of an hour the LID makes up the entirety of the observed power dependence profile. The HID concurrently 'shifts' to higher unobserved intensities. The profiles are not dependent on whether power modulation progresses from low to high intensities, or vice-versa. Figure 4.3 plots the change in HID and LID susceptibilities over time. The HID susceptibility appears to increase at roughly the same rate that the LID susceptibility decreases. There is currently insufficient data available to draw more conclusions about the time dependence of the HID as it progresses to intensities that are inaccessible/unobserved after ~45 minutes.

This effect was observed for concentrations >3 M, and were difficult to quantify reproducibly. Sometimes the solutions would provide stable second-order signals for tens of minutes, while for other solutions the HID region could progress beyond the observable incident intensities on the timescale of minutes. The effect was also more pronounced at higher concentrations and was not observed at lower concentrations (<3 M). Some solutions were allowed to age after preparation in their sealed Pyrex volumetric flasks for hours before measurement, but were found to exhibit equivalent initial signals. Therefore solution age alone is not a factor. No experiments were performed on solutions allowed to age in the presence of oxygen, excepting the oxygen that was available to the solutions in the headspace of their flasks. Figure 4.4 is a plot of some observed trends with time for a series of concentrations; the data presented use the slope of the weighted regression line (red, dashed lines in Figure 4.1 and Figure 4.2) of the entire power profile as the measure of the susceptibility reported in this figure. The higher concentration (>3 M) signals decreased in time, while lower concentrations signals remained stable for hours.

The conditions of the samples from storage to measurement undergo two changes that may serve as an initiation for the process: exposure to oxygen and exposure to the irradiation of the pump beam. Exposure to oxygen was not well-controlled, as the samples are transferred from the preparation bench to the apparatus in a Petri dish, and on dispensation, these solutions are also exposed to the lab environment. Between each measurement, the sample must be removed from the nitrogen environment of the sample chamber while reference measurements are made. The exposure to the ambient environment is an unavoidable part of the experiment due to the design of the apparatus and the effect of oxygenation remains unexplored.

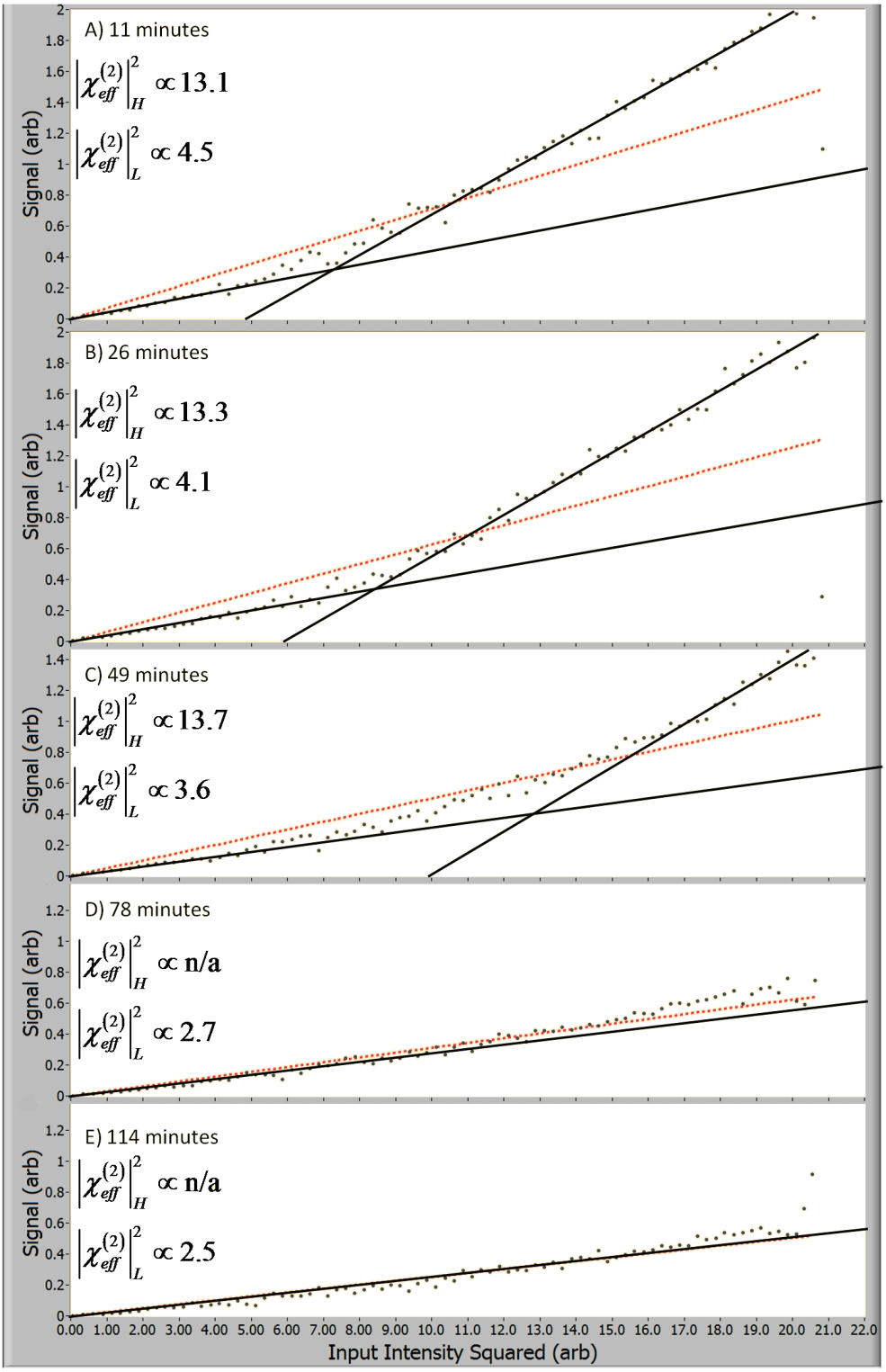

Figure 4.2- 4.7 M NaSCN power dependence profiles as a series in time for 410 nm irradiation. Solid (black) lines are fit by hand to the apparent slopes of the low (*L*) and high (*H*) intensity domains discussed in the text. Effective susceptibilities are indicated for each. The dotted (red) line is the weighted regression line, usually representing the measured susceptibility of the sample when second-order power dependence is obeyed. Time t=0 was taken on a different scale and is presented in Figure 4.1. The complete data for the series is plotted in Figure 4.3.

A slow kinetic structural change at the interface is ruled out as mixing the exposed solutions by repipetting had negligible effect, also suggesting that the evolving SHG response is not due to oxidation by air. The evidence seems to point to a chemical change in the system itself, and the obvious photochemistry occurring suggests a likely cause. The 7.0 M solution declines more rapidly than does the 4.7 M solution, indicating a concentration dependence. This is corroborated by the stability of the signals generated from lower concentration solutions. Lower concentration solutions (<3 M) do not exhibit this behavior over the time period studied, and suggest that the concentration dependence of the process is either greater than first order in SCN^- concentration, or that any changes occurring in the more dilute solutions are below our ability to resolve them.

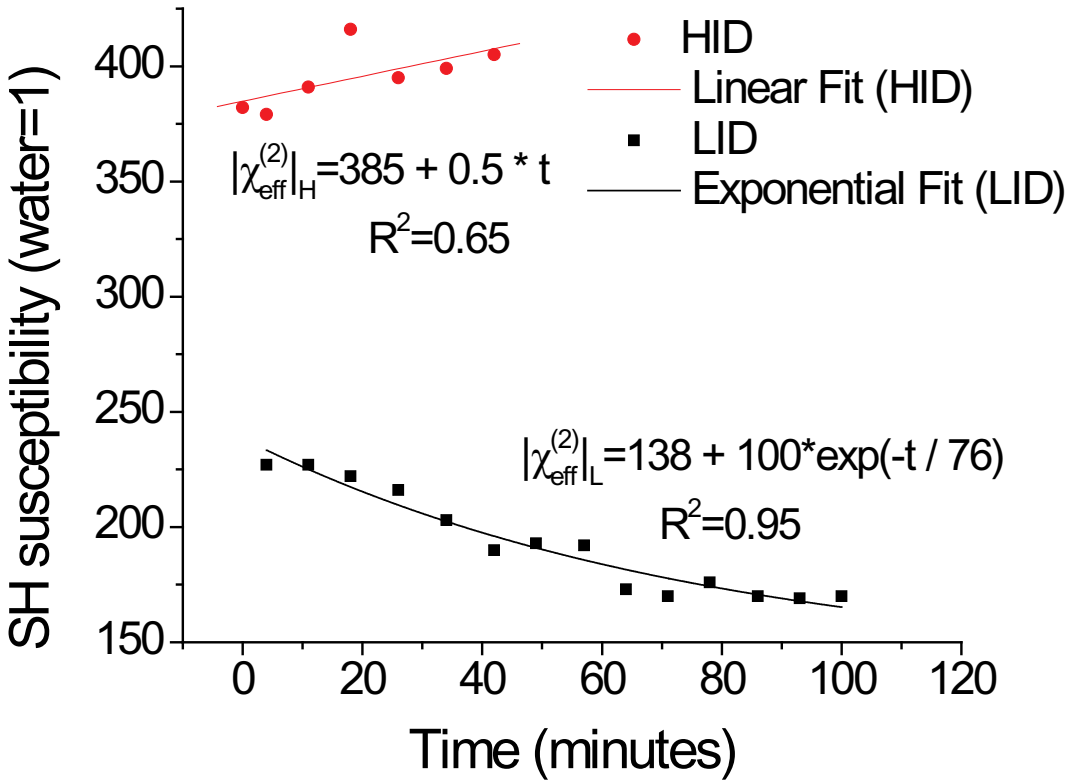

Figure 4.3- High (HID) and Low (LID) intensity domain $\left|\chi^{(2)}_{eff}\right|^2$ values of a 4.7 M NaSCN solution as a function of time. The increase in the high intensity regime response appears roughly offset by the decrease of the low intensity regime response, and the low intensity response appears to decay exponentially. Insufficient data is available for the high concentration domain to draw conclusions beyond its trend in time.

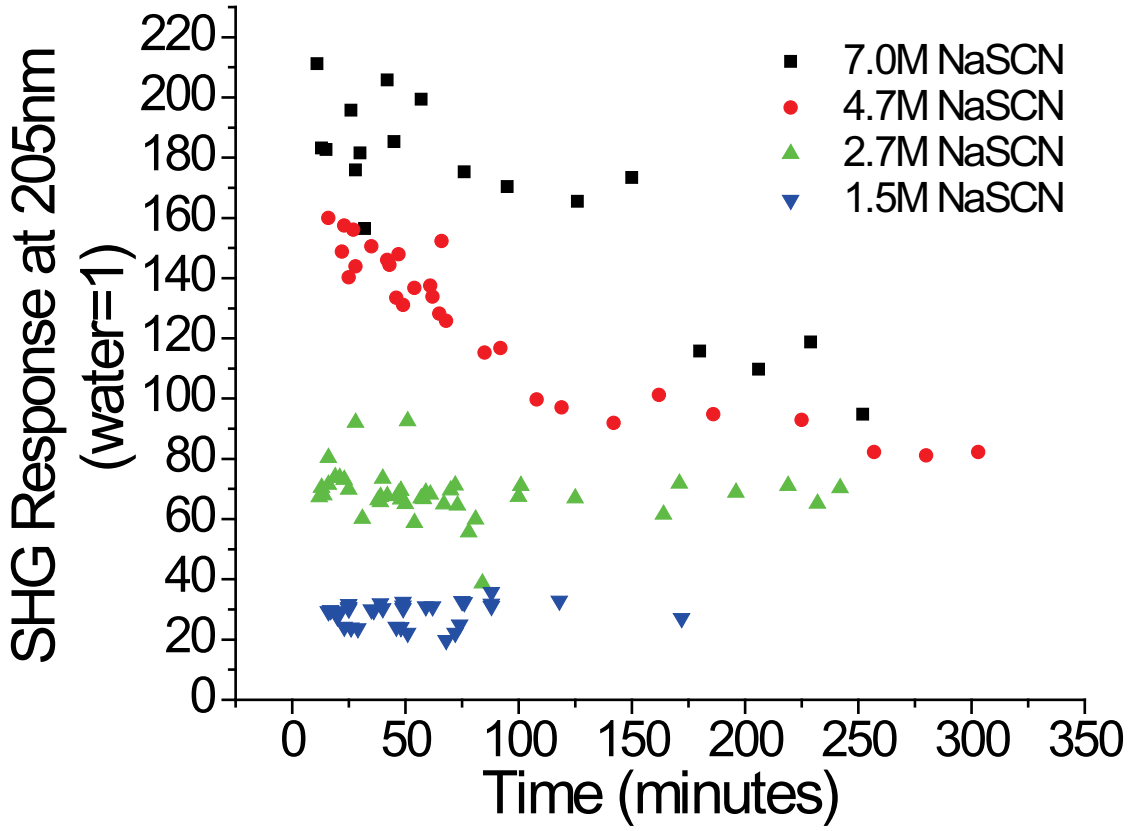

Figure 4.4- Observed SHG response (at 205nm) of various concentrations of sodium thiocyanate as a function of time. For low concentrations the signal is stable, but at concentrations exceeding ~3 M the signal is observed to decline as a function of time. The high concentration signals appear to be converging to the signal observed at 2.7 M.

The high intensity domain susceptibility (HID, Figure 4.3) clearly derives from the initial susceptibility. Based on the large concentration of thiocyanate, and the similarity of the surface second harmonic spectrum to that of bulk sodium thiocyanate (Figure 4.5)[18], we can infer that the HID is due entirely to the response of thiocyanate. The power dependence profile features appear to comprise two second-order responses (*e.g.* HID & LID) with a transition domain between them. Since the LID susceptibility is less than the HID susceptibility, we can postulate that when that in the intensity domain that we observe the LID: (A) there is less thiocyanate responding, (B) some new species is either masking, displacing, or destructively interfering with the thiocyanate response or (C) the orientation of thiocyanate is changing as a function of intensity. We can immediately eliminate (C) as a possibility, as the only feasible mechanism for this would be photo-induced heating of the sample. In this scenario we would expect the greater randomization of orientation to reduce, rather than increase the

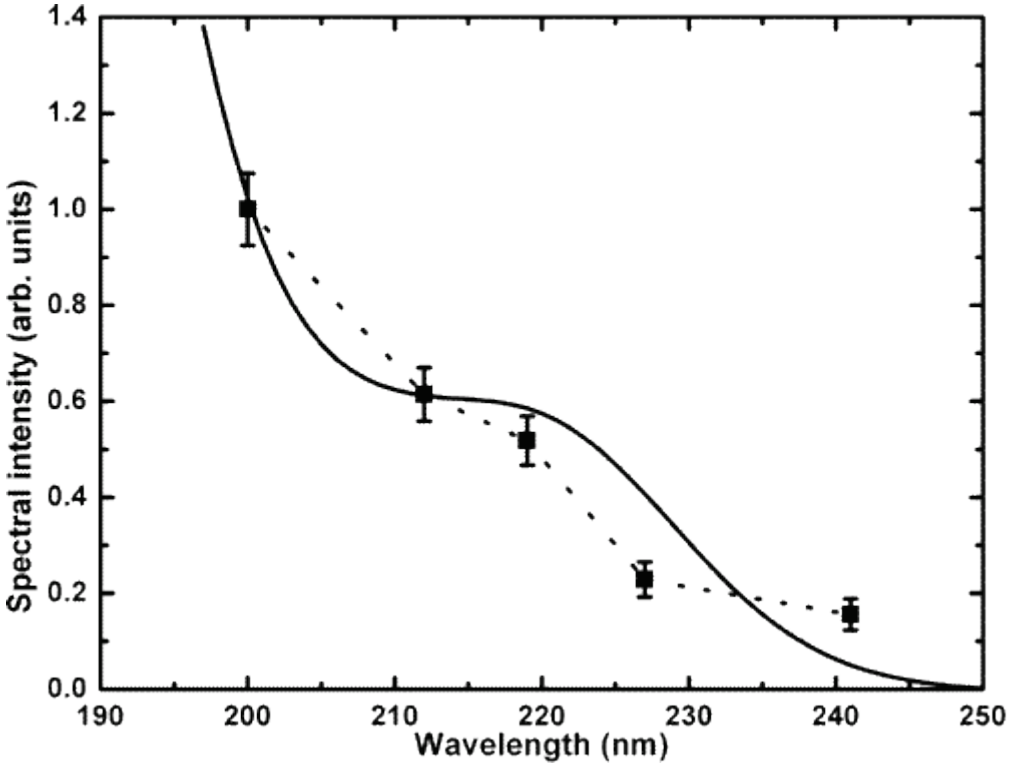

Figure 4.5- The bulk NaSCN absorption spectrum (solid line) and surface second harmonic spectrum of [18]. *Reprinted with permission from* Petersen, P.B., R.J. Saykally*, et al.*, *J. Phys. Chem. B*, **109**, 10915 (2005). *Copyright 2005 American Chemical Society.*

response as a function of power[27]. It is difficult to rationalize (A), but it is conceivable that at higher intensities SCN^- is somehow liberated from a non-SHG-responsive state to a responsive one. Since we have already excluded localized heating as a possibility, this invokes the idea of 'a new species' anyway, so we consider (B) as the most likely scenario.

Assuming some other species (hereafter, *B*) exists to limit the SH response of SCN^- to our signal, it appears that at higher intensities *B* either no longer responds, or is no longer present. It is apparent from Figure 4.2 that, as a function of time, the domain of the LID increases to higher intensities. Since it takes more intensity to induce the same effect (as a function of time) this indicates that the species must be increasing in quantity over time. Figure 4.3 demonstrates that not only does the LID domain increase, but the LID susceptibility also decreases, appearing to stabilize in the limit of long time. This also suggests that the number density of *B* saturates in the long-time domain. What we are left with is a species that isn't strongly SH active, yet present in the interface such that it either displaces or masks the signal of thiocyanate.

The intensity dependence of the susceptibility of species *B* would require at least weak resonance with either the fundamental or second-harmonic wavelengths for any appreciable interaction to occur. As a first approximation one could then model the SHG power dependence profile as a function of the time-dependent concentration of a hypothetical *B,* and the intensity dependent attenuation of the response of *B*:

$$\chi_{eff}^{(2)}(t,I) = \chi_{SCN^-,eff}^{(2)} + \left(\beta_{B,eff}^{(2)} N_B(t)\right) e^{-(\alpha I^n)} \tag{4.5}$$

where the attenuation of the signal is assumed to be due to an *n*-photon resonance with an attenuation/absorption coefficient of α. Fits of this function were made assuming that the complex phase between *B* and SCN^- did not change as a function of time, for both one and two-photon resonances. Neither fit provided results that were consistent with the assumption that both the thiocyanate effective susceptibility was a constant, and represented the entirety of the initial observed response. Similarly we considered the possibility that both the effective populations of *B* and thiocyanate were changing. The susceptibility of thiocyanate in Equation 4.5 is then expressed as

$$\chi_{SCN^-,eff}^{(2)}(t,I) = \chi_i^{(2)} + \Delta\chi_{SCN}^{(2)}\left(1 - e^{-(\alpha I^n)}\right), \tag{4.6}$$

where $\chi_i^{(2)}$ is the initial effective susceptibility and $\Delta\chi_{SCN}^{(2)}$ represents some empirical change observed at the limit of high intensities. This scenario also did not fit the data.

A different approach is to consider the possible identity of *B* based on the likely species that are present in the solution on irradiation. The most numerous species that these conditions engender are S_n, and CN^-, due to the photochemistry previously discussed. As the probe is two-photon resonant with the thiocyanate CTTS transition we could consider radical reaction products as possibilities, but clearly *B* must have lifetimes on the order of hours or greater.

The lowest energy electronic transition for cyanide in aqueous solution is <180 nm and we exclude cyanide on this basis. We do so with the caveat that interfacial anions resonances have previously been observed to undergo strong bathochromic shifts, the magnitude of which could place much of this transition into SH resonance[17, 28]. Elemental sulfur and sulfur oligimers are also strong

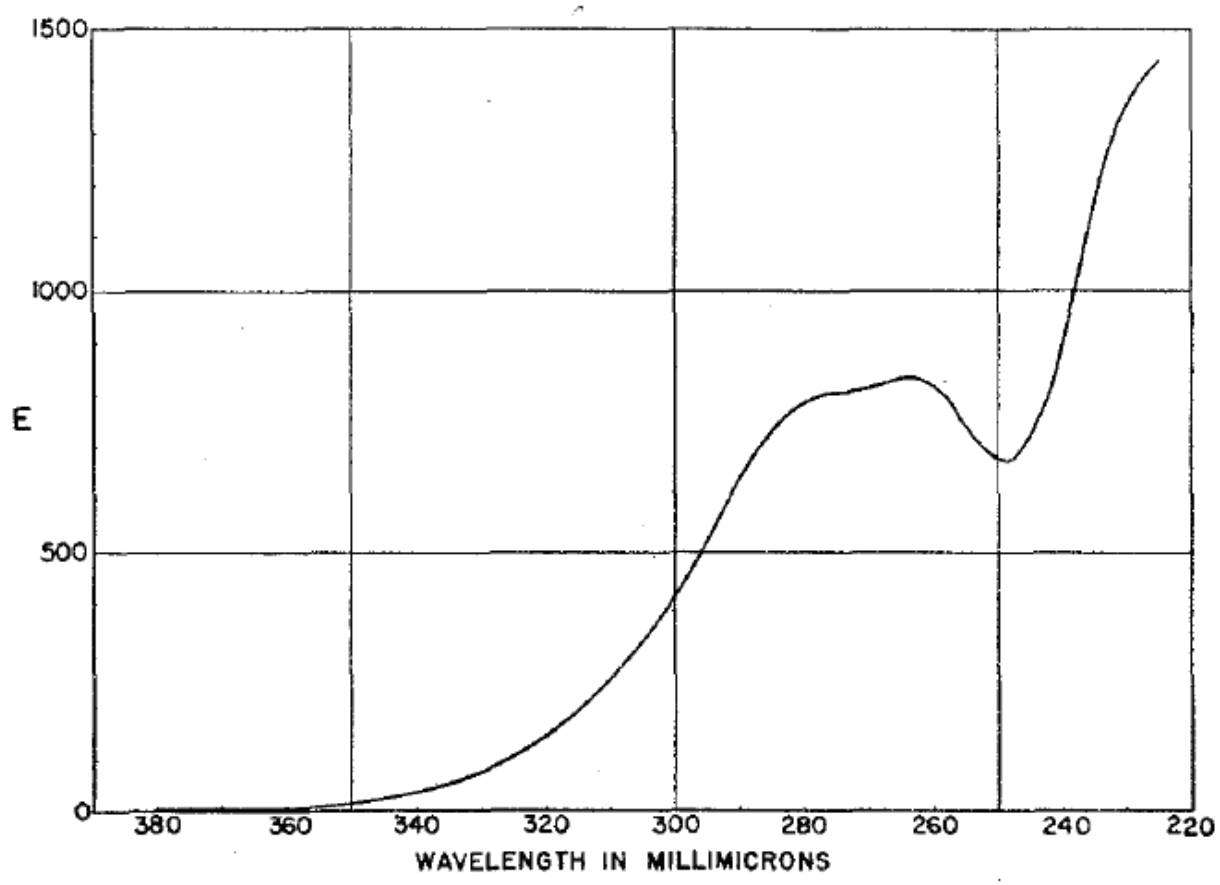

Figure 4.6-The ultraviolet spectrum of elemental sulfur in aqueous solution, interpolated from observed spectral changes observed on progressing from non-polar to polar solvents. The extinction coefficient E is expressed in terms of an absorbance calculated in base 10. The spectrum indicates that we are strongly two-photon resonant with sulfur. *Reprinted with permission from* Baer, J.E. and M. Carmack, *J. Am. Chem. Soc.*, **71**, 1215 (1949). *Copyright 1949 American Chemical Society*.

candidates for *B* in this respect due to their strong, broad UV absorptions (Figure 4.6) [29, 30].

Of these two candidates arguments can also be made regarding their respective propensities for the interface. Interfacial affinity appears to follow polarizability as an order parameter, followed closely by (and correlated with) ionic radius[3, 5, 12, 31]. Cyanide is relatively small and unpolarizable, slightly less polarizable than chloride, for which studies have indicated a negligible affinity for the interface[12, 32]. On this basis we can likely exclude it from being directly involved in the observed decrease of SHG, especially when considered in concert with the spectrum of aqueous cyanide. However, elemental sulfur and sulfur oligimers could be present in the interface, as their large size and non-polar

character makes them difficult to solvate in the bulk solution, as reflected by their low solubility[26, 29].

Under UV irradiation, elemental sulfur becomes much more susceptible to sulfur cyanolysis (abstraction of sulfur atoms), the reaction rate increasing by at least two orders of magnitude[26]. The usual rate limiting ring-opening step is mediated by the absorption of UV light:

$$S_{8,\text{ring}} \xrightarrow{h\nu} S_{8,\text{linear}} \tag{4.7}$$

$$S_n + CN^- \rightleftarrows S_{n-1} + CNS^- \tag{4.8}$$

If sulfur oligimers do reside in the interface, especially if partitioned closer to the interface than thiocyanate, it would impact the SH signal in an intensity-dependent fashion. Under low intensity conditions, there would be a net absorption of any SHG light generated from thiocyanate in sub-layers, effectively masking the pure-thiocyanate solution signal, although the sulfur itself would concomitantly add its own resonant response with its own characteristic phase, which could also interfere destructively to add to this effect. The ring form and linear oligmers display inversion symmetry however, and are unlikely to contribute significantly compared to the strong thiocyanate response. At high intensities, we could envision that the two-photon induced reaction of 4.7 then proceeds, breaking the sulfur ring and making it available for cyanolysis. The conjugated pi system of the resulting sulfur oligimers would be steadily reduced in length by succeeding (fast) cyanolysis reactions, and we could anticipate that the UV absorption band would first hypsochromically shift and then vanish as the oligmers are consumed[26].

Thus, at high intensity, two effects on the SHG signal would be observed: the first being the unmasking of the thiocyanate response, and the second being a local increase in the concentration of thiocyanate as a reaction product. Figure 4.3 supports this possibility explicitly, as the HID response is observed to increase beyond its initial value in concert with the increase of the LID domain (*i.e.* more sulfur is available to generate thiocyanate as a photo product). The data for this is unfortunately limited, but if it were possible to continue to observe the HID response as a longer function of time, we would anticipate that the HID susceptibility would saturate in concert with the LID saturation (~76 min for the solution shown, Figure 4.4), provided enough cyanide remains local to the probe region over the course of the reaction/observation. Consideration of the UV

absorption spectrum of sulfate (Figure 4.6) suggests that the phenomenological equations of 4.5 and 4.6 may have been unsuccessful due to the failure to include both one- and two- photon contributions, especially if there is a significant surface-induced bathochromic shift of the absorption bands. However, fitting with the assumption of two separate unknown attenuation/absorption coefficients was also found to be over-parameterized.

The changing nature of the UV second harmonic signal as a function of time is indicative of a systematic change in the solution itself, appearing to only occur at very high concentrations of thiocyanate (>3 M). Recently an SHG study of the dodecanol/thiocyanate solution at similar wavelengths demonstrated that the adsorption of thiocyanate to this interface deviated from the simple Langmuir model above 4 M concentrations for both potassium and sodium thiocyanate[23]. A general structural change of the interface above these concentrations was offered in explanation. The VSFG study of Viswanath and Motchmann directly probed the thiocyanate CN stretch and determined that the interface is saturated at approximately 3 M bulk concentrations of potassium thiocyanate[33]. The results of the present study also suggest a change in the nature of the interface at these concentrations, although the change in our case appears to be as a function of time and exposure to intense ultraviolet radiation.

While consideration of the transient nature of high concentration sodium thiocyanate solution SH has not yet yielded definitive conclusions, there does seem to be evidence for the surface adsorption of a photo-chemically generated species, possibly elemental sulfur, being expelled from the bulk solution. There is a low concentration limit (~3 M), below which this dynamic behavior is not observed over the timescale of the experiments. This scenario would be consistent with the results of previous studies that suggest a structural or compositional limit at ~3 M [23, 33]. However macroscopic measurements of surface tension and surface potential do not suggest any unusual surface properties in this concentration regime[34]. The observed limit may also be explained simply by the second-order rate limiting step of Reaction 4.3, which would be highly dependent on the local availability of thiocyanate to proceed and would compete with the fast geminate recombination of caged (CN^- + S).

Synthesis of the above conclusions suggests that the aqueous sodium thiocyanate interface may allow for photoproducts such as elemental sulfur to be more readily presented at the solution surface at high (>3 M) concentrations, and that the hypothesized structural/compositional changes of the interface at these

bulk concentrations may have a role in enhancing this process. Indeed, structural changes of the interface may be may be a general feature of nitrile-type solutions at these concentrations of solute[35]. The possibility for unique chemistry at the interface of highly concentrated thiocyanate solutions exists, wherein non-polar solutes such as sulfur may have an enhanced surface propensity relative to low concentration thiocyanate solutions. Such a conclusion is not at odds with thiocyanate's strong 'salting-in' behavior in the Hofmeister series, as this comparison would have to be made against other anions' ability to do the same[36, 37]. Instead one would infer that solutions of ions which are less 'structure-breaking' would exclude sulfur at lower concentrations.

Several questions are left unanswered in this study that merit further exploration, the role of oxygen being one of the more notable. Similarly, the possibility of long-lived radicals or radical reaction products was not considered, largely owing to the significant increase of complexity once these processes are invoked. Nonetheless, the potential for the presence of such species near the interface is interesting. The dithiocyanate radical anion, for example, has lifetimes greater than milliseconds in low concentration solutions, and may build up over the course of a measurement as the repetition rate of the laser is 1 kHz [38]. The reactions of dithiocyanate can lead to thiocyanogen as a possible product, elusive in aqueous solutions due to a high rate of hydrolysis, but somewhat stabilized in the presence of high concentrations of thiocyanate[39]. Thiocyanogen has recently been reported to be found in (transient) equilibrium with trithiocyanate[40, 41], a pseudo-halogen equivalent of triiodide. All of these species have strong adsorptions in the near UV and could be readily probed by this method or a pump-probe setup of the same[24, 25, 38, 41, 42]. In fact, an informal (not presented) survey of molar triiodide/iodide solution found that the SHG response was over two orders of magnitude stronger than equivalent concentrations of iodide.

4.3. The Temperature Dependence of Potassium Thiocyanate Surface Adsorption

The preceding section of study was initiated in the interest of establishing the experimental conditions necessary for the temperature dependent study of thiocyanate adsorption to the interface. In this respect, we have been able to conclude that at concentrations up to 3 M, performing measurements on only fresh solutions, and avoiding the use of high incident power at high

concentrations should permit an accurate assessment of the SHG response of such solutions without the attending photochemical complications.

4.3.1. ***Experimental***

The optical design of the apparatus employed is described generally in Chapter 2. The second harmonic signal was collected for five different temperatures, ranging from 1°C to 40°C, and for nine concentrations ranging from 10^{-3} M to 3 M (at room temperature). Incident intensities used were systematically decreased at higher concentrations to avoid the previously discussed exposure effects, and in extreme cases, to remain in the photon-counting regime of collected signal. In preliminary experiments no systematic bias was observed owing to the reduction in power, other than the avoidance of such artifacts as described above. Pulse energies varied from $2.5 - 0.2\ \mu\mathrm{J \cdot pulse^{-1}}$ at 386 nm with a repetition rate of 1 kHz, providing a power density at the sample surface of $< 5\ \mathrm{mJ \cdot cm^{-2} \cdot pulse^{-1}}$.

The apparatus sample chamber was reconstructed to allow for thermal control of the sample itself, and consisted of a thermoelectrically stabilized aluminum block that was kept in contact with the base and sides of the sample dish. K-type thermocouples were used to monitor temperature of the solutions *in-situ*, inserted to the middle of the solution bulk (~5 mm deep). Sample dishes were matched such that reproducible placement of the meniscus with respect to the focal volume was achieved, and the same sample and reference dishes were used (distinctly) throughout the study. Dry nitrogen was flowed across the nearby optics to prevent condensation on the optical faces at higher temperature measurements.

The original design was intended to control local air temperature and humidity by passing conditioned nitrogen over the sample surface. The insulation of the feed line for the nitrogen proved insufficient, however, and for the range of solution temperatures studied we were unable to generate a like-temperature nitrogen flow over the samples. Likewise, owing to the insulation issue, high-temperature humid nitrogen-flows generated condensation within the feed line and tended to leak condensate onto the sample surface.

Comparison of humid- versus dry-nitrogen flows at room temperature, as well as warm versus cold, proved to have no noticeable effect on the magnitude of SHG observed from water or solutions. Evaporation rates were found to trend as expected, observed by the rate of sample surface movement out of the focal

plane of the incident beam. The lack of change in the signal over these permutations, coupled with the unfortunate inability to control the atmosphere as intended, led to the choice of a low flow (half that necessary to perturb reflection of the probe beam) of dry room temperature nitrogen, such that, at a minimum, the atmosphere was controlled and consistent throughout these experiments. Thus, all measurements are performed with a jacketing atmosphere of 0% humidity room temperature (19.5 ±1 °C) nitrogen.

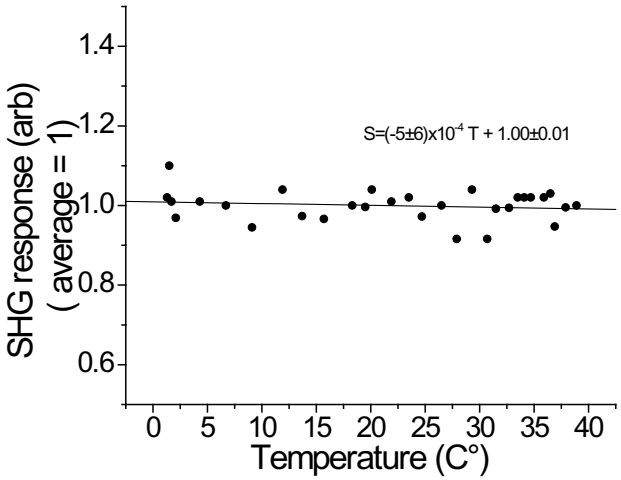

Figure 4.7- Water SHG response at 193nm as a function of temperature, normalized to the average value of the set. There is no trend within error.

Signal acquisitions were made under the constant-intensity method as noted in Chapter 2 (*i.e.* power was not modulated), with a 30 second window for each acquisition. Measurements were taken as the largest average of any three consecutive acquisitions as the sample height was scanned through the focal volume. Only one measurement is made per aliquot of water or sample and then the aliquot is discarded (due to the photochemical complications mentioned earlier). A normalized sample measurement is generated by the bracketing method described in Chapter 2 against a fresh water reference. The data presented in Figure 4.8 are the average of three to five normalized measurements, and the error bars presented are the standard deviations of that average. In most cases the standard deviation is <3% of the observed intensity.

After each measurement, the sample dish, reference dish, and pipettes used were re-rinsed thoroughly at the bench, and then rinsed again at the sample chamber prior to measurement. Solution glassware was rinsed one further time with the solution of interest. Glassware and solutions were pre-heated or chilled to reduce thermal equilibration time in the sample chamber prior to measurement. Prior to each day of measurements or sample preparation, the laboratory was swept and both the sample chamber and the local area to the experiment dusted by compressed air.

Consistent with previous studies[43, 44], the water response has no identifiable trend in the range of temperatures studied (Figure 4.7), and

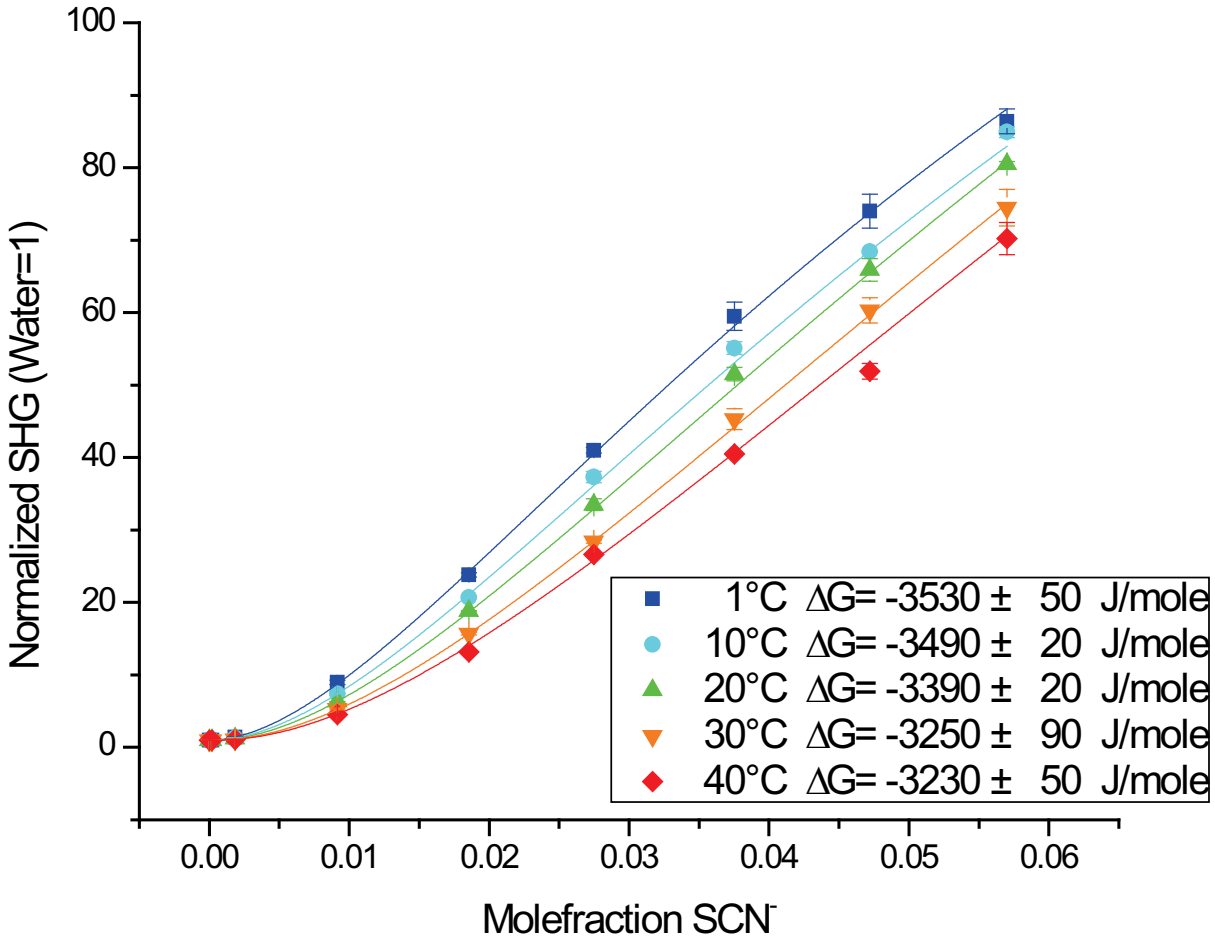

Figure 4.8- SHG response as a function of mole fraction SCN^- for the temperatures studied and the corresponding unimolecular Langmuir fits to the data. Temperatures are rainbow ordered from cold (blue) to hot (red). Error bars are the standard deviation of 3-5 measurements.

accordingly, the temperature of water was not directly monitored to avoid cross-contamination between subsequent water and sample measurements via the thermocouple. The small standard deviation of measurements indicates that this simplification had negligible impact on the normalization scheme.

The Langmuir fits used are those described as the unimolecular and bimolecular models presented in Chapter 2. However, in this study, the mole-fraction equivalent of each is used to provide a temperature-independent measure of concentration. The use of the unimolecular model herein is equivalent to previous similar studies but free energies differ by a factor of ½ owing to the explicit inclusion of the cation in the equilibrium expression. While the bimolecular model did not give a good fit of the data collected for this

T (°K ,±1)	G (kJ/mole)	A	B	C
274	-3.53 ± 0.04	0.991 ± 0.004	0.4 ± 0.3	16.2 ± 0.4
283	-3.49 ± 0.02	0.997 ± 0.001	-0.4 ± 0.2	16.8 ± 0.1
293	-3.39 ± 0.02	0.992 ± 0.004	-0.7 ± 0.2	18.1 ± 0.1
303	-3.25 ± 0.09	0.992 ± 0.003	-1.2 ± 0.8	19.5 ± 0.8
313	-3.23 ± 0.05	1.002 ± 0.004	-2.0 ± 0.3	20.0 ± 0.5

Table 4.1- Fit parameters for the unimolecular SHG/Langmuir model fit to the data presented in Figure 4.8. Error in temperature is the maximum range of temperatures measured.

experiment, the retention of the cation in the unimolecular model is still used for internal consistency.

4.3.2. ***Results***

The fits of the unimolecular Langmuir/SHG model to the collected data are plotted in Figure 4.8, and the resulting parameters are presented in Table 4.1. The bimolecular model failed to fit the data. The free energy for the adsorption process at 293°C is in agreement (within statistical error) with the results of Onorato, *et. al.* for the dodecanol/water interface but disagree by 0.7 kJ (~20x combined standard deviations) from those of Petersen, *et. al.*[18, 23]. Comparison of the absolute magnitudes of Petersen's measurements with those of the previous section suggests that that their work may have suffered from the photochemical effects described herein. Similarly, that work was performed under the constant water concentration assumption, which can lead to negative shifts in the determined free energy of the order of the observed difference, whereas the present study relies on the use of mole fraction measurements of concentration for both water and solute. The results presented here support Onorato's assertion that the lower dielectric constant of the dodecanol monolayer should result in weaker image charge repulsion of ions from the interface, whereas previously this assertion was found to be in conflict with the Peterson *et al.* study.

The net change in absolute SHG response due to increasing temperature is clearly negative, and can be attributed either to a change in SHG cross-section and/or a reduction in the number of molecules contributing to the signal. The change in cross-section could result from two possible mechanisms: a reduction in the net orientation of the surface solutes, or a shift in the energy of the CTTS transition.

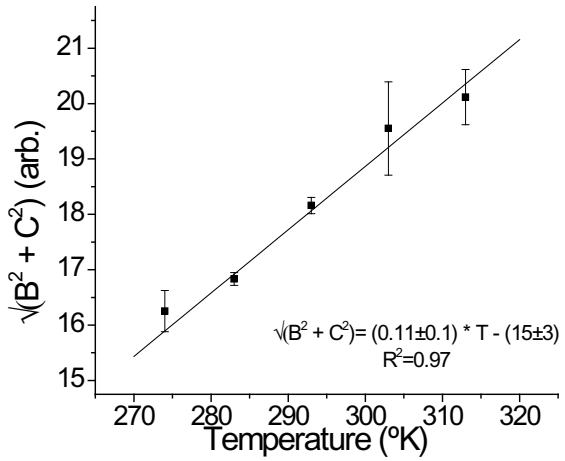

Figure 4.10- The magnitude of the effective susceptibility of thiocyanate as a function of temperature.

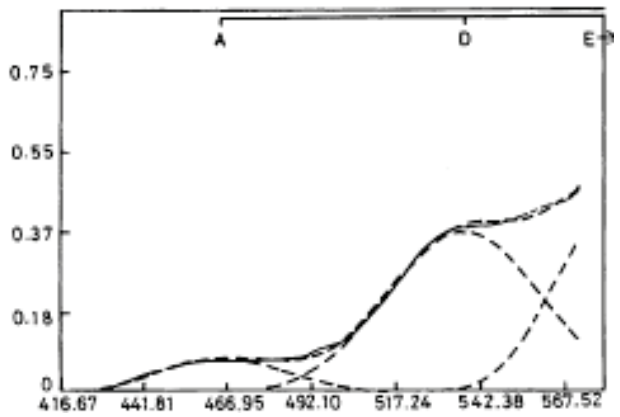

Figure 4.9- Gaussian deconvolution of the ultraviolet absorption spectrum of ~5mM tetramethyl-ammonium thiocyanate at 274°K. The *x*-axis is in units of 10^2 cm^{-1} and the *y*-axis is absorbance. The A, D, and E bands are indicated. *Reproduced from* Fox, M.F., C.B. Smith*, et al., J. Chem. Soc., Faraday Trans. 1*, **77**, 1497 (1981) *with permission of the Royal Society of Chemistry.*

The net orientation of the molecules can be expected to become more isotropic as thermal fluctuations increase the sampling of higher-energy configurations that would otherwise restrict the orientation of the molecules[27]. This would reduce the second-order surface susceptibility, as the randomization reduces the orientational average of the molecular hyperpolarizability. Several studies have used this effect as a probe of molecular order[44-48]. As the magnitude of the extracted susceptibility is observed to increase with temperature, either the energy of the CTTS maximum is shifted towards 193nm at higher temperatures or the overall transition moment has increased (Figure 4.9).

Previous studies have determined that the surface spectrum of thiocyanate in this region is equivalent to that of bulk thiocyanate, excepting a slight (2-3 nm) hypsochromic shift due to the ionic atmosphere[18]. In bulk solution it is well established that the oscillator strength of a CTTS transition is conserved as a function of temperature, and that the transition maximum undergoes a bathochromic shift with increasing temperature[49]. These properties are generally considered identifying characteristics of CTTS transitions[50]. The specific transition probed at 193 nm, identified as the D band by Fox, *et al.*, is centered at 187 nm at 274°K and is relatively free from overlapping transitions (Figure 4.10)[49]. We then expect that the resonant enhancement of the signal should increase as temperature is increased. The D-band transition-energy temperature coefficient reported in their work is $-36.5\ \mathrm{cm^{-1}\cdot K^{-1}}$, and the thermal

shift of the transition maximum can then be calculated. The observed increase in SHG susceptibility with temperature correlates well with our expectations (Figure 4.11). Thus, the (susceptibility increasing with temperature) effect of the resonant peak shift on the observed susceptibility is less than (susceptibility decreasing) effect of thermal randomization of the molecules themselves.

Figure 4.12 plots the free energy of adsorption for the process

$$H_2O \cdot S^{(+)} + H_2O \cdot S^{(-)} + SCN^- + K^+ \rightleftarrows 2H_2O + SCN^- \cdot S^{(-)} + K^+ \cdot S^{(+)}, \quad (4.9)$$

as function of temperature. The linear fit of this plot provides the standard entropy and enthalpy for this process

$$\Delta G^{\circ}_{ads} = \Delta H^{\circ}_{ads} - T\Delta S^{\circ}_{ads}, \quad (4.10)$$

which are found to be ΔH°_{ads} =-5.9 ± 0.2 kJ·mole^{-1} and ΔS°_{ads} =-8 ± 1 J·mole^{-1}·K^{-1}.

4.3.3. ***Discussion***

Significant effort has gone into explaining the affinity of large, polarizable anions for the air/solution interface[1-13]. In general the 'largeness' has been considered the driving force, *viz*. the energetic cost of cavitation in the bulk is reduced by expelling these ions from the hydrogen bonding network. The polarizable component has been considered extensively, specifically in concert with the ionic component, as the polarizability is invoked to counteract the large energetic cost of desolvating an ion as it protrudes into the lower dielectric. These efforts have met with significant success. Molecular dynamics simulations employing polarizable potentials demonstrated the potential for anionic concentration enhancement at the air/water interface[51-53]. The effects of polarizability have since been embodied in applied dielectric continuum theory in novel ways that allow for such enhancements to be modeled as well.

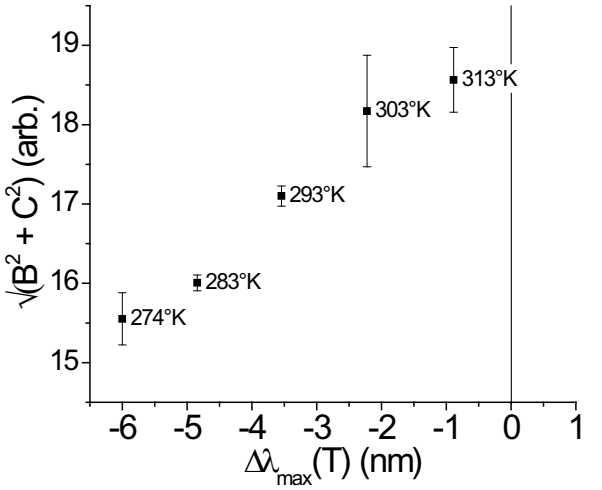

Figure 4.11- Observed thiocyanate susceptibility versus the difference between the calculated resonant wavelength and the probe wavelength based on the temperature coefficient of [50]. This confirms the expected bathochromic shift of the D band as temperature is increased.

Levin's work describes a simple sphere that is allowed to redistribute its charge asymmetrically as it protrudes into a lower dielectric[10, 54]. By empirically fitting only one parameter (the sodium ionic radius), he is able to reproduce the surface tension and surface potential for the sodium halide series, while simultaneously establishing concentration maxima for polarizable anions at the interface.

Noah-Vanhoucke and Geissler have taken a slightly different approach and found that with the proper selection of radii and charge, even non-polarizable spheres can be adsorbed to the interface, provided that interface is allowed to fluctuate in response to the ion[55]. They demonstrate that, when the surface can fluctuate in response to the perturbing ion, the benefits of expelling the ion cavity can actually be realized on approach to the Gibbs dividing surface, before the electrostatic cost of desolvation is paid. For polarizable ions, these fluctuations can delay the electrostatic cost to even further migration into the vapor phase. Their conclusion suggests that this effect may be a general characteristic of polar liquids with fluctuating interfaces.

These theories attempt to reconcile the large electrostatic cost of moving an ion towards the interface and all rely on cavitation as the primary driving force. For small inorganic ions, this force is entirely entropic in nature[56]. The effect of polarization, though enthalpically favorable, is merely to reduce the exothermic cost of dehydrating the solute. In this regard, the results obtained here are quite surprising. Not only is the adsorption process found to be exothermic, but it is also found to be entropically unfavorable.

In the broadest terms, the enthalpic result indicates a stronger average potential energy of interaction in the system as the adsorption process proceeds, and the entropic result indicates a corresponding weak increase in system correlations. As the system is described (*e.g.* the exchange of water and solute), these properties

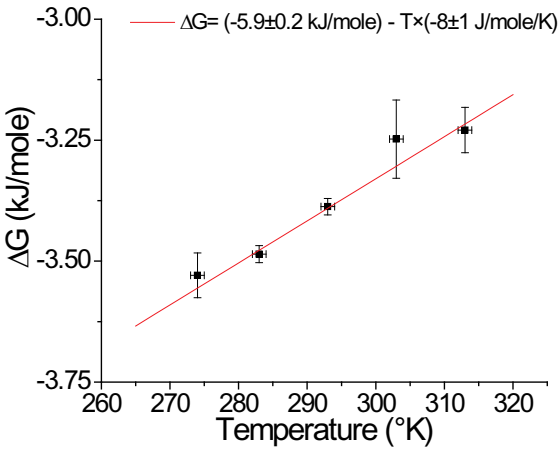

Figure 4.12- Plot of the free energy of adsorption vs. temperature as determined by the unimolecular model fits to the data (Figure 4.8). The adsorption of potassium thiocyanate to the interface by this model is exothermic, with a slightly negative change in entropy.

are due to both the removal of water from the interface region and the insertion of solutes into it. If the ion were required to partially desolvate in the process of moving to the surface, the net change in enthalpic energy would entail: a) the reduction of the ion-dipole interactions of the ion with its solvation shell while, b) simultaneously increasing the dipole-dipole interactions of the water resolvating in the bulk. The relative magnitudes of these energies suggest this process, as described, should not be exothermic. These results reasonably exclude any significant desolvation effects as part of the mechanism that drives the ions towards the surface. This conclusion effectively prohibits a molecularly close approach of thiocyanate to the vapor phase unless some mechanism is envisioned to overcome this effect.

As discussed in Chapter 3, thiocyanate, like nitrite and nitrate, is an inversion asymmetric polyatomic molecule, for which a second-harmonic response is not molecularly forbidden. Thus, the second-harmonic signal observed can quite feasibly originate from any environmentally asymmetric region that allows for a net orientation of the molecules. The study of thiocyanate adsorption to the dodecanol/water interface at 293°K yielded similar free energies to those obtained in this study, despite the termination of the water structure by hydrogen bonds[23]. That similarity suggests that there is little impact on the adsorption process due to the nature of the interface itself, a conclusion rationalized by considering the observed signal to be developed beneath the "surface" (which we take to be the outermost layer of liquid density). To the limit that we disallow desolvation, we are still left with, at best, a relatively neutral enthalpic change and have not addressed the entropic nature of the process.

As implicated for the sodium nitrite system, the mechanism of ion pairing seems a likely candidate to explain the exothermicity. There are several arguments against this proposition, however. Although there are exceptions, CTTS transitions are strongly affected by the proximity and identity of counter-ions in solution[50, 57]. For contact ion pairs this is especially true, and can be intuitively understood by recognizing that removing an electron from a net-neutral species should require more work than from a negatively charges species. The CTTS transitions of sodium iodide in THF, for example, undergoes an 18 nm hypsochromic shift from a free ion state (simulated by chelating the sodium cation in the solution), to a contact ion pair[58]. At most, the observed shift of the thiocyanate surface spectrum is on the order of unit nm (Figure 4.5).

Similarly, contact ion-pairing should occur to second-order in bulk thiocyanate concentration, yet the bimolecular fit was unsuccessful. On these basis, we can exclude the mechanism of contact-ion-pairing as the mechanism for thiocyanate adsorption to the interface.

The concept of a weaker cation-anion association bears some merit. The conclusion to be drawn from the failure of the bimolecular model is that the translational partition functions for the anion and cation must still be effectively uncoupled. Indeed, associated ion-pairs fit this criterion well, as the rates of exchange can be rapid compared to situations where the solvent shells must be penetrated (*e.g.* solvent-shared or contact ion pairs)[59, 60]. Even though association-paired ions are relatively uncoupled, there still must be some degree of correlation. The small but negative change in entropy for the process supports this hypothesis.

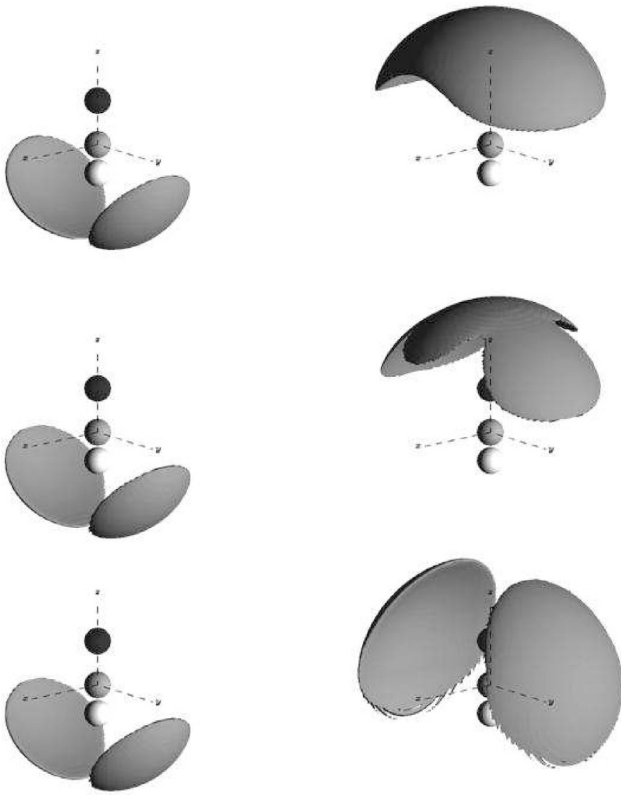

Figure 4.13- The isoprobability orientation surfaces of the water dipoles for N (left) and S (right) terminus solvating waters. Concentrations vary as 0.66 M, 1.31 M, and 2.83 M from bottom to top. Nitrogen is the darkest atom (top) and sulfur the lightest (bottom). The surfaces are visualized by that which the dipole of water would sweep out on reorientation, and appear opposite the thiocyanate molecule from which the originating water molecule is positioned. The orientation of the S terminus waters is considerably less constrained than the N terminus water, and undergoes a change in orientation as a function of concentration. *Reproduced with permission from* Botti, A., S.E. Pagnotta*, et al.*, *J. Phys. Chem. B*, **113**, 10014 (2009). *Copyright 2009 American Chemical Society.*

In a remarkable neutron diffraction study of aqueous potassium thiocyanate, Botti *et al.* considered the solvation structure of this anion in bulk solution with the aid of a Monte Carlo based simulation designed to iteratively optimize its results to match the experimental diffraction spectra[61]. In this study, they determined that solvation of the N and S terminus of thiocyanate is quite distinct, both in structure and concentration dependence. The isoprobability surfaces for the orientation of the S and N solvent dipoles are instructive (Figure 4.13), and demonstrate the potential effects that the

asymmetry of the thiocyanate anion has on bulk water, and by inference, in the interface. The solvation of the N terminus appears to be a single linear hydrogen bond of structure that is independent of concentration, of which the orientation is reasonably well-defined. However, the S terminus solvation waters are more distant and appear to be able to adopt a wider range of orientations of its dipole, and change as a function of concentration. It should be made clear that the radial distribution functions for the *positions* of solvating waters at both ends remain concentration independent. This suggests a poorly solvated S-terminus and is consistent with a previous *ab initio* simulation of thiocyanate-water clusters[62]. The poor solvation is reflected in the average number of solvating water molecules, which is reported to be <2.

These results indicate that the S-terminus, and thiocyanate in general, is weakly hydrated. The S-terminus water molecules can adopt a wide range of orientations, while the nitrogen atom is quite strongly solvated. This would engender a relatively weak cost of desolvation when brought to surface, and may be sufficient, when combined with inductive effects, to generate a net exothermic solvation reaction. This also suggests that if this molecule were to approach the solution surface, it would prefer to do so with the S terminus oriented towards the surface, the sulfur bound water molecules are held less tightly and the large and soft atom seems a much better candidate than the N terminus on the grounds of polarizability. This may be likely at low concentrations. Similarly, the change in solvation as a function of concentration does suggest that the time/intensity dependence of the SH signal discussed in the previous section may be due to a reorientation effect at high concentrations. The high viscosity of these solutions was evident during their preparation, and the kinetics of structural equilibration of the system may be exceedingly slow.

Close inspection of Figure 4.13 suggests an alternative, however. The sulfur atom appears to be undergoing a critical electronic structure transition from low to high concentrations. The symmetry of the water orientation is strongly indicative of a change in hybridization that seems to have overlooked in Botti *et al*.'s report. The low concentration orientation of the dipoles at the S-terminus suggest that the water molecules are largely pointed at ~30° angles with respect to the bond axis, suggestive of interaction with sp^2 type nonbonding electrons. As concentration is increased, the orientation develops a radial symmetry which could be due to the development of a 'blurred' sp^3 type orientation, the blurring due to overlap of orientation of three closely spaced orientational centers (*viz.*

lone pairs). This suggests that the sulfur is gradually assuming more of the net charge distribution as bulk concentration increases. While the charge distribution is clearly still resonant between nitrogen and sulfur on a timescale that is much faster than the solvating water molecules can react to translationally, it appears that they are able to react to this change via reorientation.

This could have profound consequences for solvation in the interface, and initially suggests that at higher concentrations the sulfur could tend to bury its increasing charge density in the dielectric of the solution despite its apparently weak solvation shell. However, the strongly hydrogen-bonded N terminus water would be difficult to remove, and would need to become part of the interface solvent structure for this to be plausible. Viswanath and Motschmann, were able to determine the orientation of interfacial thiocyanate to be ~45° to the surface normal, but were unable to conclude whether the S-terminus was directed towards the bulk or the interface[63]. Notably they also concluded that at concentrations over 0.5 M the orientation of the molecule becomes concentration independent. The rearrangement of charge distribution suggests that it may be the S-terminus that points towards the bulk at high concentrations, but at low concentrations this orientation may be more ambidentate.

4.4. Conclusions

It would be a remission not to add the caveat of the model explicitly here. Foremost, it is important to note that the simple model employed here engenders the usual Langmuir model assumptions discussed in Chapter 2. The fixed surface site restriction is, in effect, an assumption of constant interfacial volume as a function of concentration. Evidence in the literature suggests that, at molar concentrations, the thickness of the interface expands as a function of concentration[3, 64, 65]. If this were the case, we could expect an increase in observed surface thiocyanate that is not exclusively due to the adsorption process. The conclusions of an exothermic and entropically unfavorable adsorption process do not agree with the usual considerations for what drive polarizable anions to the interface, and certainly bear some skepticism. Nonetheless, the agreement of the data with the model is compelling.

This chapter has dealt extensively with the interfacial chemistry and spectroscopy of thiocyanate. It has been found that there is a strong signal change that appears to be a function of UV exposure and/or sample age after exposure, and it is postulated to be due to the generation and bulk exclusion of

elemental sulfur into the interface. For early times/short exposures to UV, this species probably undergoes photo-induced cyanolysis to expose the underlying thiocyanate layer at high applied intensities. After long exposures, the accumulation of sulfur is likely to be too dense to remove by this means. However, the possibility of other chemical effects, such as radical products and oxygenation, remain unexplored, as the study was intended for other purposes. Further study of this system is certainly merited to either confirm or refute the observed trends in signal changes and to ascertain their chemical origin. The possibility of radical thiocyanate products is of special interest, especially owing to the possibility of the formation of the trihalogen-like trithiocyanate, which is likely to have similar properties to triiodide.

The determination of the thermodynamic parameters for thiocyanate adsorption to the interface, under the assumptions of the unimolecular Langmuir model, indicates an exothermic process with a weakly unfavorable entropic change. This conclusion is in disagreement with usual views of the mechanism of adsorption, *viz*. that it is generally driven chiefly by cavitation forces with electrostatic penalties being mitigated by inductive forces. The failure of the bimolecular model to fit the present data indicates that ion-pairing can only be a factor if the ions are still relatively free to independently explore the interface region, *e.g.* associative pairing rather than contact pairing. Consideration of our results in context with related work suggests that the adsorption mechanism may be also be enhanced due to the specific (and weak) solvation of the thiocyanate anion, reducing the endothermic cost of desovlation to an extent that may allow for a net exothermic process when inductive effects are considered. There is no definitive evidence to suggest that thiocyanate actually penetrates the outermost layer of liquid water, and the exothermicity of the reaction implies that such an excursion is energetically unlikely.

4.5. References

1) Wang, H., E. Borguet*, et al.*, *J. Phys. Chem. A*, "*Polarity of Liquid Interfaces by Second Harmonic Generation Spectroscopy*," **101**, 713 (1997)

2) Fan, Y., X. Chen*, et al.*, *J. Phys. Chem. B*, "*On the Structure of Water at the Aqueous/Air Interface*," **113**, 11672 (2009)

3) Allen, H.C., N.N. Casillas-Ituarte*, et al.*, *Phys. Chem. Chem. Phys.*, "*Shedding light on water structure at air-aqueous interfaces: ions, lipids, and hydration*," **11**, 5538 (2009)

4) Shen, Y.R. and V. Ostroverkhov, *Chem. Rev.*, "*Sum-Frequency Vibrational Spectroscopy on Water Interfaces: Polar Orientation of Water Molecules at Interfaces*," **106**, 1140 (2006)

5) Petersen, P.B. and R.J. Saykally, *Annu. Rev. Phys. Chem.*, "*On the nature of ions at the liquid water surface*," **57**, 333 (2006)

6) Wilson, K.R., B.S. Rude*, et al.*, *J. Phys. Chem. B*, "*X-ray Spectroscopy of Liquid Water Microjets*," **105**, 3346 (2001)

7) Ohshima, H. and H. Matsubara, *Surface tension of electrolyte solutions*, in *Colloid & Polymer Science*. 2004, Springer Berlin / Heidelberg.

8) Levin, Y., *J. Chem. Phys.*, "*Interfacial tension of electrolyte solutions*," **113**, 9722 (2000)

9) Tamashiro, M.N. and M.A. Constantino, *J. Phys. Chem. B*, "*Ions at the Water-Vapor Interface*," **114**, 3583 (2010)

10) Levin, Y., A.P. dos Santos*, et al.*, *Phys. Rev. Lett.*, "*Ions at the Air-Water Interface: An End to a Hundred-Year-Old Mystery?*," **103**, 257802 (2009)

11) Ishiyama, T. and A. Morita, *J. Phys. Chem. C.*, "*Molecular Dynamics Study of Gas-Liquid Aqueous Sodium Halide Interfaces. I. Flexible and Polarizable Molecular Modeling and Interfacial Properties*," **111**, 721 (2006)

12) Mucha, M., T. Frigato*, et al.*, *J. Phys. Chem. B*, "*Unified Molecular Picture of the Surfaces of Aqueous Acid, Base, and Salt Solutions*," **109**, 7617 (2005)

13) Garrett, B.C., *Science*, "*Ions at the Air/Water Interface*," **303**, 1146 (2004)

14) Petersen, P.B., J.C. Johnson*, et al.*, *Chem. Phys. Lett.*, "*Direct experimental validation of the Jones-Ray effect*," **397**, 46 (2004)

15) Petersen, P.B. and R.J. Saykally, *Chem. Phys. Lett.*, "*Confirmation of enhanced anion concentration at the liquid water surface*," **397**, 51 (2004)

16) Petersen, P.B., *Dissertation: Surface Structure of Aqueous Electrolyte Solutions Probed by UV Second Harmonic Generation*, in *Department of Chemistry*. 2005, University of California, Berkeley: Berkeley.

17) Petersen, P.B. and R.J. Saykally, *J. Am. Chem. Soc.*, "*Adsorption of Ions to the Surface of Dilute Electrolyte Solutions: The Jones-Ray Effect Revisited*," **127**, 15446 (2005)
18) Petersen, P.B., R.J. Saykally*, et al.*, *J. Phys. Chem. B*, "*Enhanced Concentration of Polarizable Anions at the Liquid Water Surface: SHG Spectroscopy and MD Simulations of Sodium Thiocyanide*," **109**, 10915 (2005)
19) Petersen, P.B. and R.J. Saykally, *J. Phys. Chem. B*, "*Evidence for an Enhanced Hydronium Concentration at the Liquid Water Surface*," **109**, 7976 (2005)
20) Petersen, P.B. and R.J. Saykally, *J. Phys. Chem. B*, "*Probing the Interfacial Structure of Aqueous Electrolytes with Femtosecond Second Harmonic Generation Spectroscopy*," **110**, 14060 (2006)
21) Petersen, P.B. and R.J. Saykally, *Chem. Phys. Lett.*, "*Is the liquid water surface basic or acidic? Macroscopic vs. molecular-scale investigations*," **458**, 255 (2008)
22) Onorato, R.M., D.E. Otten*, et al.*, *J. Phys. Chem. C.*, "*Measurement of Bromide Ion Affinities for the Air/Water and Dodecanol/Water Interfaces at Molar Concentrations by UV Second Harmonic Generation Spectroscopy*," **114**, 13746 (2010)
23) Onorato, R.M., D.E. Otten*, et al.*, *Proc. Natl. Acad. Sci. USA*, "*Adsorption of thiocyanate ions to the dodecanol/water interface characterized by UV second harmonic generation*," **106**, 15176 (2009)
24) Dogliotti, L. and E. Hayon, *J. Phys. Chem.*, "*Flash photolysis study of sulfite, thiocyanate, and thiosulfate ions in solution*," **72**, 1800 (1968)
25) Luria, M. and A. Treinin, *J. Phys. Chem.*, "*Photochemistry of thiocyanate ion in solution*," **72**, 305 (1968)
26) Bartlett, P.D. and R.E. Davis, *J. Am. Chem. Soc.*, "*Reactions of Elemental Sulfur. II. The Reaction of Alkali Cyanides with Sulfur, and Some Single-Sulfur Transfer Reactions1*," **80**, 2513 (1958)
27) Boyd, R.W., *Nonlinear Optics*. Second ed. 2003, San Diego: Academic Press.
28) Otten, D.E., P.B. Petersen*, et al.*, *Chem. Phys. Lett.*, "*Observation of nitrate ions at the air/water interface by UV-second harmonic generation*," **449**, 261 (2007)
29) Friedman, H.L. and M. Kerker, *Journal of Colloid Science*, "*Ultraviolet absorption of aqueous sulfur solutions*," **8**, 80 (1953)
30) Baer, J.E. and M. Carmack, *J. Am. Chem. Soc.*, "*The Ultraviolet Absorption Spectra of Aliphatic Sulfides and Polysulfides*," **71**, 1215 (1949)

31) Cheng, J., C.D. Vecitis*, et al.*, *J. Phys. Chem. B*, "*Experimental Anion Affinities for the Air/Water Interface*," **110**, 25598 (2006)
32) Marcus, Y. and G. Hefter, *Chem. Rev.*, "*Ion Pairing*," **2006**, 4585 (2006)
33) Viswanath, P. and H. Motschmann, *J. Phys. Chem. C.*, "*Effect of Interfacial Presence of Oriented Thiocyanate on Water Structure*," **112**, 2099 (2008)
34) Jarvis, N.L. and M.A. Scheiman, *J. Phys. Chem.*, "*Surface potentials of aqueous electrolyte solutions*," **72**, 74 (1968)
35) Zhang, D., J.H. Gutow*, et al.*, *J. Chem. Phys.*, "*Sudden structural change at an air/binary liquid interface: Sum frequency study of the air/acetonitrile--water interface*," **98**, 5099 (1993)
36) Collins, K.D. and M.W. Washabaugh, *Q. Rev. Biophys.*, "*The Hofmeister effect and the behaviour of water at interfaces*," **18**, 323 (1985)
37) Cacace, M.G., E.M. Landau*, et al.*, *Q. Rev. Biophys.*, "*The Hofmeister series: salt and solvent effects on interfacial phenomena doi:10.1017/S0033583597003363*," **30**, 241 (1997)
38) Milosavljevic, B.H. and J.A. LaVerne, *J. Phys. Chem. A*, "*Pulse Radiolysis of Aqueous Thiocyanate Solution*," **109**, 165 (2004)
39) Gardner, W.H., H. Weinberger*, et al.*, *Thiocyanogen Solution*. Inorganic Syntheses. 2007: John Wiley & Sons, Inc.
40) Barnett, J.J., M.L. McKee*, et al.*, *Inorg. Chem.*, "*Acidic Aqueous Decomposition of Thiocyanogen*," **43**, 5021 (2004)
41) Barnett, J.J. and D.M. Stanbury, *Inorg. Chem.*, "*Formation of Trithiocyanate in the Oxidation of Aqueous Thiocyanate*," **41**, 164 (2002)
42) Baxendale, J.H., P.L.T. Bevan*, et al.*, *Trans. Faraday Soc.*, "*Pulse radiolysis of aqueous thiocyanate and iodide solutions*," **64**, 2389 (1968)
43) Du, Q., R. Superfine*, et al.*, *Phys. Rev. Lett.*, "*Vibrational spectroscopy of water at the vapor/water interface*," **70**, 2313 LP (1993)
44) Fordyce, A.J., W.J. Bullock*, et al.*, *Mol. Phys.*, "*The temperature dependence of surface second-harmonic generation from the air-water interface*," **99**, 677 (2001)
45) Rodriguez, V., F. Adamietz*, et al.*, *J. Phys. Chem. B*, "*Quantitative Determination of the Polar Order Induced under High Electric Field in Amorphous PDR1M Azobenzene Polymer Films*," **107**, 9736 (2003)
46) Fokin, Y.G., T.V. Murzina*, et al.*, *Surf. Sci.*, "*Phase transitions in ferroelectric liquid crystals probed by optical second harmonic generation*," **507-510**, 724 (2002)

47) Slyadneva, O., A. Harata*, et al.*, *Surf. Sci.*, "*Phase transitions in Langmuir monolayers of a rhodamine dye as studied by a second harmonic generation technique*," **507-510**, 713 (2002)
48) Uesu, Y., R. Nakai*, et al.*, *Ferroelectrics*, "*SHG Microscopic Studies on Low Temperature Phase Transitions of SrTi 16 O 3 and SrTi 18 O 3*," **285**, 19 (2003)
49) Fox, M.F., C.B. Smith*, et al.*, *J. Chem. Soc., Faraday Trans. 1*, "*Far-ultraviolet solution spectroscopy of thiocyanate*," **77**, 1497 (1981)
50) Blandamer, M.J. and M.F. Fox, *Chem. Rev.*, "*Theory and applications of charge-transfer-to-solvent spectra*," **70**, 59 (1970)
51) Jungwirth, P. and D.J. Tobias, *J. Phys. Chem. B*, "*Molecular Structure of Salt Solutions: A New View of the Interface with Implications for Heterogeneous Atmospheric Chemistry*," **105**, 10468 (2001)
52) Jungwirth, P. and D.J. Tobias, *J. Phys. Chem. B*, "*Ions at the Air/Water Interface*," **106**, 6361 (2002)
53) Taylor, R.S., L.X. Dang*, et al.*, *J. Phys. Chem.*, "*Molecular Dynamics Simulations of the Liquid/Vapor Interface of SPC/E Water*," **100**, 11720 (1996)
54) Levin, Y., *Phys. Rev. Lett.*, "*Polarizable Ions at Interfaces*," **102**, 147803 (2009)
55) Noah-Vanhoucke, J. and P.L. Geissler, *Proc. Natl. Acad. Sci. USA*, "*On the fluctuations that drive small ions toward, and away from, interfaces between polar liquids and their vapors*," **106**, 15125 (2009)
56) Chandler, D., "*Interfaces and the driving force of hydrophobic assembly*," **437**, 640 (2005)
57) Sauer, M.C., I.A. Shkrob*, et al.*, *J. Phys. Chem. A*, "*Electron Photodetachment from Aqueous Anions. 2. Ionic Strength Effect on Geminate Recombination Dynamics and Quantum Yield for Hydrated Electron*," **108**, 10414 (2004)
58) Bragg, A.E. and B.J. Schwartz, *J. Phys. Chem. A*, "*Ultrafast Charge-Transfer-to-Solvent Dynamics of Iodide in Tetrahydrofuran. 2. Photoinduced Electron Transfer to Counterions in Solution*," **112**, 3530 (2008)
59) Atkinson, G. and S. Petrucci, *J. Phys. Chem.*, "*Ion Association of Magnesium Sulfate in Water at 25Â°*," **70**, 3122 (1966)
60) Watanabe, D. and H.-o. Hamaguchi, *J. Chem. Phys.*, "*Ion association dynamics in aqueous solutions of sulfate salts as studied by Raman band shape analysis*," **123**, 034508 (2005)
61) Botti, A., S.E. Pagnotta*, et al.*, *J. Phys. Chem. B*, "*Solvation of KSCN in Water*," **113**, 10014 (2009)

62) Sansone, R., C. Ebner*, et al.*, *J. Mol. Liq.*, "*Quantum chemical and molecular dynamics study on the hydration of cyanide and thiocyanate anions*," **88**, 129 (2000)
63) Viswanath, P. and H. Motschmann, *J. Phys. Chem. C.*, "*Oriented Thiocyanate Anions at the Airâˆ'Electrolyte Interface and Its Implications on Interfacial Water - A Vibrational Sum Frequency Spectroscopy Study*," **111**, 4484 (2007)
64) Feng, R.-r., Y.-y. Xu*, et al.*, *Phys. Chem. Chem. Phys.*, "*Increased interfacial thickness of the NaF, NaCl and NaBr salt aqueous solutions probed with non-resonant surface second harmonic generation (SHG)*," **10**, 4920 (2008)
65) Xu, M., R. Spinney*, et al.*, *J. Phys. Chem. B*, "*Water Structure at the Air-Aqueous Interface of Divalent Cation and Nitrate Solutions*," **113**, 4102 (2009)

Chapter 5 - Second Harmonic Generation Spectroscopy of the Charge-Transition-To-Solvent Band of Iodide

5.1. Introduction

Electronic surface second-harmonic generation (SHG) spectroscopy seems a path of much potential for the study of aqueous interfaces, owing to the success of the related vibrational sum-frequency spectroscopy,[1-9] and represents a shift in focus from a Beer's law analogue employed in previous chapters to a true electronic spectroscopy of the interface. The iodide anion is an excellent proof-of-principle candidate owing to its well resolved charge-transition-to-solvent (CTTS) spin-orbit bands[10], the wealth of studies on the transition itself[10-18], and the previously reported lower-resolution second harmonic (SH) spectrum, which indicated a concentration dependent bathochromic shift of these bands[19-21].

As found for thiocyanate, iodide was observed to have a variable SHG signal over time and these results are considered in view of the oxidation of iodide into surface active products. The collected spectrum also appears to deviate from that previously reported[19, 22, 23], both at high and low concentrations. These results are considered in terms of possible oxidation interference, or the result of a difference in experimental configuration (*viz*. angle of incidence) between this study and the previous report.

5.2. Experimental

The optical setup used is described in Chapter 2. The bracketing methodology described in Chapter 2 is used for the time-dependent study discussed below. Further details of that study will be discussed with the results. All wavelengths referenced herein refer to the SH wavelength.

The SHG spectra of 10^{-3}, 0.01, and 0.12 mole fraction aqueous sodium iodide solutions (~6 M, 0.5 M, 0.05 M) were collected over 200-225 nm in 2.5 nm increments. The concentrations were chosen to reflect the high, mid, and low concentration regimes discussed in previous reports[19-21]. Due to the limited bandwidth of the detection-side mirrors, the spectrum was collected in two segments, $\lambda_{2\omega}$=200-225 nm and $\lambda_{2\omega}$=215-225 nm. The collection of the oxidation-

prone sodium iodide SH spectrum required that the sample not be removed from the sample chamber during acquisition of a given spectral segment (hereafter, segment) owing to the oxygen sensitivity that will be discussed below. Instead of bracketing a single sample measurement with two single reference measurements, a segment of the sample was collected and bracketed by two reference segments. Segments were taken three times for each concentration studied, overlapping portions of the segments taken six times total. One of the three segments was taken in reverse order of wavelength progression to randomize the effect of any systematic bias in time.

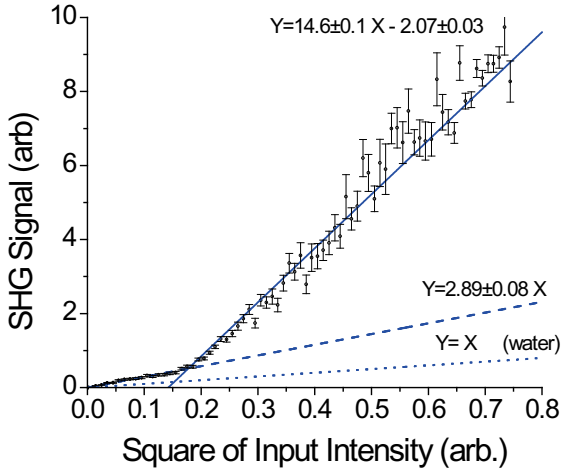

Figure 5.1- Power dependence profile of 0.12x NaI at 210 nm, 35 minutes after dispensation to it Petri-dish. The initial slope was ~15. The behavior is similar to that observed for SCN^-, as discussed in chapter 4.

Samples were prepared gravimetrically, and special attention was paid towards protecting the samples from oxygen before use. Samples were prepared in volumetric flasks with glass stoppers, and when prepared, the head space was purged with nitrogen before sealing. The samples prepared this way provided consistent results for up to three hours after preparation, but were compromised once exposed to oxygen. Thus, freshly prepared samples were used for every measurement. Samples were dispensed to Petri dishes and transferred as rapidly as possible to the nitrogen-purged (100% humidity) sample chamber immediately before measurements.

5.3. Time Dependence of the Sodium Iodide SHG Response

The SH signal of 0.12x NaI was found to decrease in time. The power dependence profile taken at 210 nm is quite similar to that observed for the thiocyanate ion at 205 nm (Figure 5.1). This effect was followed in time for four samples at 230 nm over a period of hours and days. The results are summarized in Figure 5.2. These measurements were taken by the bracketing method: for every measurement the sample must be removed from the nitrogen atmosphere of the sample chamber and stored for a minimum of four minutes in the lab

environment (covered by the Pyrex Petri-dish top) before a subsequent measurement can be made.

The time domain behavior of sodium iodide is very similar to that of the signals observed for sodium thiocyanate. A notable exception is in the decline of the signal to values below that of water (<1 in Figure 5.2), indicating the possible destructive interference or masking of the water non-resonant response, or perhaps an outright displacement of surface water. The instability of the iodide SHG response has been noted in the literature[24], and the possibility of chemical- or photo-induced oxidation has been cautioned against in a related study[20]. Based on the monotonic decline of the signal, even below the water non-resonant response, it seems quite likely that destructive interference is not occurring. Were this the case, we would anticipate that at some time the signal would regain intensity as the out-of-phase signal decreases beyond the maximum of interference. However, the signal may, in fact do so beyond the time scale of our observations or at differing concentrations.

Samples that were allowed to sit overnight in the lab environment

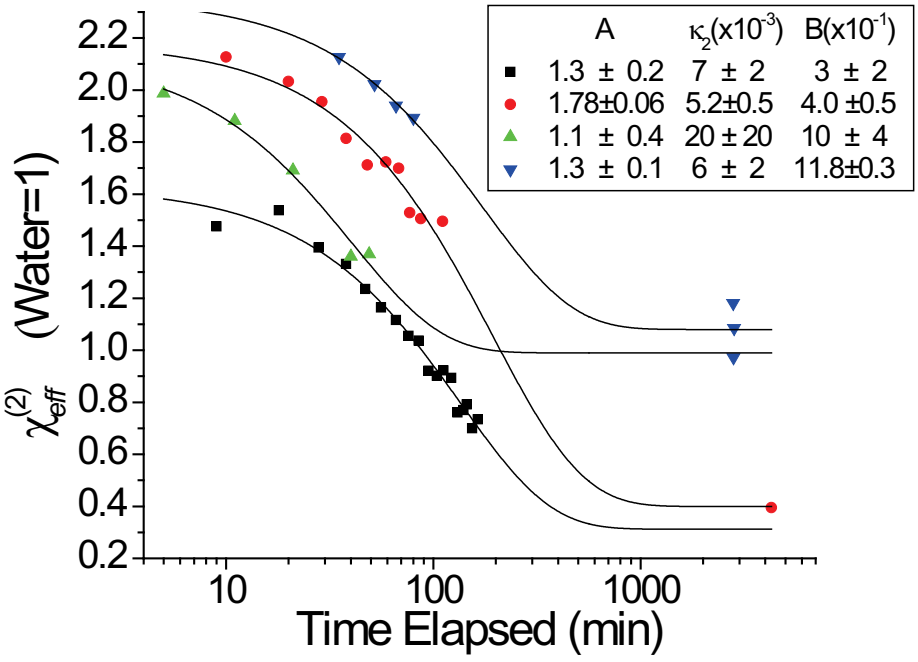

Figure 5.2- The effective susceptibility for four 0.12x NaI solutions observed at 230 nm, plotted as a function of time-elapsed since transferred from the preparation flask to Petri-dish. Solid (black) lines are fits to the rate-law expression of equation 5.7 which models the adsorption of oxygen into the sample. The large gaps in data are from overnight periods where the Petri dishes were allowed to sit in the lab atmosphere, covered but not sealed.

(covered, but not sealed) appear to have continued to decline in signal, in spite of the absence of irradiation. This suggests that the process is not photochemically sustained, although it is perhaps initiated or enhanced by irradiation; the yellow color of triiodide was evident along the beam path after irradiation. While photoproducts for even a monatomic anion are numerous and well studied[10-18], thermal mechanisms can also result in the oxidation of iodide[25]. Both mechanisms lead to two secondary products that are most likely to be present over such a prolonged timescale and in sufficient numbers to affect the observed second-harmonic signal[12, 14, 25]. Triiodide is the obvious candidate, as it has been observed by its distinctive yellow color after irradiation. The spectrum of triiodide consists of two adsorption bands centered at 291 nm and 434 nm[26], which are non-resonant for the wavelength of observation in Figure 5.2. The other likely species is iodate, which forms slowly through the disproportion of hypoiodous acid intermediate[27]:

$$I_2 + H_2O \rightleftarrows I^- + H^+ + HOI \tag{5.1}$$

$$3HOI \rightleftarrows 2I^- + IO_3^- + 3H^+ . \tag{5.2}$$

The presence of hypoiodous acid is neglected due to the high concentration of iodide in the competing reaction at pH 7[27]:

$$HOI + 2I^- \rightleftarrows I_3^- + OH^- . \tag{5.3}$$

Both species are plausible candidates for interfacial solvation, particularly since they carry all of the same qualities of polarizability and size that the surface active iodide does, except in even greater magnitude. The slow decline of SH signal is suggestive of the rate limiting disproportionation step, but the *relatively* high concentration of triiodide is compelling as well. Of note, the iodate ion consists of a broad shoulder that begins at ~270 nm but extends into the VUV and exhibits trigonal pyramidal structure (inversion-asymmetric), and would likely provide a strong second-order response relative to iodide and triiodide[28]. The SH signal seems to be continually decaying, which implies a true surface adsorption that is either displacing or masking up to half of the water response. As these are all ionic species, it seems unlikely that they could populate a surface so completely. To this end we consider iodine as a possibility as well, relying on arguments of poor solubility, lack of charge, and somewhat large size as a possible driving force.

The simplest way to approach the kinetic component of the signal is to assume that the buildup of some surface species is proportional to the oxygen content of the system. Both iodine and triiodide rates can be approached by applying the steady-state approximation to the concentration of iodine. Thus, we can state as a first approximation:

$$-\frac{d\chi_{eff}^{(2)}}{dt} \propto \frac{d[\mathrm{O}_2]}{dt} = k_1 p_{\mathrm{O}_{2(g)}} - (k_{-1} + k_2)[\mathrm{O}_2] \equiv \kappa_1 - \kappa_2[\mathrm{O}_2], \tag{5.4}$$

where k_1 (k_{-1}) is the rate constant for gas uptake (release) by the solution, and k_2 describes the loss of dissolved oxygen to the reactions via I_2 in the solution. We recognize that k_2 will decrease with time as our approximations become invalid. The oxygen concentration, and change in signal is then given by

$$-\Delta\chi_{eff}^{(2)} \propto [\mathrm{O}_2] = \left([\mathrm{O}_2]_0 - \frac{\kappa_1}{\kappa_2}\right)e^{-\kappa_2 t} + \frac{\kappa_1}{\kappa_2} \tag{5.5}$$

$$\left(\chi_{eff}^{(2)}\right)_f \propto \left(\frac{\kappa_1}{\kappa_2} - [\mathrm{O}_2]_0\right)e^{-\kappa_2 t} - \frac{\kappa_1}{\kappa_2} + \left(\chi_{eff}^{(2)}\right)_i. \tag{5.6}$$

This allows for the three parameter fit

$$\left(\chi_{eff}^{(2)}\right)_f = Ae^{-\kappa_2 t} + B, \tag{5.7}$$

applied to the date presented in Figure 5.2. While little can be quantitatively extracted from this fit, it has the reassuring quality of not generating a non-physical κ_2 value and supports the notion of an oxygen-mediated change in signal. Measurements that were subsequently performed for the electronic spectroscopy were kept under nitrogen throughout the measurement set, and when observed 30 minutes later were found to be unchanged.

5.4. Iodide SHG CTTS spectra

The collected spectra for the concentrations studied are found in the panels of Figure 5.3. The high concentration solution (0.12x NaI) was examined to capture the 'bulk-like' surface spectrum previously reported (Figure 5.4), while the low concentration (10^{-3}x NaI) was chosen to ideally exhibit the destructive interference reported in the 'Jones-Ray' concentration regime (Figure 5.5)[19, 20]. The high-concentration spectrum is featureless, consisting of a large, smoothly decaying shoulder tailing from the vacuum ultraviolet. There is some slight

evidence of structure in the mid-concentration spectrum, but it otherwise resembles the high-concentration spectrum. The low-concentration spectrum is indistinguishable the response of from neat water.

There is very little about the spectra collected in this study that can be considered in detail due to the lack of features exhibited. The high- and mid-

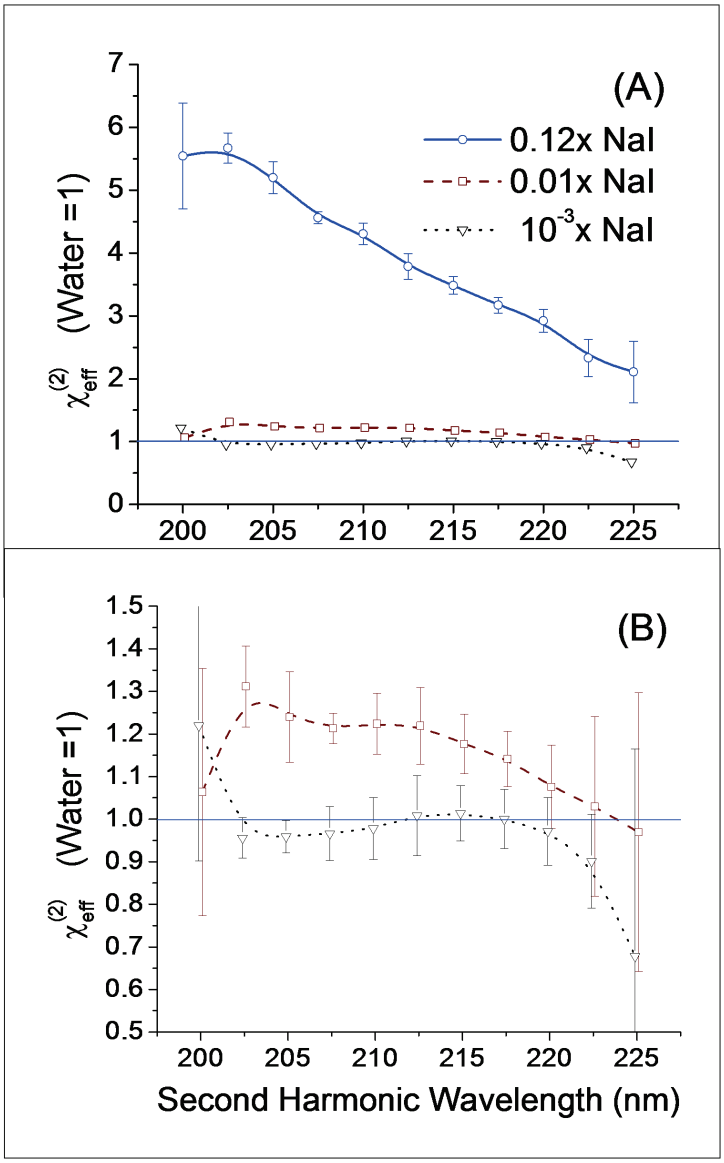

Figure 5.3- UV second harmonic spectra for 0.12x, 0.01x and 10^{-3}x NaI. Panel (B) is a magnification of the low concentration spectra of panel (A). Lines are guides for the eye. The Y-axis scale is the effective susceptibility as opposed its modulus. Data points at the ends of spectra suffer from large errors due to: (blue end) the weakness of the laser line used, and (red end) reflection limit of the detection mirrors used. 0.12x NaI spectrum is a broad, featureless shoulder extending from the VUV. 0.01x NaI spectrum shows evidence of a peak at 211 nm. The 10^{-3}x NaI is not distinguishable from water.

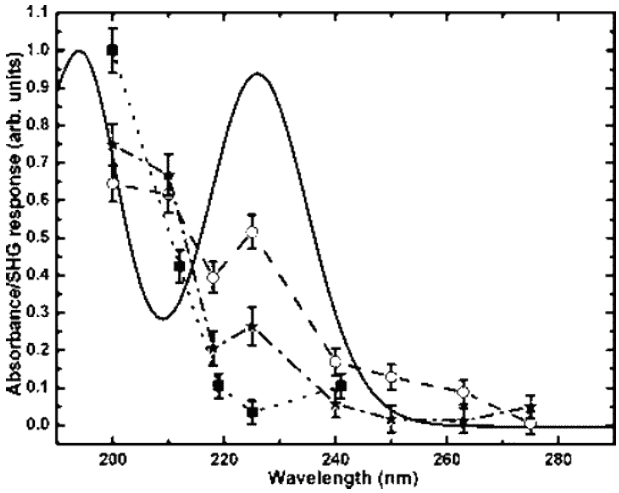

Figure 5.4- The linear absorption spectrum of NaI (solid line) overlaid by the surface second-harmonic spectrum of molar concentrations of NaI (open circles), KI (stars), and HI (solid squares). The alkali iodide spectra demonstrate evidence of the resolution of the bulk iodide spin-orbit features. *Reprinted with permission from* Petersen, P.B. and R.J. Saykally, *J. Phys. Chem. B*, 109, 7976 (2005). *Copyright 2005 American Chemical Society.*

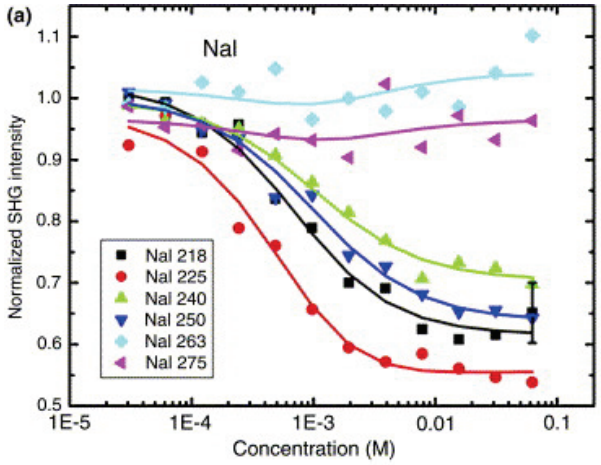

Figure 5.5- The sodium iodide second harmonic concentration profile as a series of second-harmonic wavelength in the Jones-Ray concentration regime collected by Petersen *et. al* [19]. The solutions exhibit a marked (up to ~40%) decrease of the second-harmonic signal relative to water, indicating destructive interference of the resonant iodide and non-resonant water responses. *Reprinted from Chem. Phys. Lett.,* ***397****,* Petersen, P.B. *et al. "Direct experimental validation of the Jones-Ray effect,"* p46, *Copyright 2004, with permission from Elsevier.*

concentration spectra collected here most resemble those of 5 M HI presented by Petersen and Saykally (Figure 5.4)[20]. There is no evidence here of the low-energy spin-orbit peak observable in that work.

While the experimental configuration differs in several respects, there are only two differences that may have resulted in such a discrepancy. The focal lengths and power densities are not reported in the referenced or related works[19, 20, 29-33], although the two quoted incident intensities used are comparable to those used for this study ($<10\ \mu\mathrm{J}\cdot\mathrm{pulse}^{-1}$; Ref [31]; and $<3\ \mu\mathrm{J}\cdot\mathrm{pulse}^{-1}$, Ref [32]). The potential effect of incident power density on the second-order responses in the presence of photo-chemically active systems has already been demonstrated in Chapter 4. This could indicate that the previously observed spectra are an artifact of intensity induced changes in the system.

The only other difference that could result in such a gross change in spectral character is the difference in incident angle, 60° herein, and 45° for the previous study. Brief consideration of the Fresnel factors[34] indicates that of the four independent components of the response tensor, only the magnitude of the $\chi^{(2)}_{zxx}$ component of will be observed to change more than

~5% (at 225 nm) between the two incident angles, assuming the dielectric of the interface region is an average of the vapor and bulk. However, on shifting the angle of incidence from 45° to 60°, the contribution from the $\chi^{(2)}_{zxx}$ component drops by ~60%. The angle for maximum response from this component is 43°, suggesting that the observations of Petersen and Saykally were performed at a near optimal configuration for this particular component. This suggests that the dominant contribution to iodide CTTS second-harmonic response may be due to a single component of the response tensor and, if so, represents the reason for the variation between the results reported herein, and those of Petersen and Saykally.

The observation of a resonant SHG signal that destructively interferes with the neat water non-resonant signal had also been reported at millimolar concentrations of NaI, and the corresponding Langmuir fit to that signal led to the conclusion that iodide is observed by SHG to be strongly surface adsorbing species in this concentration regime[19]. At the concentration used here (10^{-3}x NaI≈0.05 M), we had expected to see a strongly destructively interfering signal, by as much as 40% of the water response (see Figure 5.5), but instead the observed spectrum was indistinguishable from that of water. However, in consideration of the change in Fresnel factors mentioned above, the collected low-concentration spectrum may be in agreement with the previous study[19].

It is also plausible that the chemical change discussed earlier may have led to the depression of the signal, and subsequently interpreting it as destructive interference. It seems clear from the observed time dependent response of iodide that the signal values can decrease to even less than that of water. At higher concentrations, the process can quench significant amounts of SH signal. Thus, this process is a possible candidate for the cause of a sub-unity response from the iodide solution surface. The following establishes the possibility that the chemical changes in the system are what lead to the previously reported Jones-Ray SHG response of sodium iodide.

The general methodology employed by Petersen and Saykally was demonstrated in the presence of this researcher and can be commented on here with more detail than has been published in the literature[21, 33]. The solutions used were freshly prepared in a similar fashion as done in this study: they were generated the day of the experiment, using sparged 18 MΩ water, and sealed in volumetric flasks until used. It is unknown if the precaution of flushing the

headspace of the flasks with nitrogen was performed. Notably, subsequent dilutions were performed from the irradiated samples themselves: the stock sample first placed into a Petri dish, observed by SHG, and then varying amounts of the solution from the Petri dish was removed into a freshly rinsed volumetric flask to form the basis of the next dilution. Low concentration work (<1 M) was done similarly, starting from a 1 M bulk solution and diluting by ½ for each dilution: 10ml of previously used sample and 10ml of fresh, sparged water. However, the sample surface may also have been aspirated off in some instances.

Clearly, if the buildup of an oxidative product (hereafter, *B*) is proportional to the concentration of iodide in the system, and the *B* is known to depress the SH response to values below that of water, the destructive interference observed by Petersen, *et al.* can readily be explained. At initial concentration conditions there is no buildup of *B* in the system and the SH response is entirely due to the contributions of iodide and water. On the next dilution, there will now be some increased concentration of *B* and a decreased concentration of iodide. This is sufficient to demonstrate that, as long as the response of *B* depresses the SH signal more than iodide and water contribute to it, the SH will then be observed to be less than water, *viz.* 'destructive interference'.

Furthermore *B* will tend to increase concentration with succeeding dilutions, leading to greater depression of the signal, provided the rate of *B* generation is greater than the rate of loss due to dilution. Since we assume that iodide is responsible for the generation of *B*, we can anticipate that eventually dilutions will reduce the concentration of iodide such that the rate *B* generation is no longer greater than the rate of loss to dilution; the SH signal will then begin to return to the value of water with succeeding dilutions. This qualitative description of events describes the shape of the second harmonic response of iodide observed as a function of concentration in the Jones-Ray concentration regime.

Aspirating the surface away could mitigate such an effect. However if *B* has any appreciable concentration in the bulk this precaution would be of limited use. The population of bulk *B* would still remain to re-populate the interface, limited only by diffusion. However, we could anticipate that the agitation induced during the pipetting processes would certainly enhance the rate of oxygen adsorption into the system compared to the rates observed here for effectively stagnant systems.

5.5. Conclusions

It seems likely that the presence of oxidizing species in the iodide system can drastically change the nonlinear optical nature of and, quite likely, the chemical nature the air/solution interface. The SHG response of interfacial iodide is observed to decrease to levels below that of the non-resonant water background and indicates the buildup of an SHG inactive or otherwise undetected species. This suggests that the availability of interfacial iodide for chemistry on aerosols may be limited to reductive or neutral conditions, while concomitantly oxidative conditions may engender a new available species. The parallels between the photochemistry of thiocyanate and the processes observed here may indicate that trihalides and tri-pseudo halides are strongly surface active, and suggest that the results of the photo-chemical section of Chapter 4 could be reconsidered in this light. A model for consideration of the kinetic behavior of this process is developed, demonstrating that SHG can be used as a tool to monitor the dynamic chemical processes occurring at an interface.

The SH spectrum obtained from 200 nm-225 nm for the sodium iodide liquid water surface shows markedly little structure and differs significantly from that previously observed[19, 20]. This discrepancy may be due to a change of experimental configuration that leads to the dominating tensor component of the susceptibility being suppressed. Alternatively may have been due to a methodology artifact that stems from the above described oxidation process. The need for independent verification of these experiments is evident.

5.6. References

1) Allen, H.C., N.N. Casillas-Ituarte*, et al.*, *Phys. Chem. Chem. Phys.*, "*Shedding light on water structure at air-aqueous interfaces: ions, lipids, and hydration*," **11**, 5538 (2009)

2) Liu, D., G. Ma*, et al.*, *J. Phys. Chem. B*, "*Vibrational Spectroscopy of Aqueous Sodium Halide Solutions and Air-Liquid Interfaces: Observation of Increased Interfacial Depth*," **108**, 2252 (2004)

3) Du, Q., R. Superfine*, et al.*, *Phys. Rev. Lett.*, "*Vibrational spectroscopy of water at the vapor/water interface*," **70**, 2313 LP (1993)

4) Du, Q., E. Freysz*, et al.*, *Science*, "*Surface Vibrational Spectroscopic Studies of Hydrogen Bonding and Hydrophobicity*," **264**, 826 (1994)

5) Du, Q., E. Freysz*, et al.*, *Phys. Rev. Lett.*, "*Vibrational spectra of water molecules at quartz/water interfaces*," **72**, 238 LP (1994)

6) Shen, Y.R. and V. Ostroverkhov, *Chem. Rev.*, "*Sum-Frequency Vibrational Spectroscopy on Water Interfaces: Polar Orientation of Water Molecules at Interfaces*," **106**, 1140 (2006)

7) Zhuang, X., P.B. Miranda*, et al.*, *Physical Review B*, "*Mapping molecular orientation and conformation at interfaces by surface nonlinear optics*," **59**, 12632 (1999)

8) Raymond, E.A. and G.L. Richmond, *J. Phys. Chem. B*, "*Probing the Molecular Structure and Bonding of the Surface of Aqueous Salt Solutions*," **108**, 5051 (2004)

9) Tarbuck, T.L., S.T. Ota*, et al.*, *J. Am. Chem. Soc.*, "*Spectroscopic Studies of Solvated Hydrogen and Hydroxide Ions at Aqueous Surfaces*," **128**, 14519 (2006)

10) Blandamer, M.J. and M.F. Fox, *Chem. Rev.*, "*Theory and applications of charge-transfer-to-solvent spectra*," **70**, 59 (1970)

11) Schmitz, G., *Phys. Chem. Chem. Phys.*, "*The oxidation of iodine to iodate by hydrogen peroxide*," **3**, 4741 (2001)

12) Jortner, J., M. Ottolenghi*, et al.*, *J. Phys. Chem.*, "*THE EFFECT OF OXYGEN ON THE PHOTOCHEMISTRY OF THE IODIDE ION IN AQUEOUS SOLUTIONS*," **66**, 2042 (1962)

13) Jortner, J., M. Ottolenghi*, et al.*, *J. Phys. Chem.*, "*THE EFFECT OF NITROUS OXIDE AND THE NATURE OF INTERMEDIATES IN THE PHOTOCHEMISTRY OF THE IODIDE ION IN AQUEOUS SOLUTION*," **66**, 2037 (1962)

14) Jortner, J., M. Ottolenghi*, et al.*, *J. Phys. Chem.*, "*On the Photochemistry of Aqueous Solutions of Chloride, Bromide, and Iodide Ions*," **68**, 247 (1964)

15) Jortner, J., M. Ottolenghi*, et al.*, *J. Phys. Chem.*, "*SOLVENT EFFECTS ON THE PHOTOCHEMISTRY OF THE IODIDE ION*," **67**, 1271 (1963)

16) Grossweiner, L.I. and M.S. Matheson, *J. Phys. Chem.*, "*The Kinetics of the Dihalide Ions from the Flash Photolysis of Aqueous Alkali Halide Solutions*," **61**, 1089 (1957)
17) Lian, R., D.A. Oulianov*, et al.*, *J. Phys. Chem. A*, "*Electron Photodetachment from Aqueous Anions. 3. Dynamics of Geminate Pairs Derived from Photoexcitation of Mono- vs Polyatomic Anionsâ€* " **110**, 9071 (2006)
18) Choi, H., R.T. Bise*, et al.*, *J. Chem. Phys.*, "*Photodissociation dynamics of the triiodide anion (I_3^-)*," **113**, 2255 (2000)
19) Petersen, P.B., J.C. Johnson*, et al.*, *Chem. Phys. Lett.*, "*Direct experimental validation of the Jones-Ray effect*," **397**, 46 (2004)
20) Petersen, P.B. and R.J. Saykally, *J. Phys. Chem. B*, "*Evidence for an Enhanced Hydronium Concentration at the Liquid Water Surface*," **109**, 7976 (2005)
21) Petersen, P.B., *Dissertation: Surface Structure of Aqueous Electrolyte Solutions Probed by UV Second Harmonic Generation*, in *Department of Chemistry*. 2005, University of California, Berkeley: Berkeley.
22) Petersen, M.K., S.S. Iyengar*, et al.*, *J. Phys. Chem. B*, "*The Hydrated Proton at the Water Liquid/Vapor Interface*," **108**, 14804 (2004)
23) Petersen, P.B. and R.J. Saykally, *Annu. Rev. Phys. Chem.*, "*On the nature of ions at the liquid water surface*," **57**, 333 (2006)
24) Feng, R.-r., Y.-y. Xu*, et al.*, *Phys. Chem. Chem. Phys.*, "*Increased interfacial thickness of the NaF, NaCl and NaBr salt aqueous solutions probed with non-resonant surface second harmonic generation (SHG)*," **10**, 4920 (2008)
25) Evans, G.J., S.M. Mirbod*, et al.*, *The Canadian Journal of Chemical Engineering*, "*The volatilization of iodine species over dilute iodide solutions*," **71**, 761 (1993)
26) Mizuno, M., J. Tanaka*, et al.*, *J. Phys. Chem.*, "*Electronic spectra and structures of polyiodide chain complexes*," **85**, 1789 (1981)
27) Rahn, R.O., *Anal. Chim. Acta*, "*Determination of iodide formed from inorganic iodine in aqueous solution*," **248**, 595 (1991)
28) Awtrey, A.D. and R.E. Connick, *J. Am. Chem. Soc.*, "*The Absorption Spectra of I2, I3-, I-, IO3-, S4O6= and S2O3=. Heat of the Reaction I3- = I2 + I-*," **73**, 1842 (1951)
29) Petersen, P.B. and R.J. Saykally, *Chem. Phys. Lett.*, "*Is the liquid water surface basic or acidic? Macroscopic vs. molecular-scale investigations*," **458**, 255 (2008)
30) Petersen, P.B. and R.J. Saykally, *Chem. Phys. Lett.*, "*Confirmation of enhanced anion concentration at the liquid water surface*," **397**, 51 (2004)

31) Petersen, P.B. and R.J. Saykally, *J. Am. Chem. Soc.*, "*Adsorption of Ions to the Surface of Dilute Electrolyte Solutions: The Jones-Ray Effect Revisited*," **127**, 15446 (2005)
32) Petersen, P.B., R.J. Saykally*, et al.*, *J. Phys. Chem. B*, "*Enhanced Concentration of Polarizable Anions at the Liquid Water Surface: SHG Spectroscopy and MD Simulations of Sodium Thiocyanide*," **109**, 10915 (2005)
33) Petersen, P.B. and R.J. Saykally, *J. Phys. Chem. B*, "*Probing the Interfacial Structure of Aqueous Electrolytes with Femtosecond Second Harmonic Generation Spectroscopy*," **110**, 14060 (2006)
34) Shen, Y.R., *Surf. Sci.*, "*Surfaces probed by nonlinear optics*," **299-300**, 551 (1994)

Chapter 6 - Conclusions

In Chapter 1, we considered the development of the current picture of the air/water and air/aqueous-electrolyte interface, noting in particular that the molecular level study of small inorganic ions in the interface is a relatively new field of exploration. Nonlinear spectroscopic techniques have been successful in elucidating some of the finer details about the nature of the molecularly thin layers of water and solute that comprise the interface region. The presence of inorganic anions in the interface is now well accepted, but consideration of the mechanism of adsorption remains an active field of study.

In Chapter 2, we considered the previous application of ultraviolet second-harmonic generation (SHG) to electrolyte interface, utilizing the strong charge-transition-to-solvent (CTTS) bands to monitor the relative concentration change of such small inorganic anions as a function of bulk concentration. These studies utilized an adaptation of the Langmuir adsorption isotherm to extract the free energy of adsorption of such anions to the interface. However, we determined that the nature of the model imposes an exchange process whereby the number of water molecules replaced is fixed at a somewhat arbitrary value of 1:1. This imposition also constrains the maximum number of surface sites and therefore affects the apparent free energy of the adsorption. Hence, the energies of adsorption determined by the isotherms are very specific to the model used and are most useful when compared with like-modeled systems. Nonetheless, more realistic models increase complexity such that the very information we seek to attain is a prerequisite: the requirement of simultaneously modeling the SHG response with unknown molecular response constants, along with the unknowns of the adsorption process itself, renders the simplification of the problem a necessity.

At a minimum, we established that we could consider the effect of the cation in the context of the adapted Langmuir adsorption model, and, in fact, must require this as a consequence of the electroneutrality of the interface. In doing so, we are able to distinguish between adsorption processes where anions may adsorb independently, or co-adsorb with counter-ions as ion-pairs. In Chapter 3, we applied this model to the sodium nitrate and nitrite system, finding that the nitrite anion adsorbs to the interface in a second-order mechanism that is indicative of ion-pairing. This suggests that some anions may solvate in the interface with their counter-ion as a result of net charge reduction, the lower

dielectric of the interface enhancing the likelihood of such pair formation. The nitrate anion was concluded to be largely excluded from the interface, yet observable, and little mechanistic information could be determined as such. This work also demonstrated the success of using mechanistic modeling (*viz.* bimolecular vs. unimolecular adsorption) as a means to address the relative translational freedom of the cation in its concomitant approach to the interface.

In Chapter 4, we proceeded to consider the possible thermodynamic properties of ionic adsorption by measuring the temperature dependence of the interfacial adsorption process of potassium thiocyanate. It was determined that the process of adsorption of this anion was exothermic by the model used, and (weakly) unfavorable entropically. Similarly, it was determined that the unimolecular model held where the bimolecular model did not, indicating that the cation independently explores the interface volume. Whereas ion-pairing could have explained the exothermic result, the only means to rationalize the failure to fit the bimolecular model was to invoke weakly-bound solvent-separated ion-pair. Other consideration was made for the possibility that hydration of the thiocyanate ion is sufficiently weak that inductive forces may be sufficient to cause a net exothermicity.

Chapter 4, and subsequently, Chapter 5 also considered some of the dynamic effects observed in (unintentionally) non-equilibrium systems. The photochemistry induced in concentrated thiocyanate suggested the expulsion of a photo-product species which is postulated to be elemental sulfur, ultimately causing a time dependent decline in the SHG response attributed to thiocyanate alone. The time-dependent SHG study of iodide suggests that, on exposure to oxygen, triiodide or iodine, perhaps even iodate, may be present at the interface in concentrated iodide solutions. We also established the principle of applying a kinetic study, based on rate law, to the iodide solution change. Further directed study is required to draw quantitative conclusions, but the potential to monitor such processes is evident. The relationship of the power dependence profiles of the irradiated thiocyanate and iodide solutions suggests some similarity, which may indicate that trithiocyante production may offer a further explanation for the photochemical results of Chapter 4.

Chapter 5 concluded with the presentation of the deep-UV SHG spectrum of iodide, finding it to be different than that previously reported.[1-3] The difference of incident probe angle, or the possibility of oxidation chemistry were indicated as possible reasons for this variance.

To perform the above experiments some innovations were made in the experimental technique which allowed for some of these results to be obtained, and these were outlined in Chapter 2. The use of photon counting and the real-time collection of the power dependence profile was a tremendous boon towards identifying and then elucidating the nature of the dynamic signals discussed in Chapters 4 and 5. The evidence of two intensity regimes of response would have otherwise been unobserved. Similarly, while the development of a sighting laser and target for surface alignment was of tremendous importance, the subsequent determination of the dimensions of the second-harmonic depth of field brought to light just how sensitive the response of a sample is to this parameter. Not only did subtle alignment changes drastically effect the signals observed, it was determined that the stability of the temporal pulse width was also a critical factor in femtosecond generation of SHG, wherein small changes of laboratory environmental conditions at could lead to large relative changes in power density at the sample surface.

While the determination of these properties of concentrated electrolyte solutions is valuable, the fact is that actually performing these experiments is difficult. Diagnosing the variances of a response when contamination, photochemistry, short- and long-lived laser fluctuations, and the native response of a system are all independent variables is no small task. There is no question that the technique provides interesting insight into the nature of the liquid surface, but there is also no question that the potential for these experiments has been significantly impeded by the inability to control many of these factors. If there was one change I could make to these experiments it would be to perform them in a sealed environment. As such, further studies would *ideally* be carried out on a renewing surface, in a controlled atmosphere, and with a truly stable photon source. The dream would be to perform these experiments and preparation in a clean room. The application of these studies on a liquid microjet holds great potential for sample handling in this regard, although such a technique will undoubtedly engender its own difficulties.

A methodology that holds great potential for SHG spectroscopy as well as handling the stability issue includes the possibility of broadband *UV* SFG. The impact that vibrational sum frequency generation has already been discussed, and there is no fundamental reason why the same technique cannot be applied in the visible and UV spectrum through the use of modern white-light continuum sources. The collection of a full spectrum, rather than a single energy response,

has the benefits of self-normalization, multiplexed information, and would be operationally less complex if designed adequately. Accomplishing this would require some consideration for the detection sensitivity, as signals generated from these surfaces are already less than one photon per pulse, but even a scanning methodology could be successful under the right conditions.

A final consideration is given to the possibility of performing pump-probe surface chemistry studies. The photochemical interactions discussed in Chapter 4 certainly provide a basis for this, and the recent detection of the interfacial hydrated electron is an excellent example of this potential.[4] The iodide system could be an excellent starting point, owing to its rich photochemistry, and the (relatively) simple number of compounds that can result.

6.1. References

1) Petersen, P.B., J.C. Johnson*, et al.*, *Chem. Phys. Lett.*, "*Direct experimental validation of the Jones-Ray effect*," **397**, 46 (2004)
2) Petersen, P.B. and R.J. Saykally, *J. Phys. Chem. B*, "*Evidence for an Enhanced Hydronium Concentration at the Liquid Water Surface*," **109**, 7976 (2005)
3) Petersen, P.B., *Dissertation: Surface Structure of Aqueous Electrolyte Solutions Probed by UV Second Harmonic Generation*, in *Department of Chemistry*. 2005, University of California, Berkeley: Berkeley.
4) Sagar, D.M., C.D. Bain*, et al.*, *J. Am. Chem. Soc.*, "*Hydrated Electrons at the Water/Air Interface*," **132**, 6917 (2010)